Degenerative Joint Diseases

9

9.1 Osteoarthritis

Degenerative joint diseases include osteoarthritis, osteoarthrosis, osteochondrosis, and others and are the most common joint disorders that gradually disable patients. These recently receive greater attention because of the unprecedented prolongation of life expectancy and the availability of efficient prosthetic therapy. The terms describing "degenerative joint diseases" are many and used more or less loosely and even interchangeably. Osteoarthritis and osteoarthrosis designate degraded states of a synovial joint with and without significant inflammation, respectively. Osteoarthritis is classified into primary or idiopathic and secondary and inflammatory when there is significant synovial involvement with effusion.

A number of factors have been implicated as causative, but mechanical wearing down of the articular cartilages and supportive structures due to aging and obesity appears most important. According to Mitchel and Cruess (1977), osteoarthritis results from an abnormal concentration of stress across a normal joint or conversely a normal concentration of stress across an abnormal joint with an altered cartilage or subchondral bone. On the other hand, a hereditable element of osteoarthritis has been demonstrated in 50–65% in a twin epidemiological study (Cicuttini and Spector 1997), and one most recent study has indicated the existence of vertical transmission of primary osteoarthritis (Spencer et al. 2005).

9.2 Pathology

Osteoarthritis is initiated by either the enzymatic disruption of the cartilaginous matrix or microfractures in the subchondral bone trabeculae that are rendered vulnerable due to the thinning of the covering articular cartilage (Radin et al. 1977). Mild synovitis may develop after the appearance of histological alterations in the cartilage and bone as a result of the removal of the cartilage breakdown products through the synovial interstitium (Howell et al. 1976). Occasional cases show significant inflammation with effusion.

9.3 Radiographic Manifestations

The radiographic features include (a) narrowing of the joint space, (b) bone erosion, (c) eburnation in the contact area, (d) osteophytosis in the noncontact area, and (e) cyst in the subarticular bone (Fig. 9.1). When osteoarthritis is attended by local synovitis, that part of the joint becomes blurred with effusion and para-articular soft-tissue thickening and bulging (Fig. 9.2a). An important differential diagnostic feature of osteoarthritis is that changes are asymmetrical and focal and occur most typically in the area under stress and pressure. Such areas are in the lateral or medial aspect of the acetabu-

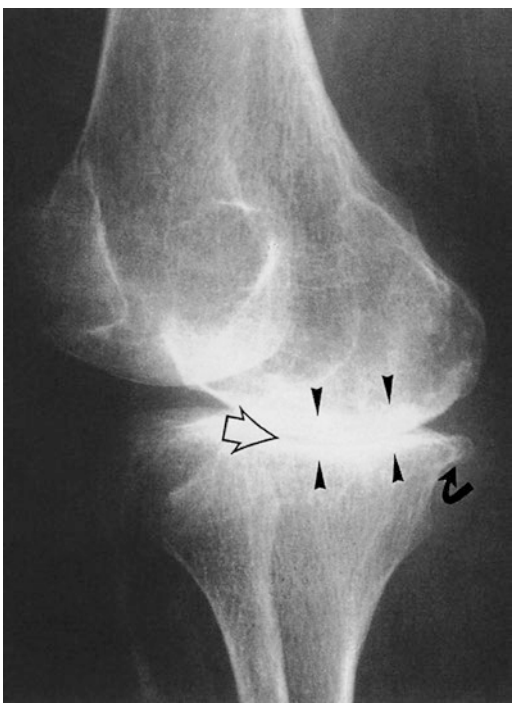

Fig. 9.1 Radiographic manifestations of osteoarthritis. Oblique radiograph of the right knee in a 51-year-old woman shows marked narrowing of the medial femorotibial compartment (*open arrow*) with subchondral eburnation (*arrowheads*) and a marginal osteophyte at the posterior tibial edge (*curved arrow*). The same case as Fig. 9.3

Y.-W. Bahk, *Combined Scintigraphic and Radiographic Diagnosis of Bone and Joint Diseases*,
DOI 10.1007/978-981-10-2759-8_9

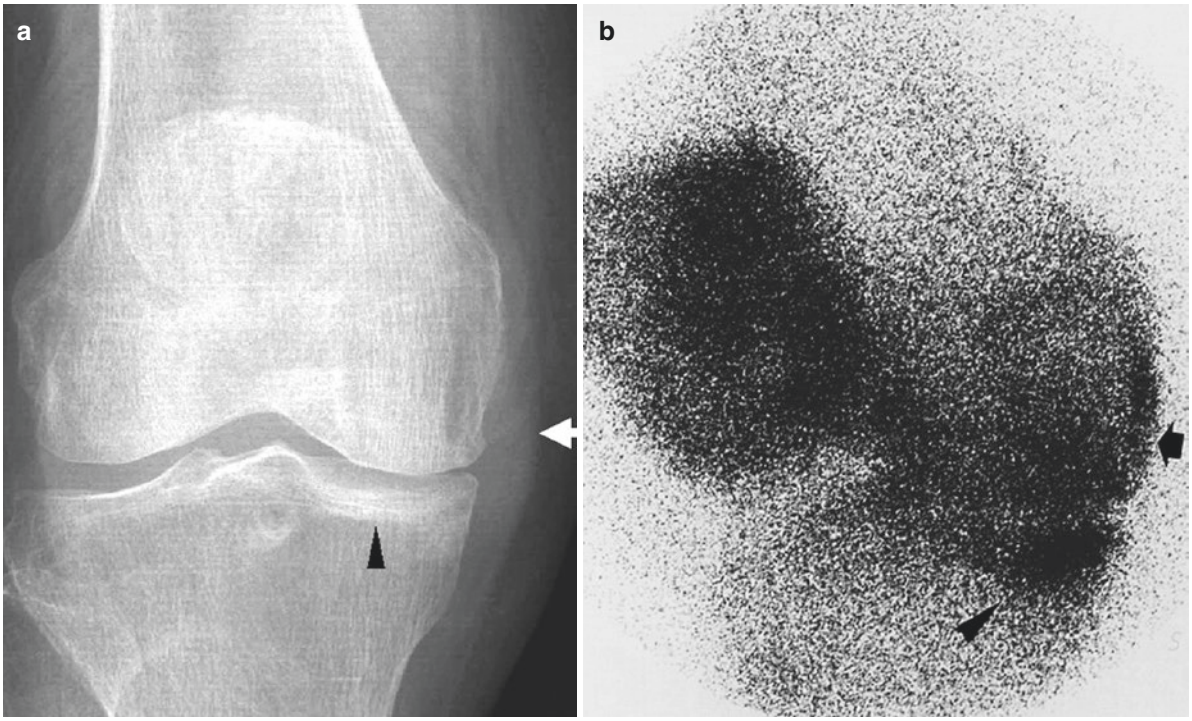

Fig. 9.2 Osteoarthritis with local synovitis. (**a**) Anteroposterior radiograph of the right knee in an 85-year-old female shows a narrowed medial articular compartment with a thickened capsule and collateral ligament (*arrow*) and sclerosis in the medial tibial plateau (*arrowhead*). (**b**) Anterior pinhole scan shows subchondral bone uptake with a narrowed joint space denoting synovitis with local bone reaction (*arrow*). Note focal sclerosis (*arrowhead*)

lar roof in the hip and in the medial, patellofemoral, or less frequently the lateral compartment, in the knee. Degeneration may occur both in the synovial and nonsynovial joints. The knee, the hip, the acromioclavicular joint, and the phalangeal joints belong to the former, and the diskovertebral joints, the manubriosternal joints, and the symphysis pubis belong to the latter. The apophyseal and costovertebral joints of the spine are well-known seats of osteoarthritis.

9.4 Pinhole Scintigraphic Manifestations

Pinhole scan features include focal articular narrowing, segmental or patchy uptake, and malalignment or deformity (Fig. 9.3). Tracer uptake appears to closely correlate with cortical erosion, eburnation, and subchondral cystic change. It is to be noted that the cystic change in the cancellous bone beneath the cortex accumulates tracer more intensely than in eburnation or mature osteophytes (Fig. 9.4). On the other hand, the mature osteophytes found in the marginal, nonstress area of a joint accumulate tracer only minimally, indicating that they are metabolically inert (Fig. 9.5). Pinhole scintigraphy can often show area(s) of very subtle uptake in a painful yet radiographically normal joint (Fig. 9.6). Many such lesions are not visualized on ordinary scintigraphs.

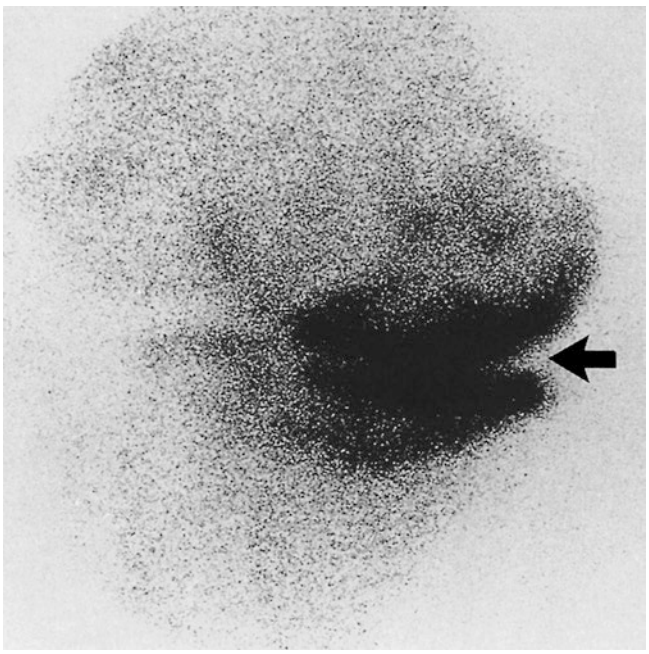

Fig. 9.3 Asymmetrical, discrete, periarticular segmental, and spotty tracer uptake with articular narrowing in osteoarthritis in the knee. Anterior pinhole scan of the right knee in the same patient as in Fig. 9.1 shows irregular, asymmetrical, segmental intense tracer uptake in the medial femorotibial compartment and the distal femoral bone end with narrowed articular space (*arrow*)

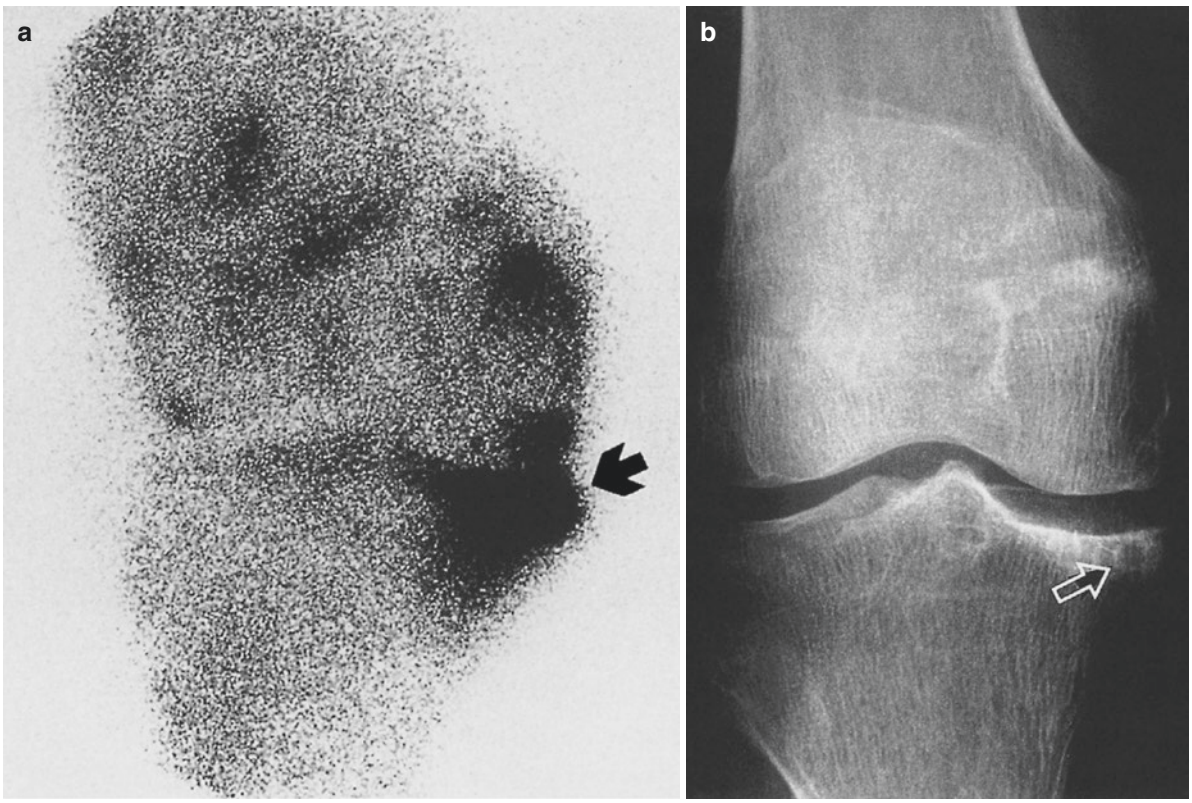

Fig. 9.4 Intense intraosseous tracer uptake in the cystic change of osteoarthritis. (**a**) Minimally rotated anterior pinhole scan of the right knee in a 74-year-old woman shows an extremely intense, triangular tracer uptake deep in the trabecular bone of the medial tibial condyle surrounded by less intense uptake (*arrow*). The joint is preserved and other asymmetrical, patchy tracer uptake can be seen in the femoral condyles. (**b**) Anteroposterior radiograph shows a small subcortical cyst and sclerosis in the medial tibial condyle (*arrow*)

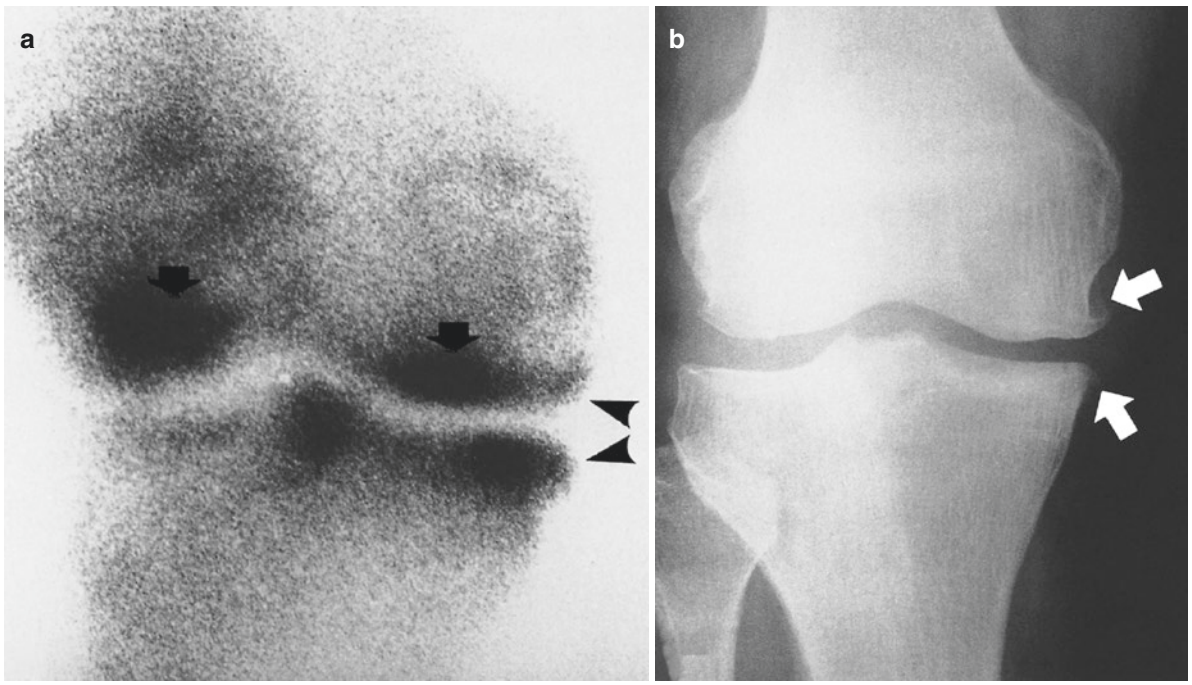

Fig. 9.5 Osteophytes in nonstress, marginal areas with little tracer uptake. (**a**) Anterior pinhole scintigraph of the right knee in a 72-year-old man shows insignificant tracer uptake in the osteophytes in the medial aspects (*arrowheads*). In contrast very intense uptake is seen in the articular surfaces of femoral condyles, medial plateau, and tibial tubercle, all of which are radiographically unremarkable (*arrows*). These denote preradiographic change. (**b**) Anteroposterior radiograph shows mature osteophytes in medial aspect of the knee (*arrows*). Note that periarticular bones are normal despite very intense tracer uptake

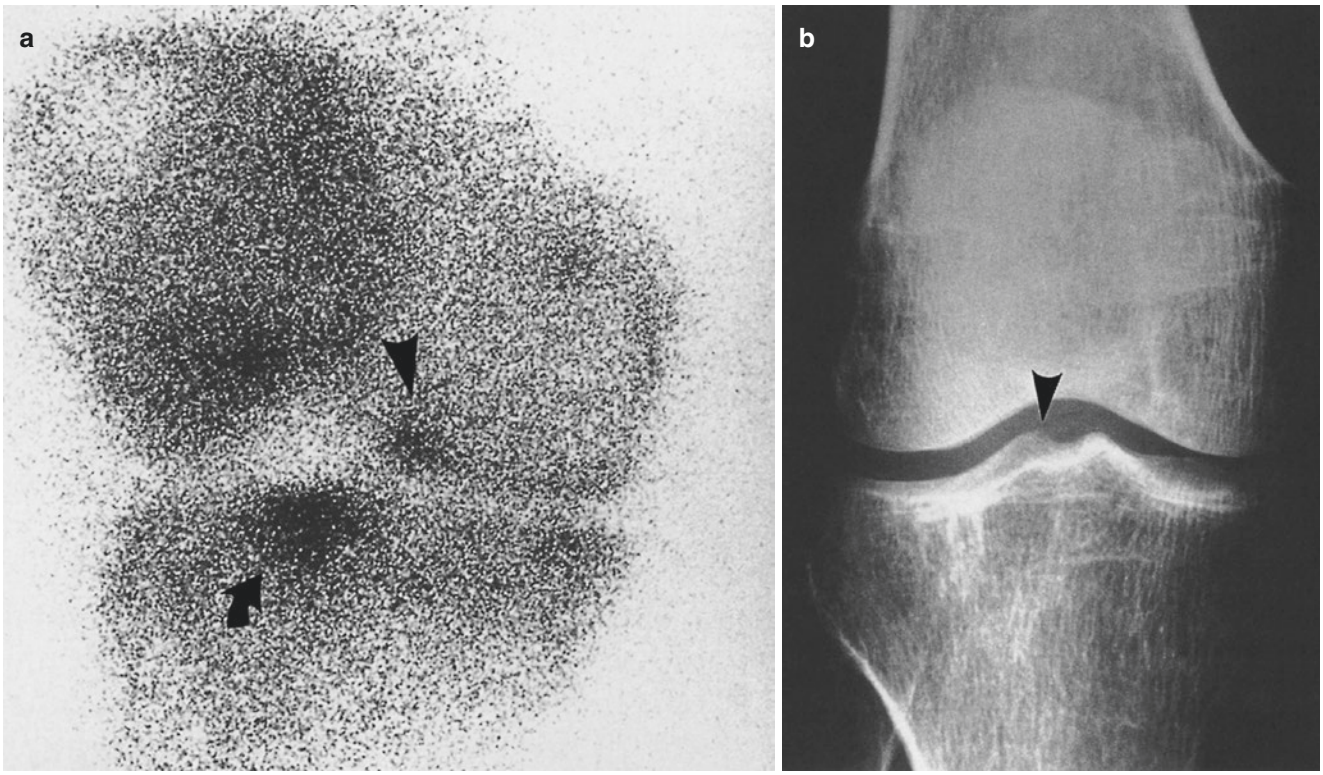

Fig. 9.6 Preradiographic manifestation of osteoarthritis and incipient osteophyte. (**a**) Slightly rotated pinhole scintigraph of the right knee in a 61-year-old woman with pain shows indeed subtle tracer uptake in the lateral aspect of the medial femoral condyle (*arrowhead*) and also in the lateral tibial tubercle (*arrow*). The medial femorotibial compartment is narrowed. (**b**) Anteroposterior radiograph appears normal, except for questionable pointing of the tip of the lateral tibial tubercle (*arrowhead*). The pointing may not have drawn enough attention if it had not been for the scan abnormality

9.5 Sacroiliac Joint

This is the articulation between the sacral and iliac auricular surfaces that are reciprocally curved and roughened or sinuous. This curvature and roughness restricts joint movements and biomechanically contributes to the stability and strength of the joint so that it can efficiently transmit weight from the spine to the lower limbs. The articulation is divided into two parts: (1) the synovial joint in the anteroinferior half or two-thirds and (2) the ligamentous (fibrous) joint in the remaining posterosuperior part (Brower 1988). The iliac surface is covered by thin hyaline cartilage (1 mm) and the iliac surface by thick fibrous cartilage (3–5 mm). The thinness of the cartilage in the iliac side explains why the disease involves this side first and the sacral side next. The degenerative changes of the sacroiliac joint may develop before the age of 30 years and become prominent after middle age. Pathological

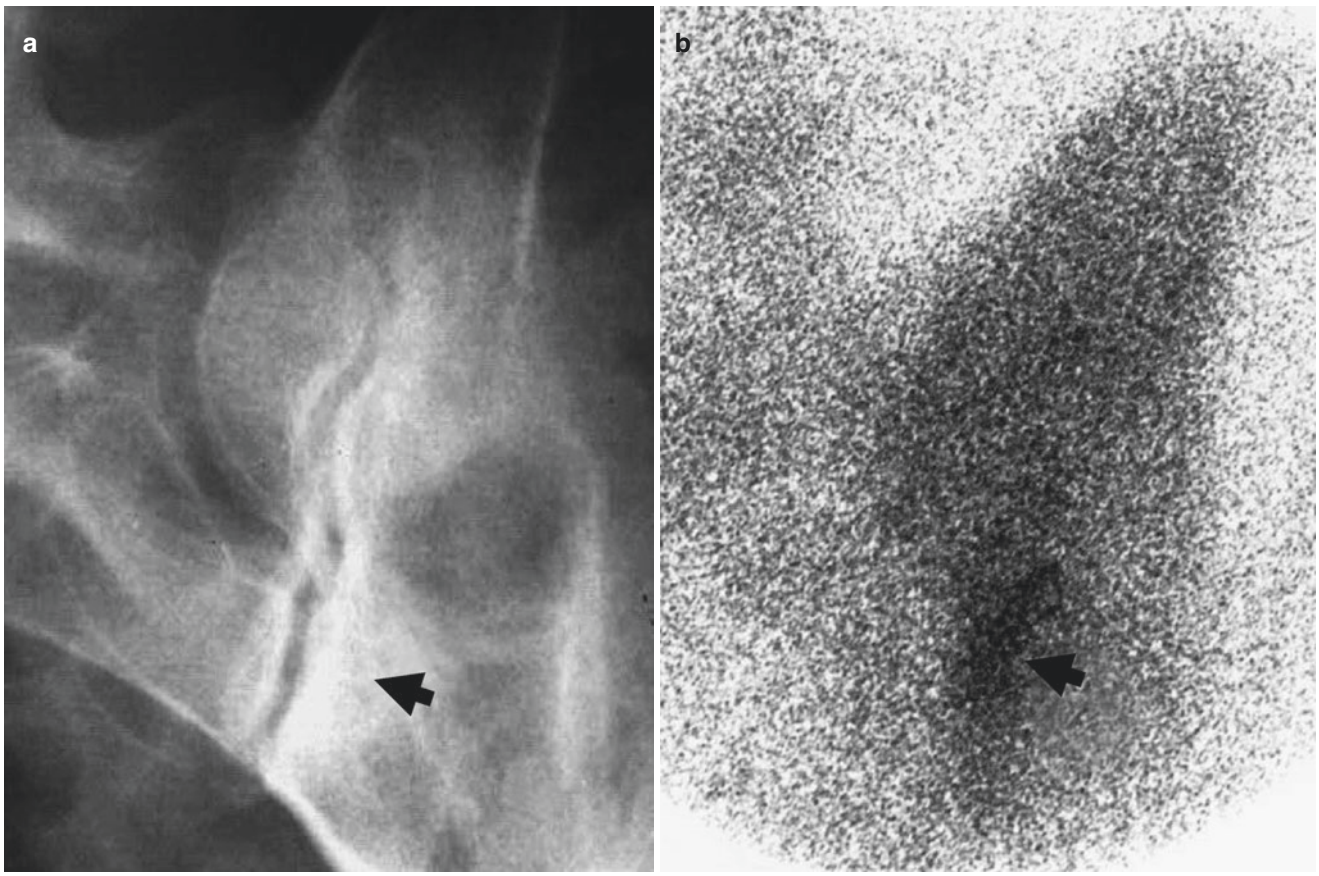

Fig. 9.7 Osteoarthritis in the sacroiliac joint. (**a**) Anteroposterior radiograph of the left sacroiliac joint in a 33-year-old male shows paraarticular sclerosis in the lower compartment (*arrow*). Note that sclerosis is more prominent on the iliac side than on the sacral side. (**b**) Anterior pinhole scan shows tracer uptake to be more intense in the iliac bone (*arrow*)

sequences are cartilage fibrillation, erosion, necrosis, and denudation followed by fibrous ankylosis. Bony eburnation and osteophytosis are common findings of the disease in the late stage. The involvement may be either unilateral or bilateral.

Radiographic manifestations include irregular cortical erosion, subchondral sclerosis, articular narrowing, and osteophytosis (Fig. 9.7a). In general articular narrowing is not a prominent feature in the sacroiliac joint, and osteophytosis typically occurs in the lower anterior aspect of the joint with beaking. Conventional tomography (CT) is extremely helpful in the analysis of all these features (Fig. 9.8b)

Pinhole scintigraphy demonstrates increased tracer uptake that is localized to the lower aspect of the joint in the early stages (Figs. 9.7b and 9.8c). Radiographic correlation reveals the uptake to specifically occur in the sclerotic bone that is in the iliac edge.

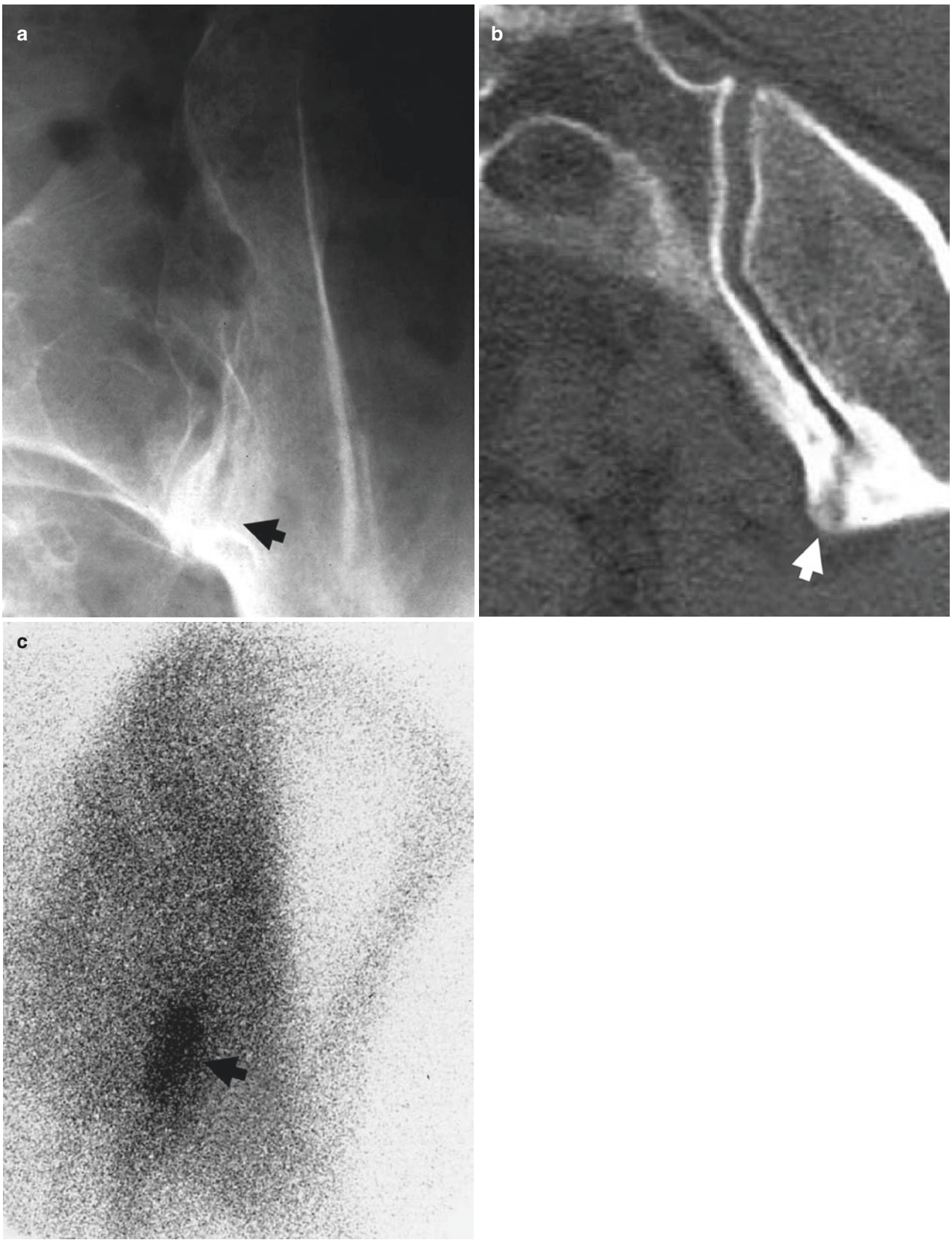

Fig. 9.8 Osteoarthritis in the sacroiliac joint with osteophytosis. (**a**) Anteroposterior radiograph of the left sacroiliac joint in a 49-year-old female shows sclerosis and articular obliteration in the lower articular compartment (*arrow*). (**b**) CT demonstrates anteriorly protruding hyperostosis with more prominent change occurring in the ilium (*arrow*). (**c**) Anterior pinhole scan shows tracer uptake in osteophytosis (*arrow*)

9.6 Hip

The hip is a ball-and-socket joint that permits multiaxial movement. It is surrounded by a dense, strong, and fibrous capsule. Along with the knee, the hip joint is the most typical site of osteoarthritis. Clinical symptoms are rotation or extension difficulty and pain that may be referred to the buttock, thigh, groin, greater trochanteric region, and knee.

The radiographic features, as in all other joints, include articular narrowing, osteosclerosis, osteophytosis, subchondral cystic change, and ankylosis (Fig. 9.9). Rarely, osteochondral or loose bodies may be present. The articular narrowing is accompanied by asymmetrical migration of the femoral head with respect to the acetabulum. On anterior radiographs the migration is mostly superolateral or superomedial and infrequently axial or central. The finding contrasts with the concentric migration of the femoral head in infective arthritis (Fig. 8.12) and rheumatoid arthritis (see Chap. 10).

Ordinary scintigraphy may show marked tracer uptake in the affected hip without topographic detail. In contrast, pinhole scintigraphy shows tracer uptake that is eccentric in location either in the uppermost (Fig. 9.10) or innermost aspect of the acetabulum, reflecting cranial or medial migration, respectively. On occasion, moderate uptake may also be observed in the medial aspect of the femoral neck due to buttressing (Fig. 9.10). It is important to note that the tracer uptake in the acetabular side of the joint is usually less intense than that in the femoral head unless the disease is advanced. The joint space becomes extinct when sealed by ankylosis (Fig. 9.11). Osteophytes may be indicated by ovoid tracer uptake hanging from the acetabulum like a necklace (Fig. 9.12). As mentioned above, differentiation from pyogenic arthritis or rheumatoid arthritis is possible by noting concentric narrowing of the joint space in these conditions. As elsewhere, the preradiographic or early change can be indicated by subtle uptake in the femoral head. The sign is reliable especially when it is eccentric in location. Frequently, such a small uptake may pass undetected on ordinary scintigraphs.

Fig. 9.9 Advanced osteoarthritis in the hip joint. Anteroposterior radiograph of the right hip in a 73-year-old female with long-standing arthritis shows articular narrowing, sclerosis, osteophytosis, subchondral cystic change, and osseous ankylosis (the same patient as in Fig. 9.11)

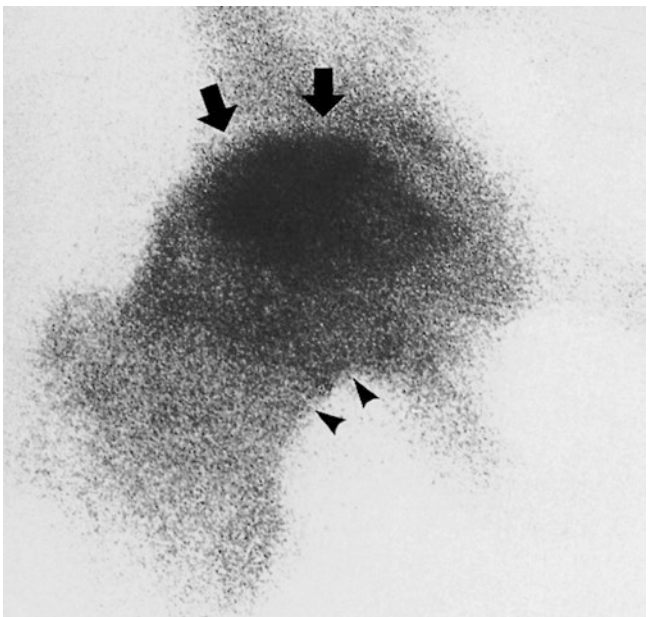

Fig. 9.10 Eccentric tracer uptake in the uppermost aspect of the femoral head in osteoarthritis. Anterior pinhole scintigraph of the right hip in a 62-year-old woman with advanced osteoarthritis shows intense tracer uptake localized eccentrically in the uppermost part of the femoral head (*arrows*) with narrowed joint. Modest tracer uptake can be seen also in the medial aspect of the neck, denoting buttress (*arrowheads*). The acetabulum shows little alteration. All these findings were validated by radiography (not shown here)

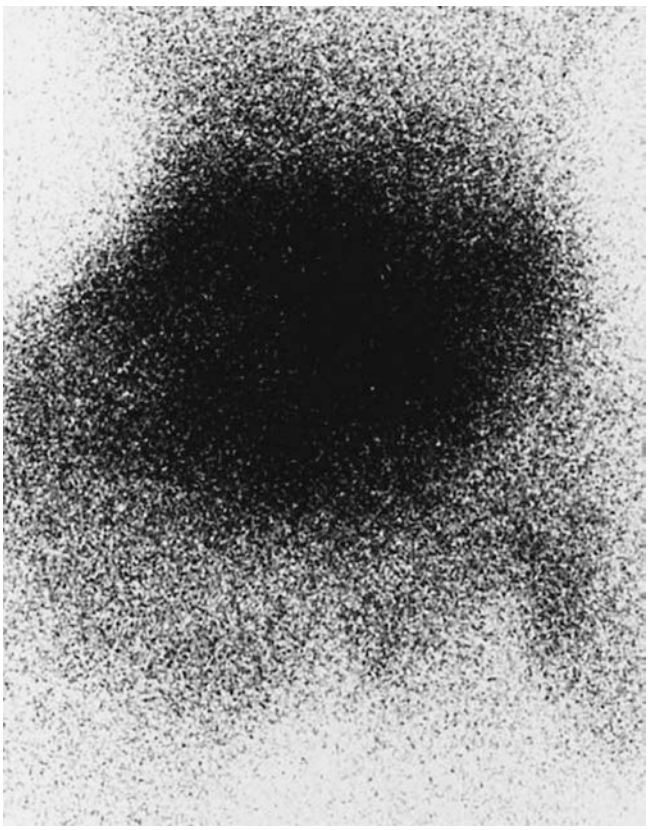

Fig. 9.11 Anterior pinhole scan of the right hip joint shows diffusely increased tracer uptake with dominant uptake involving the femoral head with extinct joint space due to ankylosis (same patient as in Fig. 9.9)

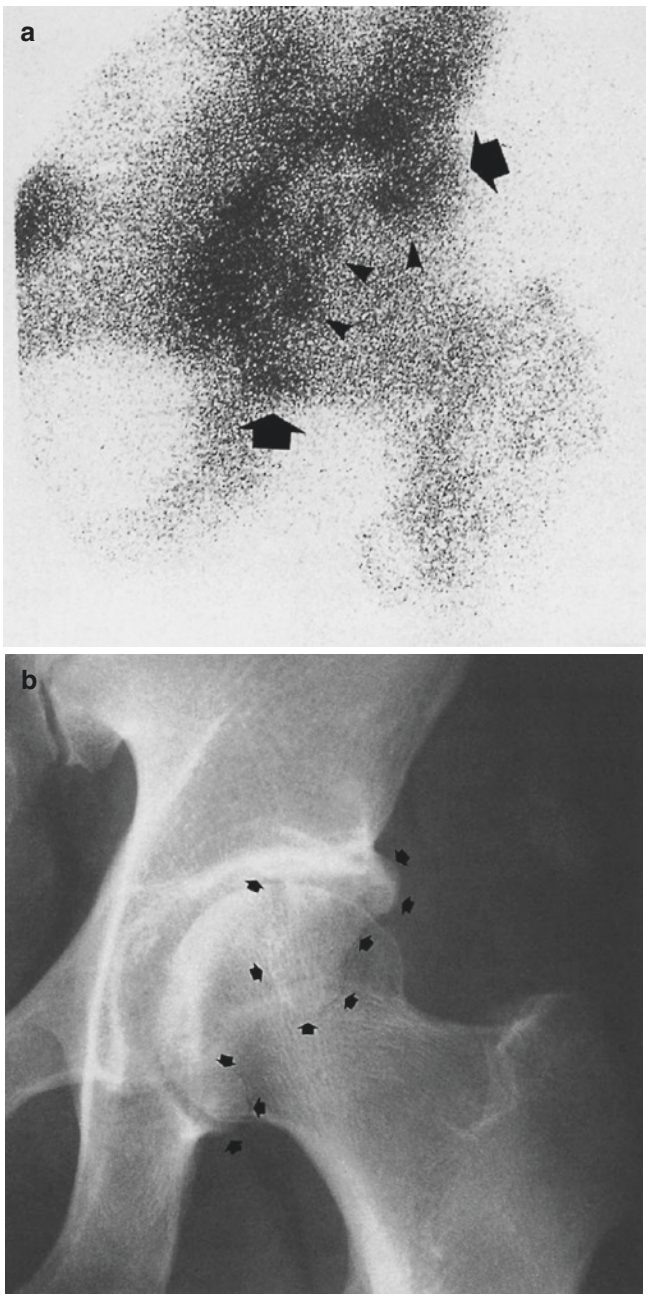

Fig. 9.12 Scintigraphic demonstration of the marginal osteophytes in osteoarthritis in the hip. (**a**) Anterior pinhole scintigraph of the left hip in a 33-year-old man with osteoarthritis secondary to dislocation reveals several beaded areas of increased tracer uptake along the acetabular brim as well as an eccentric, patchy uptake in the medial edge (*lower arrow*). Beaded lesions represent stalactic osteophytes; those at the lateral and medial edges are imaged in profile (*arrows*) and those at the anterior and posterior edges en face (*arrowheads*). The eccentricity of the patchy tracer uptake is characteristic of osteoarthritis. (**b**) Anteroposterior radiograph shows the stalactic bony excrescences along the acetabular brim (*arrows*)

9.7 Knee

The knee is the most common site of osteoarthritis. The anatomy of the knee is compound, having two condylar joints between the femur and tibia and the sellar joint between the patella and femur. The joint is provided internally with the menisci and the cruciate ligaments and externally with the bursae above, in front of, and below the patella. The causes for osteoarthritis in the femorotibial compartment (knee) and the patellofemoral compartment (patella) are many and varied. For example, femorotibial osteoarthritis has been related to trauma, meniscus surgery, osteonecrosis, deformity and obesity, and femoropatellar osteoarthritis to trauma, deformity, and chondromalacia patellae (Bahk et al. 1994; Resnick 2002). Symptoms may be surprisingly lacking during the early stage despite the presence of radiographic spurs or scintigraphic change, or conversely pain and limited motion may antedate the appearance of the radiographic or scintigraphic abnormality. Sooner or later, however, instability, awkward gait, limb deformity, and subluxation may ensue with severe disablement. Radiographic features include articular narrowing of various grades, subchondral osteosclerosis, eburnation, cystic change, and periarticular osteophytosis or spur formation. When acute synovitis supervenes, the para-articular soft tissue becomes bulged due to effusion and synovial edema, and

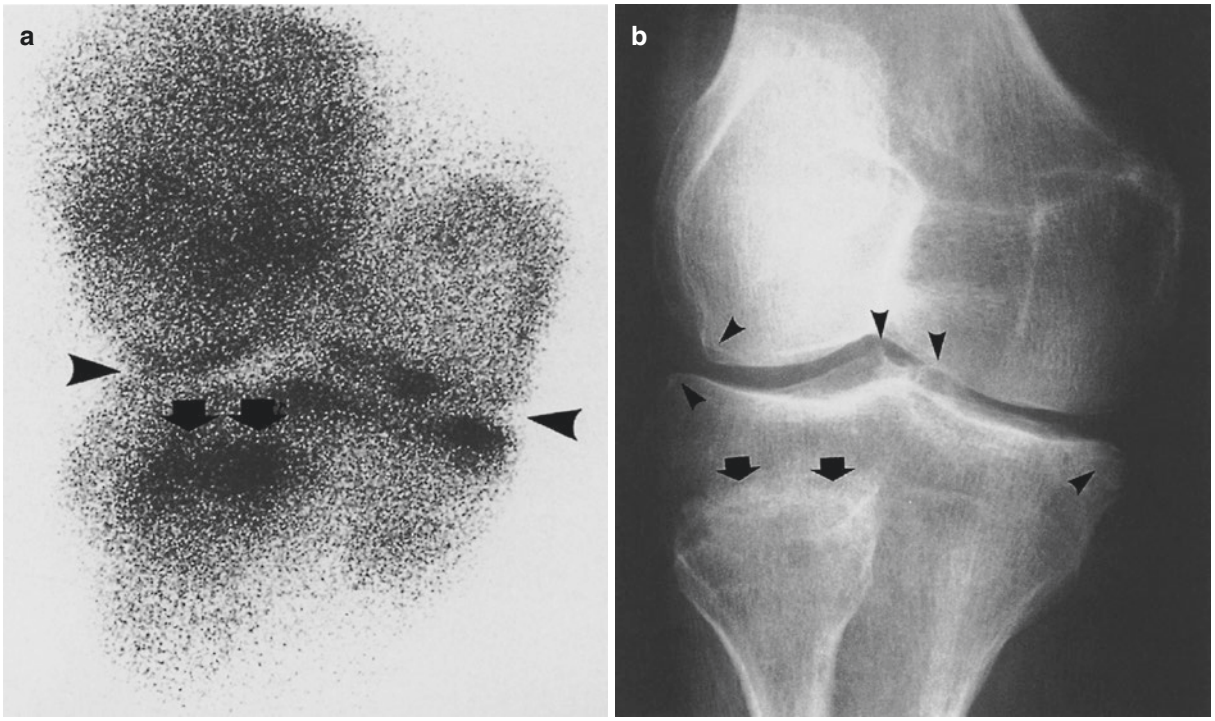

Fig. 9.13 Multicompartmental involvement in osteoarthritis in the knee. (**a**) Anterior pinhole scan of the right knee in a 35-year-old man shows multiple, asymmetrical areas of segmental, spotty, and patchy tracer uptake in the femorotibial compartments including the tibial tubercles and the proximal tibiofibular joint (*arrows*) with narrowed articular space (*arrowheads*). (**b**) Anteroposterior radiograph reveals minimal marginal osteophytes (*arrowheads*), the pointing of the tibial tubercles (*middle arrowheads*), and the narrowing of the joint. The proximal tibiofibular joint also shows periarticular sclerosis and articular obliteration (*arrows*)

it occurs typically in the medial femorotibial compartment (Fig. 9.2a). Occasionally, vacuum shadow and loose bodies may be seen. Except for marginal spurs, most changes occur in the contact joint surfaces. In advanced cases, the joint becomes subluxed and sealed due to osseous ankylosis.

Pinhole scintigraphy in the earliest stage of osteoarthritis demonstrates spotty "hot" area(s) in the subchondral zones of the femorotibial compartment that is in close contact and weight bearing (Fig. 9.6). The degree of uptake varies widely from subtle to extreme, and the appearance may be spotty, mottled, patchy, or segmental. Tracer uptake and radiographic changes do not necessarily match each other, and a hot area may be seen where there is no radiographic change (Fig. 9.6). As the disease progresses, focal uptake appears in the eburnation and spurs formed in the tibial plateaus, femoral condylar undersurfaces, and tibial tubercles (Fig. 9.13). The uptake is discrete and asymmetrical, mainly involving the medial and central femorotibial compartments (Figs. 9.4, 9.5, and 9.6). When cystic change supervenes, uptake becomes markedly intensified. Cystic change is commonly observed in the medial tibial condylar edge, giving rise to the "hot edge" sign (Fig. 9.4). In occasional cases the whole knee joint compartments including the medial and lateral femorotibial compartments, the proximal tibiofibular compartment, and the patellofemoral compartment are involved (Fig. 9.13). The involvement of the tibial tubercles is indicated by uptake localized in the central elevation of the tibial head (Fig. 9.13).

In summary, unlike in infective arthritis and rheumatoid arthritis, the lesions in osteoarthritis are discrete and the joint is not completely affected. When acute synovitis supervenes, uptake becomes diffuse, but is still confined to one side of the knee, more commonly the medial side. Subchondral cysts accumulate tracer most intensely, presenting the "hotter spot within hot area" sign. In contrast, mature osteophytes accumulate little or no tracer. Their location in the nonstress area keeps metabolism as inert and stable as that in the normal long bones (Fig. 9.5).

9.8 Patella

The patella, the largest sesamoid bone, is situated anterior to the knee. It is buried cranially in the rectus femoris muscle tendon and caudally in the infrapatellar tendon. The convex anterior surface, subcutaneous with a bursa between, is roughened to permit tendinous attachment, and the posterior or retropatellar facet is provided with a

smooth articular surface divided by a vertical ridge. Along with the knee proper, the retropatellar facet is a notorious site of degenerative diseases including osteoarthritis and chondromalacia.

9.8.1 Patellar (Femoropatellar) Osteoarthritis

Patellar osteoarthritis is characterized by tracer uptake at the lower or upper edge of the retropatellar facet (Figs. 9.14 and 9.15). The narrowing of the patellofemoral joint and increased uptake in other articular compartments of the knee are important diagnostic features of osteoarthritis. Due to altered locomotion, osteoarthritis in genu valgum and genu varus tends to occur in the lateral and medial femorotibial compartment, respectively, whereas osteoarthritis in flexion deformity is prone to affect the posterior compartment. As discussed below chondromalacia patellae is not osteoarthritis in the strict sense and, hence, usually not accompanied by osteoarthritis in other parts of the knee (Fig. 9.16).

9.8.2 Chondromalacia Patellae

Chondromalacia of the patella is a condition characterized by a series of degenerative changes that involve the cartilage and subchondral bone in the retropatellar facet. Clinically, two different types have been described on the basis of the age and symptom. The first type, which is traditionally referred to as chondromalacia patellae, manifests as pain and crepitus over the patella in young adults and adolescents. The second type is a disease of older age. It is not necessarily associated with osteoarthritis in the femoropatellar joint.

Pathologically, in the initial stage, the cartilage on the retropatellar facet undergoes softening and swelling, in the second and third stages fissuring and fibrillation with a "crab meat" appearance, and in the final stage thinning and ulceration. As a result, the subchondral bone becomes exposed (Wiles et al. 1956). According to Goodfellow et al. (1976), the changes in the articular cartilage of the patella may be categorized as the surface type or the basal type.

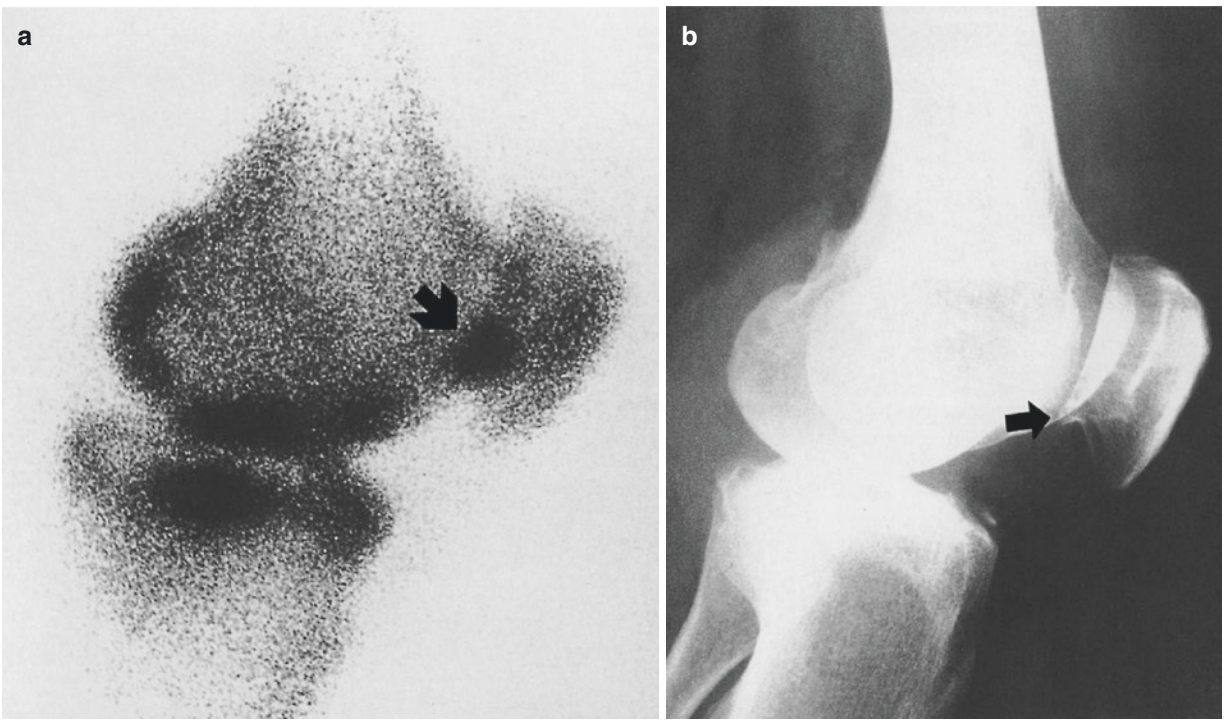

Fig. 9.14 Patellar involvement in osteoarthritis. (**a**) Medial pinhole scintigraph of the left knee in a 61-year-old woman shows a spotty "hot" area in the inferoposterior aspect of the patella (*arrow*) with associated spotty intense tracer uptake in the other periarticular bones. (**b**) Mediolateral radiograph demonstrates a small osteophyte in the inferoposterior aspect of the patella (*arrow*) and suspicious erosion in the apposing femoral cortex

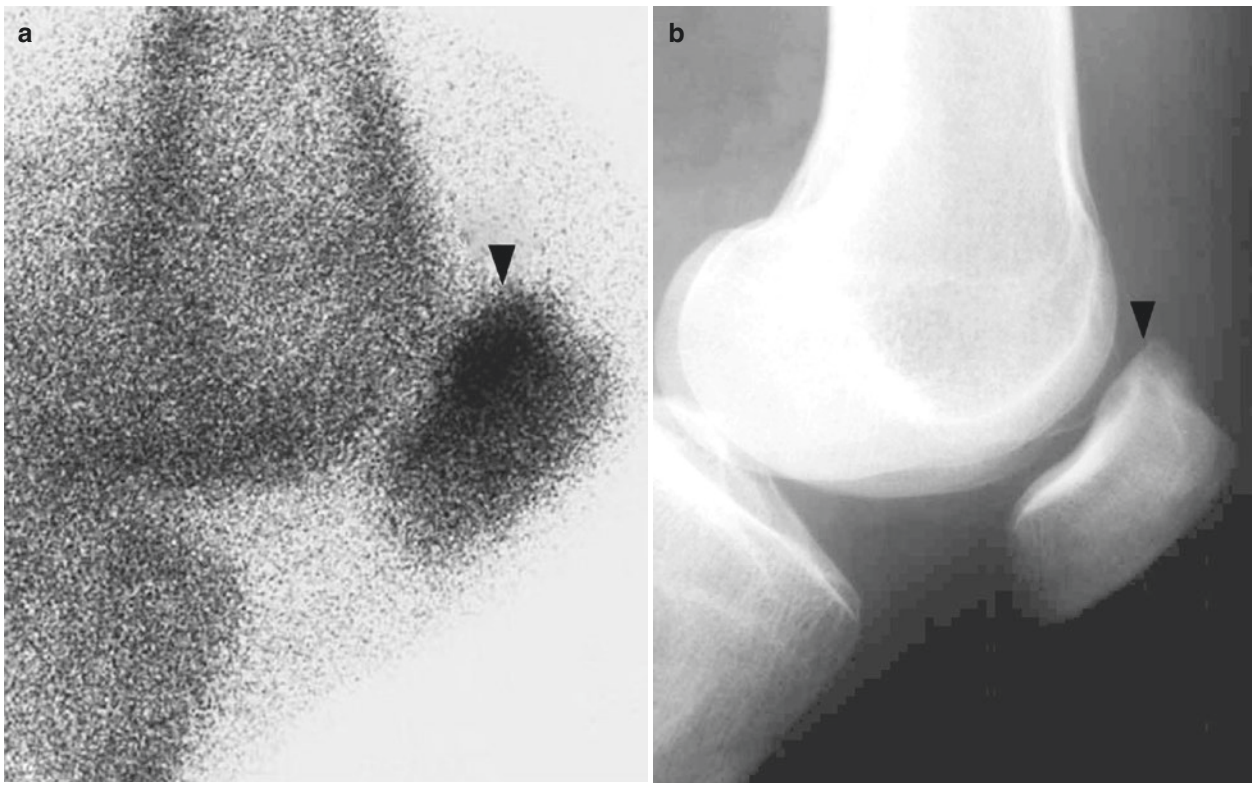

Fig. 9.15 Patellar osteoarthritis. (**a**) Lateral pinhole scan of the right patella in a 63-year-old male shows increased tracer uptake localized to the upper edge of the retropatellar facet (*arrow*). (**b**) Lateral radiograph reveals a small spur with sclerosis (*arrow*)

The former is age dependent, and its incidence increases precipitously with age, predisposing to osteoarthritis in later years, and the latter is a disease of young adults with more or less self-limited symptoms and clinical course.

Conventional radiography is of limited value in diagnosing this condition (Lund and Nilsson 1980), but arthrography and CT and MRI play a decisive role. Occasionally, simple radiography may reveal focal osteopenia in the retropatellar facet with or without subchondral bone changes (Figs. 9.16a and 9.17b). CT may reveal the roughening, thinning, or denudation of cartilage (Fig. 9.16b) and cystic change (Fig. 9.18a) in the subchondral bone. Concomitant degenerative change may occur, although this is not essential.

Scintigraphy reveals abnormal tracer uptake in 54% of patients with patellar pain (Dye and Boll 1986). Pinhole scintigraphy can reveal a specific sign (Bahk et al. 1994). This consists of small "hot" spotty uptake localized to the central retropatellar facet, denoting cartilage aberration and cystic change (Figs. 9.16c and 9.18b). Less intense reactive uptake may be present in the remaining patella. In the classic cases, no associated lesions are present in other parts of the affected knee. The chondromalacia patellae associated with osteoarthritis can be readily recognized as such by pinhole scanning because, in addition to the characteristic retropatellar uptake, accompanying changes appear in the other articular compartments of the knee (Fig. 9.17a). Occasionally, the lesion may be doubled (Fig. 9.18). For differential diagnosis it is to be pointed out that osteoarthritis of the patella characteristically involves the lower or upper edge of the retropatellar facet with small osteophytosis (Figs. 9.14 and 9.15).

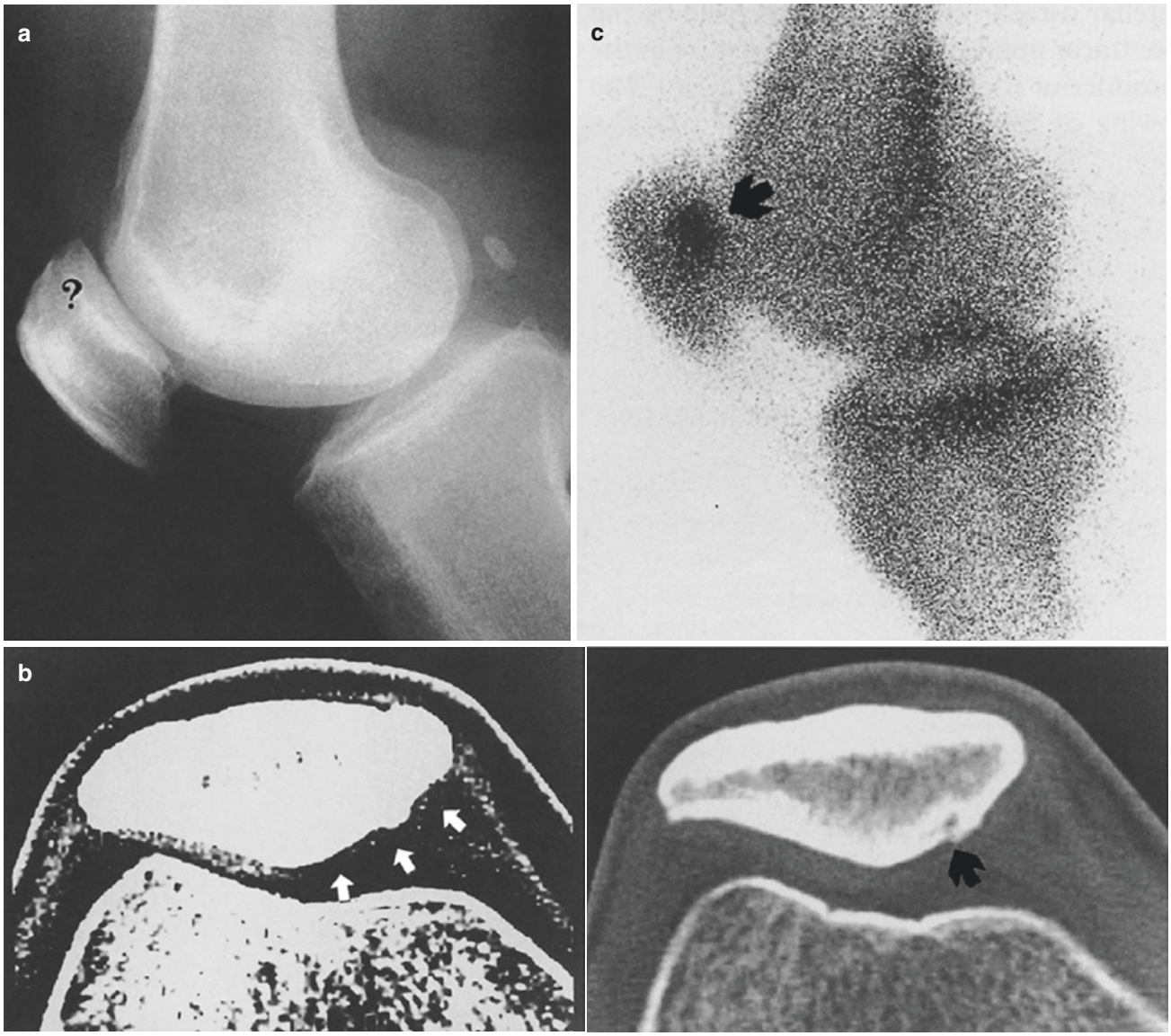

Fig. 9.16 Scintigraphic manifestation of chondromalacia patellae. (**a**) Mediolateral radiograph of the right knee in a 61-year-old man with painful chondromalacia patellae reveals suspicious pointing of the upper patellar pole (*?*). (**b**) (*Upper panel*) axial measure-set CT section through the upper patella reveals the denudation of the cartilaginous layer with subchondral bone elevation in the lateral facet (*arrows*). (*Lower panel*) with a different CT window setting, a small cystic change is apparent just beneath the elevated bone (*arrows*). (**c**) Medial pinhole scan shows spotty intense tracer uptake that is characteristically localized in the central zone of the retropatellar facet (*arrow*). The other articular compartments are normal

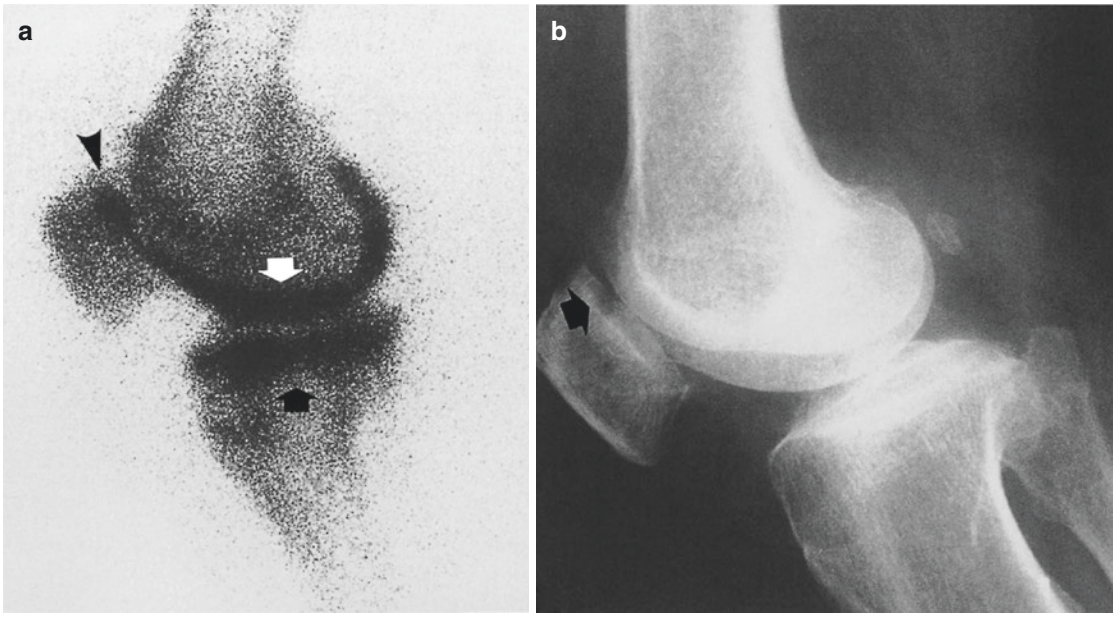

Fig. 9.17 Chondromalacia patellae associated with osteoarthritis. (**a**) Medial pinhole scan of the right knee in a 70-year-old woman shows spotty intense tracer uptake typically localized in the upper posterior aspect of the patella surrounded by less intense uptake (*arrowhead*). The patellofemoral and lateral femorotibial compartments accumulate tracer diffusely, designating associated osteoarthritis (*arrows*). (**b**) Mediolateral radiograph shows a small cystic change in the upper posterior aspect of the patella (*arrow*) and diffuse periarticular sclerosis in the patellofemoral and femorotibial compartments. CT scan confirmed roughened cartilage with subchondral cysts (not shown here)

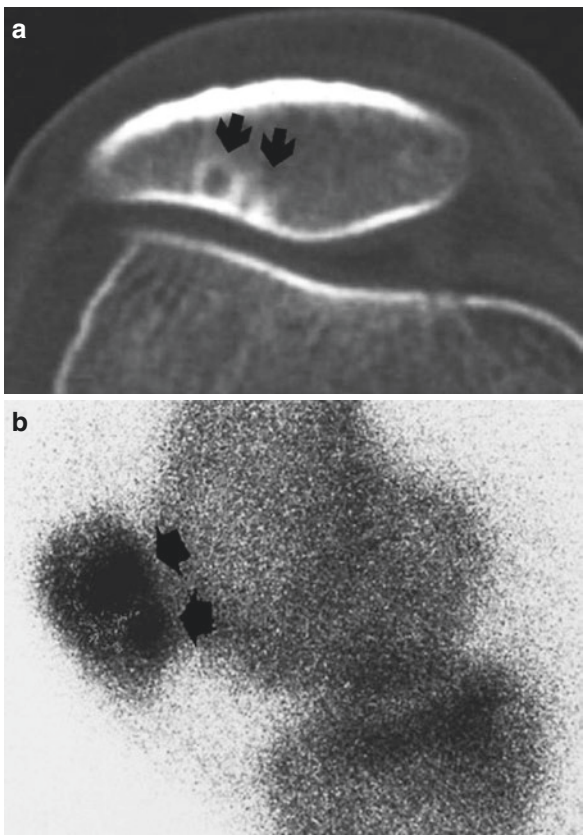

Fig. 9.18 Bone scintigraphic sign of chondromalacia patellae. (**a**) CT of the left patella in a 63-year-old male shows a small sharply defined subchondral cyst with sclerosis in the medial retropatellar facet (*arrow*). (**b**) Lateral pinhole scan reveals two spotty "hot" areas (*arrows*)

9.9 Ankle and Tarsal Joints

The ankle (talocrural joint) is uniaxial articulation between the lower tibial end together with the medial and lateral malleoli and the trochlear surface of the talus. Beneath the talus are the anterior, middle, and posterior subtalar joints and the talonavicular joint in front. The ankle is not a common site of osteoarthritis, and when involved it is usually the consequence of a significant trauma or the cumulative effects of repeated minor physical insults. In most cases, the talocrural joint and the subtalar and talonavicular joints are involved.

Radiographic manifestations of osteoarthritis of the ankle are inconspicuous in the early stage, as in any joint. However, established osteoarthritis manifests as articular narrowing, subchondral sclerosis, and osteophytosis. Our limited observation has indicated that the change starts in the anterior subtalar joint followed by involvement of the talocrural joint, the middle and posterior subtalar joints, and the talonavicular joint seemingly in sequence.

The earliest change of talar osteoarthritis appears to start from the anterior subtalar joint of a painful ankle as a focal, spotty "hot" area (Fig. 9.19). Not infrequently, such a "hot" area is seen in the absence of radiographic change. As the disease progresses, the talocrural joint becomes involved (Fig. 9.20) and then the subtalar and talonavicular joints (Fig. 9.21). The initial involvement of the anterior subtalar and talocrural joints is presumably related to the fact that these joints are constantly subjected to great stress and strain.

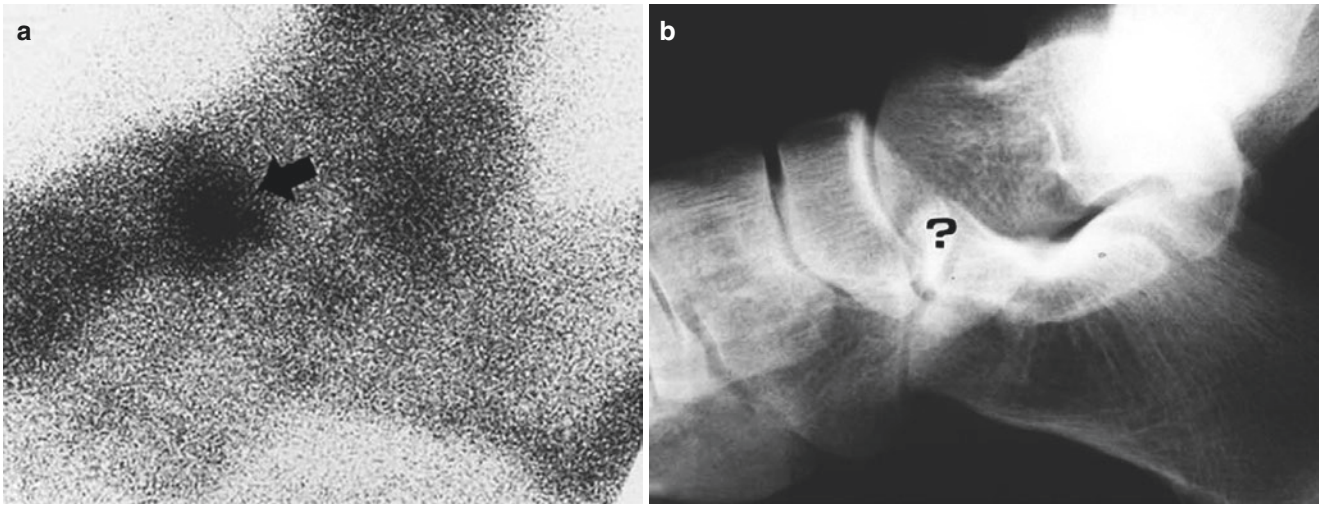

Fig. 9.19 Preradiographic manifestation of talar osteoarthritis. (**a**) Lateral pinhole scan of painful right ankle in a 31-year-old female shows spotty uptake in the anterior subtalar joint (*arrow*). (**b**) Lateral radiograph shows no abnormality (*?*)

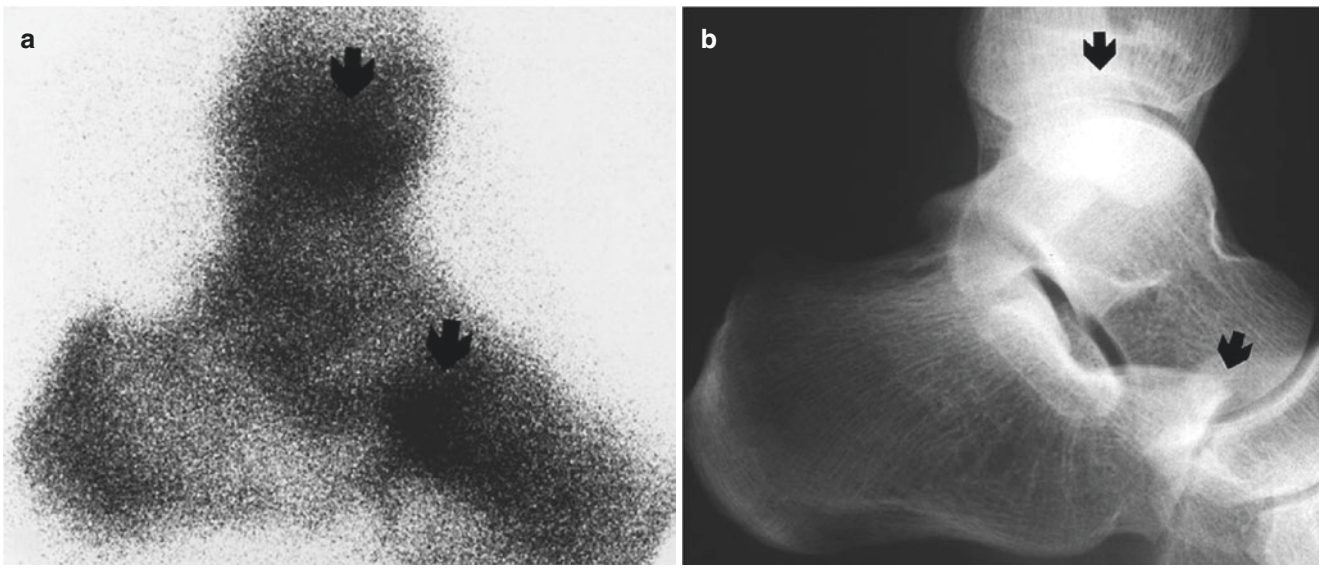

Fig. 9.20 Talocrural joint involvement in slightly advanced talar osteoarthritis. (**a**) Lateral pinhole scan of the left ankle in a 21-year-old male shows patchy areas of increased uptake in the anterior subtalar joint (*lower arrow*) and the talocrural joint (*upper arrow*). (**b**) Lateral radiograph demonstrates sclerosis in the anterior articular surface of the calcaneus (*lower arrow*) and talocrural articular narrowing and sclerosis (*upper arrow*)

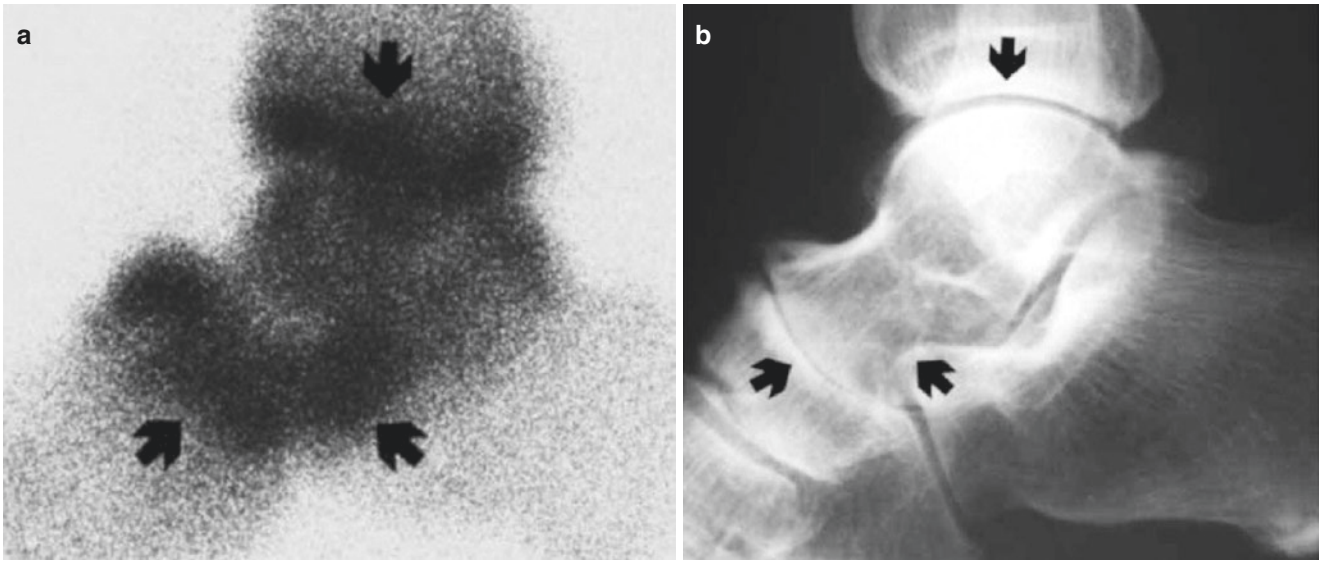

Fig. 9.21 Advanced talar osteoarthritis. (**a**) Lateral pinhole scan of the right ankle in a 36-year-old female shows diffuse tracer uptake in the subtalar and talonavicular joints (*lower arrows*) as well as the talocrural joint (*upper arrow*). (**b**) Lateral radiograph demonstrates sclerosis with marked articular narrowing (*arrows*)

9.10 Shoulder

The shoulder has two articulations: the acromioclavicular joint and the glenohumeral joint. The former is a synovial joint formed between the medial acromial margin and the lateral clavicular end that are covered with fibrocartilage. It is completely surrounded by the fibrous capsule and provided with an articular disk in the upper part or rarely in the entire joint (de Palma 1957). The latter is a multiaxial joint formed between the roughly hemispherical humeral head and the shallow glenoid fossa of the scapula, possessing motion freedom but an insecure structure. The joint is deepened with the fibrocartilaginous rim, the glenoid labrum.

9.10.1 Acromioclavicular Joint

Degenerative change of this joint is primarily related to aging. The disease may start as early as the second decade of life, becoming severe by the fifth decade (de Palma 1957). The disease causes discomfort or pain that may be aggravated by motion, radiating to the upper arm.

Radiography in the early stage shows mild cortical thickening and subcortical osteopenia in the para-articular bones, giving rise to a pencil-line appearance and apparent articular widening (Fig. 9.22a). With the progress of pathological change, the articulation becomes narrowed with prominent osteopenia (Fig. 9.23a). The articular change appears to be more prominent in the clavicular side than in the acromial side, and it is indeed peculiar to note that the acromion remains insignificantly affected on radiographs although tracer uptake is intense.

The pinhole scintigraphic findings are the mirror image of the radiographic findings with additional information on altered bone metabolism, featuring varied para-articular uptake and articular obliteration. The extent and intensity of tracer uptake appear to vary according to the severity of degenerative change and arthritic activity. Uptake is mild to moderate and predominantly localized to the clavicular end in the early phase when the articular space is relatively preserved (Fig. 9.22b). However, in the active chronic phase with advanced articular narrowing uptake becomes markedly intensified and spreads to the acromion with articular obliteration (Fig. 9.23b). Thus, pinhole scintigraphic analysis shows that degenerative arthritis in the acromioclavicular joint characteristically starts from the clavicular end, at least as far as bone metabolic change is concerned. On occasion, osteophytes are shown by increased tracer uptake. Increased uptake in acromioclavicular osteoarthritis is usually unilateral, and the side involved is related to the side of the hand used most.

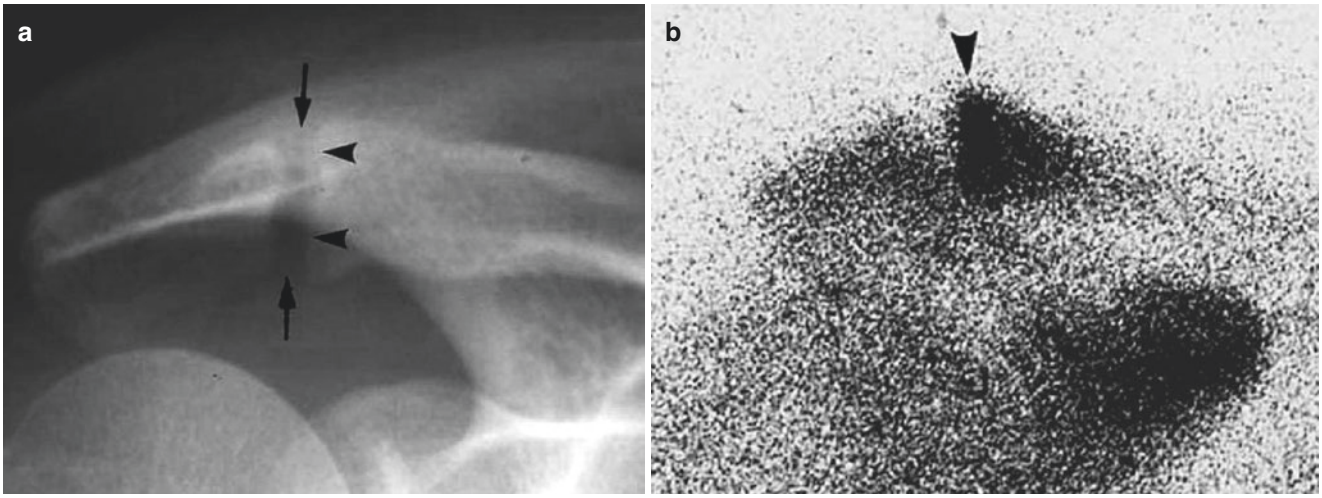

Fig. 9.22 Early acromioclavicular osteoarthritis. (**a**) Anteroposterior radiograph of a painful right shoulder in a 39-year-old female shows mild cortical thickening and osteopenia in the para-articular bones (*arrowheads*), producing the pencil-line sign with apparent articular widening (*arrows*). (**b**) Anterior pinhole scan reveals tracer to characteristically accumulate in the clavicular end (*arrowhead*) but not in the acromion

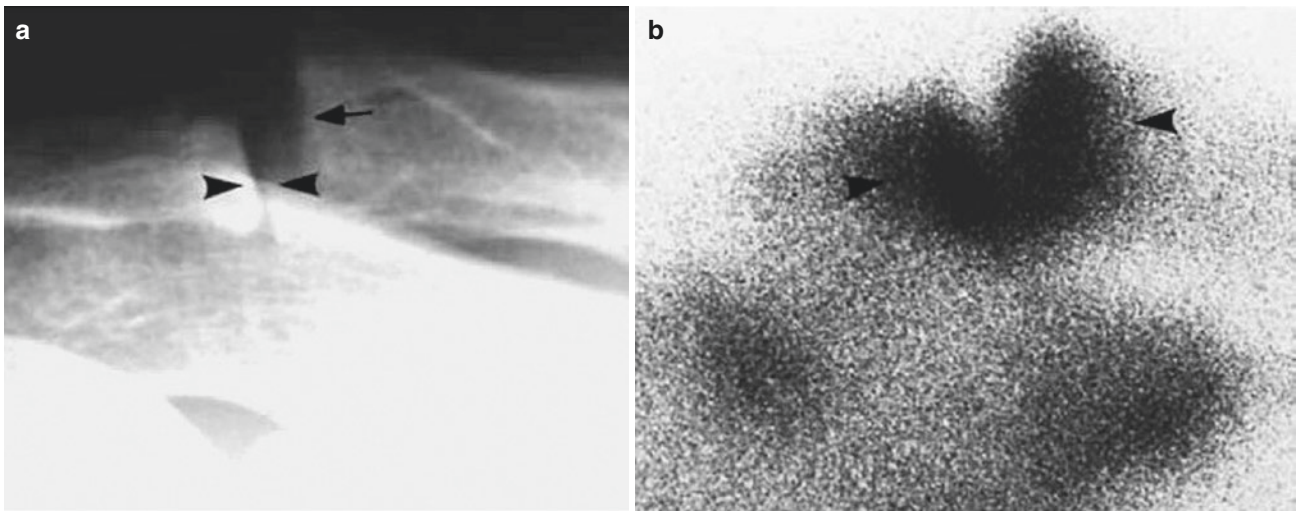

Fig. 9.23 Advanced acromioclavicular osteoarthritis. (**a**) Anteroposterior radiograph of a chronic painful right shoulder in a 22-year-old male shows marked narrowing of the lower articular space (*arrowheads*) with paradoxical widening of the upper compartment due to bony erosion (*arrow*). (**b**) Anterior pinhole scan reveals intense uptake now in both the clavicular end and the acromion (*arrowheads*)

9.10.2 Glenohumeral Joint

Osteoarthritis of the glenohumeral joint may be associated with aging, occupation, sports, or accidental trauma. Bone diseases such as epiphyseal dysplasia, crystal deposition, hemophilia, or alkaptonuria may also cause osteoarthritis in this joint. The usual pathological sequence is chondrolysis with articular narrowing, hypertrophy with eburnation and osteophytosis, and cystic formation.

Radiography shows eburnation, marginal sclerosis, and cystic change with articular narrowing most typically in the anterior and inferior aspects of the joint. The inferomedial aspect of the humeral head and apposing rim of the glenoid fossa are also involved (Fig. 9.24). Glenohumeral osteoarthritis is often associated with the shoulder impingement syndrome (Fig. 9.25) and rarely complicated with subluxation (Fig. 9.26). When osteoarthritis is associated with impingement, cystic change may occur in the greater tuberosity at the site of the supraspinatus tendon attachment along with subacromial spur (Fig. 9.25). Our observation has indicated that the radiographic change in the humeral head is often less impressive than

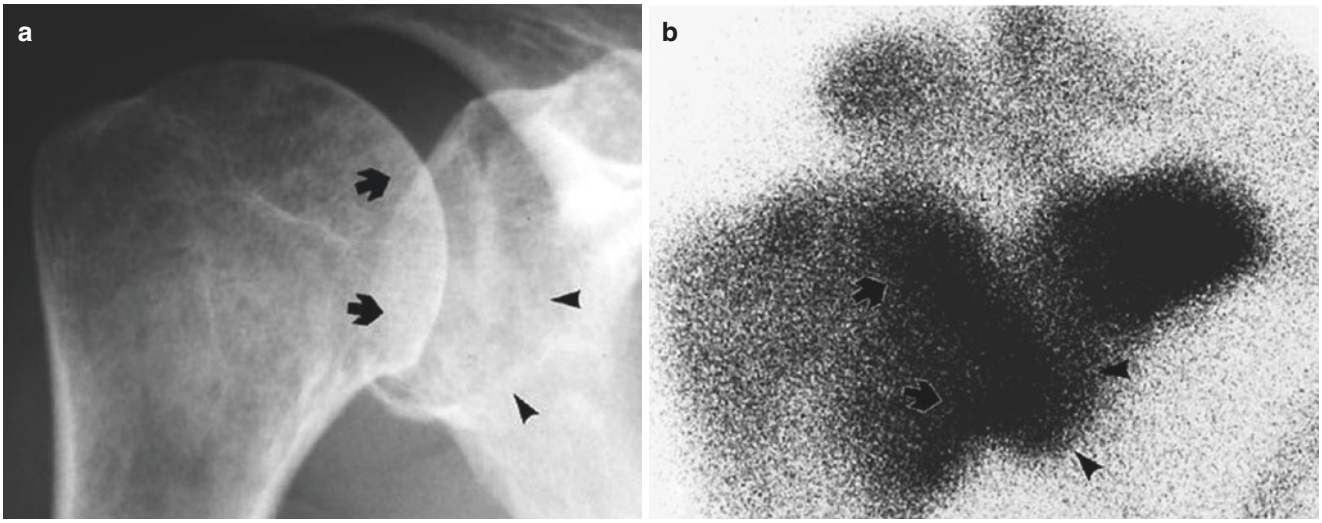

Fig. 9.24 Chronic osteoarthritis in the glenohumeral joint. (**a**) Anteroposterior radiograph of a painful right shoulder of several years duration in a 48-year-old female shows osteopenia and pencil-line cortex (*arrows*) in the humeral head and irregular erosion in the glenoid (*arrowheads*). (**b**) Anterior pinhole scan reveals intense uptake in the inferomedial aspect of the humeral head (*arrows*) and the apposing glenoid (*arrowheads*)

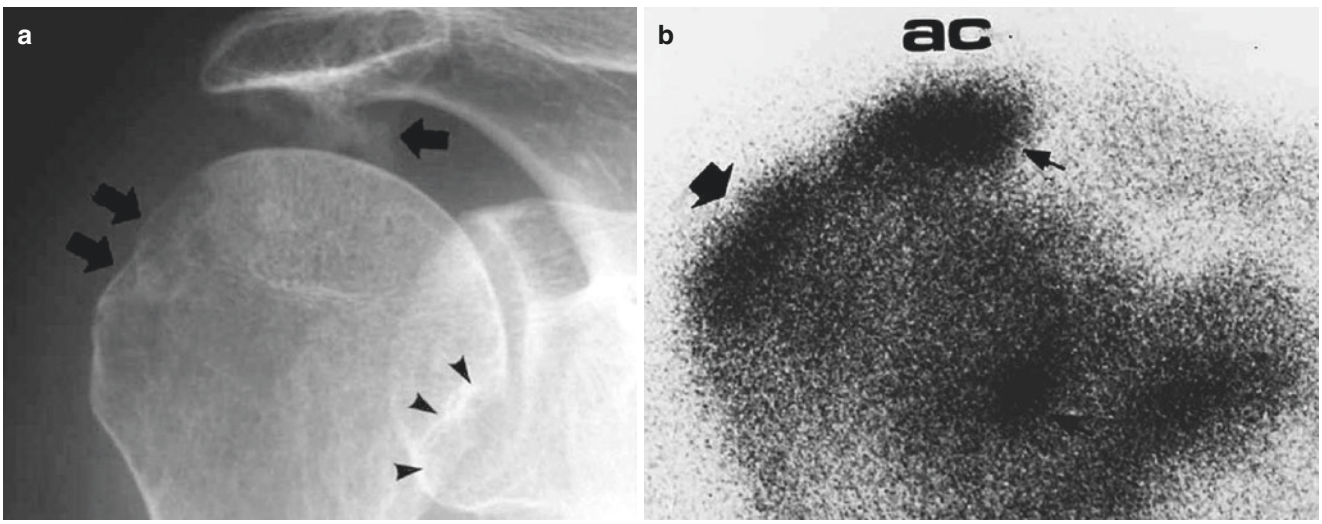

Fig. 9.25 Glenohumeral osteoarthritis associated with shoulder impingement syndrome. (**a**) Anteroposterior radiograph of a chronic painful right shoulder in an 82-year-old male shows marked narrowing of the lower glenohumeral articular compartment (*arrowheads*) and also osteopenia and cystic changes in the greater tuberosity (*pair of arrows*) and subacromial spur (*single arrow*). (**b**) Anterior pinhole scan reveals intense tracer uptake in the respective lesions including the greater tuberosity (*large arrow*) and the acromion (*ac*) where the supraspinatus tendon attaches (*small arrow*)

the scintigraphic change in the relatively early or active chronic stage of the disease when the metabolic activity is at its height (Fig. 9.27). Such a mismatch can be explained at least in part by disuse that can be diagnosed by osteopenia.

Pinhole scintigraphy shows increased tracer uptake in the articular surface of the glenoid fossa and humeral head (Fig. 9.24b). As mentioned above, the scintigraphic features often precede the radiographic change (Fig. 9.27). In moderately advanced cases, the joint becomes diffusely obliterated and subcortical cyst, if formed, is indicated by "hotter area within hot area" (Fig. 9.25b). Subluxation is represented by the displacement of the humeral head and widened joint space (Fig. 9.26b).

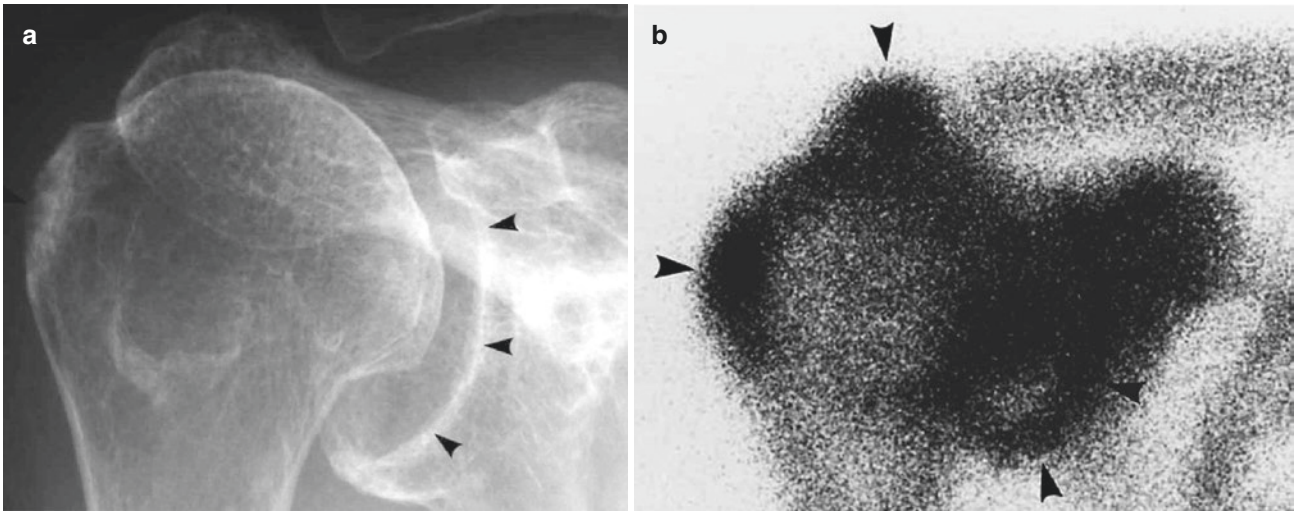

Fig. 9.26 Glenohumeral osteoarthritis complicated with subluxation. (**a**) Anteroposterior radiograph of the right shoulder in a 64-year-old female shows craniolateral displacement of the humeral head with widened articular space (*arrowheads*). Bones are markedly porotic with accentuated cortices. (**b**) Anterior pinhole scan reveals prominent tracer uptake in the widened glenohumeral joint (*lower arrowheads*). Note increased tracer uptake in the acromion (*top arrowhead*) and greater tuberosity (*left arrowhead*) suggesting impingement or rotator cuff syndrome

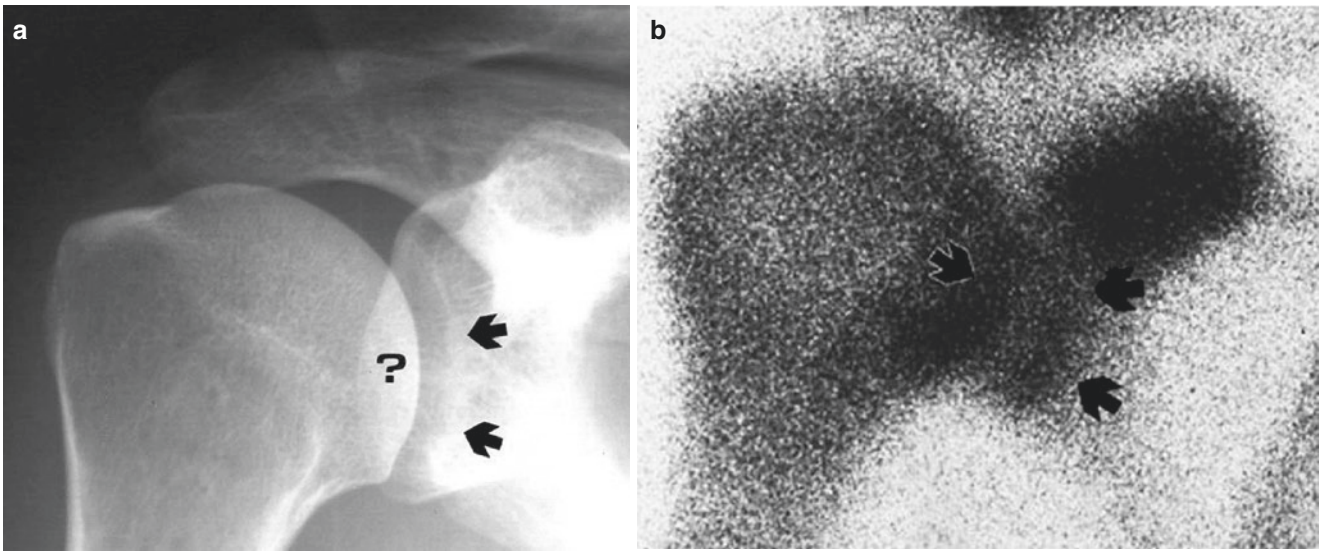

Fig. 9.27 Disparity between scintigraphic and radiographic osteoarthritic change in the early stage. (**a**) Anteroposterior radiograph of a painful right shoulder in a 56-year-old male shows no abnormality on the humeral side (*?*) and mild sclerosis in the lower glenoid (*arrows*). (**b**) In contrast, the anterior pinhole scan reveals prominent tracer uptake in both the humerus and the glenoid (*arrows*)

9.11 Sternum

The sternum has two joints: the sternoclavicular joint and the manubriosternal joint. The former is the synovial joint and the latter is a symphysis.

9.11.1 Sternoclavicular Joint

The sternoclavicular joint is the synovial articulation between the medial end of the clavicle and the sternal clavicular notch, together with the upper part of the subjacent first

costal cartilage. The movements and structures including the articular disk are much like those of the acromioclavicular joint. The fibrocartilaginous layer is much thicker on the clavicular surface than the sternal notch. This joint is also a common seat of osteoarthritis. Men are more frequently affected than women. Motion pain, local tenderness, and enlargement of the joint are the main presenting symptoms. The involvement is usually unilateral, but the bilateral type is not rare.

Radiographic manifestations include periarticular bone erosions, joint space narrowing, eburnation, and osteophytosis. Understandably, these changes are mild or even dubious in the early stage (Fig. 9.28a). In general, the sternal facet is affected more prominently than the clavicular facet whose fibrocartilaginous layer is thicker. More often than not, chondrolysis and bone erosion may be disguised as joint space widening (Fig. 9.28a). Conventional tomography or CT is useful for the delineation of the true state of affairs (Fig. 9.29a).

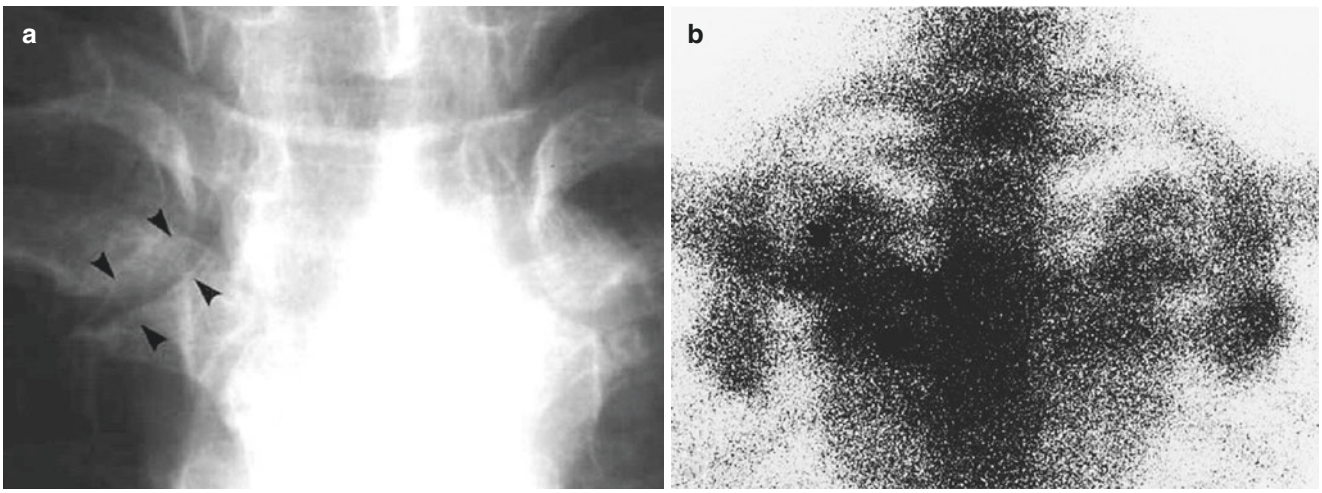

Fig. 9.28 Relatively early osteoarthritis in the sternoclavicular joint. (**a**) Plain anteroposterior radiograph of a painful right sternoclavicular joint in a 50-year-old female shows periarticular bone erosion, osteopenia, and eburnation (*arrowheads*). Note false articular widening due to chondrolysis and osteopenia. (**b**) Anterior pinhole scan reveals slightly increased uptake in periarticular bones (*arrows*). The uptake is not impressive

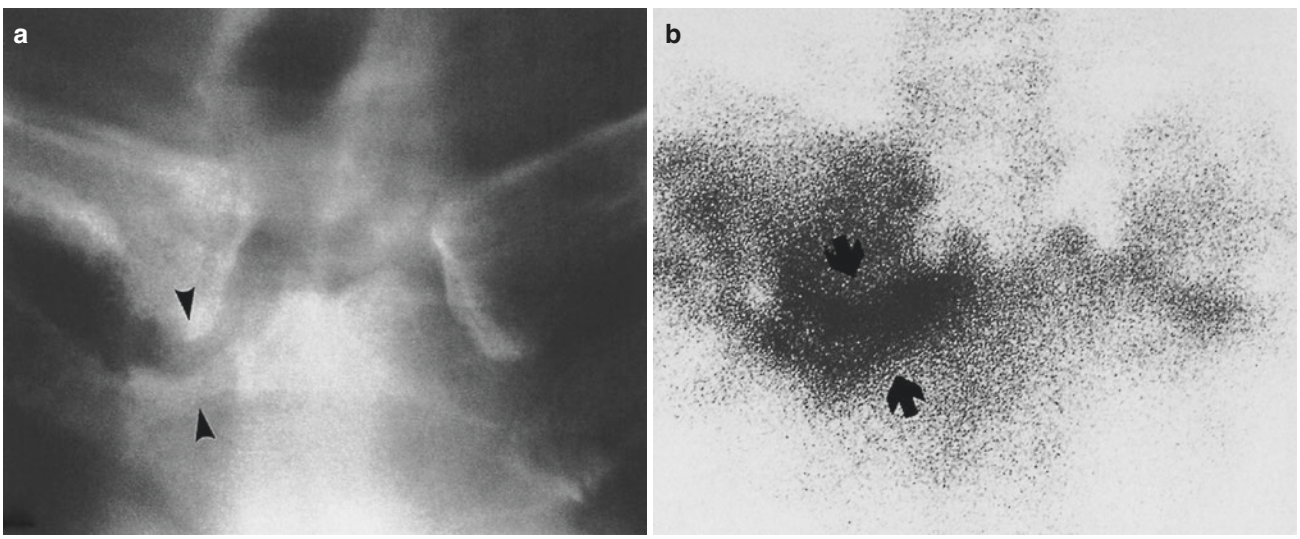

Fig. 9.29 Well-established osteoarthritis in the sternoclavicular joint. (**a**) Anteroposterior conventional X-ray tomogram of the sternum with a painful right sternoclavicular joint in a 49-year-old man reveals irregular subchondral erosions and sclerosis with small osteophytes in the bones about the joint (*arrowheads*). The joint is irregularly and eccentrically narrowed. (**b**) Anterior pinhole scan shows intense tracer uptake in the sternal margin (*lower arrow*) and the medial clavicular end (*upper arrow*) with eccentric articular narrowing. Note that the most intense tracer uptake is localized in the joint, the characteristic feature of osteoarthritis

Pinhole scintigraphy in the early stage shows an ill-defined area of minimally increased tracer uptake in the affected joint, vaguely denoting mild eburnation in the clavicular and sternal facets (Fig. 9.28b). With the progression of osteoarthritis, the articular space becomes obliterated and tracer uptake intensified. The uptake is typically more prominent at the sternal facet (Fig. 9.29b). Generally, the joint space is indiscernible even in the early stage and on a magnified scan, obviously due to the smallness of the joint and the ball-and-socket type of articular structure.

9.11.2 Manubriosternal Joint

Osteoarthritis also affects the manubriosternal joint, which is one of the largest fibrocartilaginous articulations. Degenerative arthritis mainly involves the central portion of the articular fibrocartilage with resultant articular narrowing and periarticular eburnation.

Radiographically, the manubriosternal joint shows diffuse or partial narrowing with irregular sclerosis of the subchondral bones. Occasionally, the joint may be totally closed (Fig. 9.30a). Conventional or computed tomography is extremely useful for a definitive demonstration of the joint. Pinhole scintigraphy shows intense tracer uptake that fills up the joint, spreading to the lower manubrium and upper gladiolus (Fig. 9.31). It is to be mentioned that the tracer uptake in manubriosternal osteoarthritis is maximal in the central portion of the joint (Figs. 9.30b and 9.31).

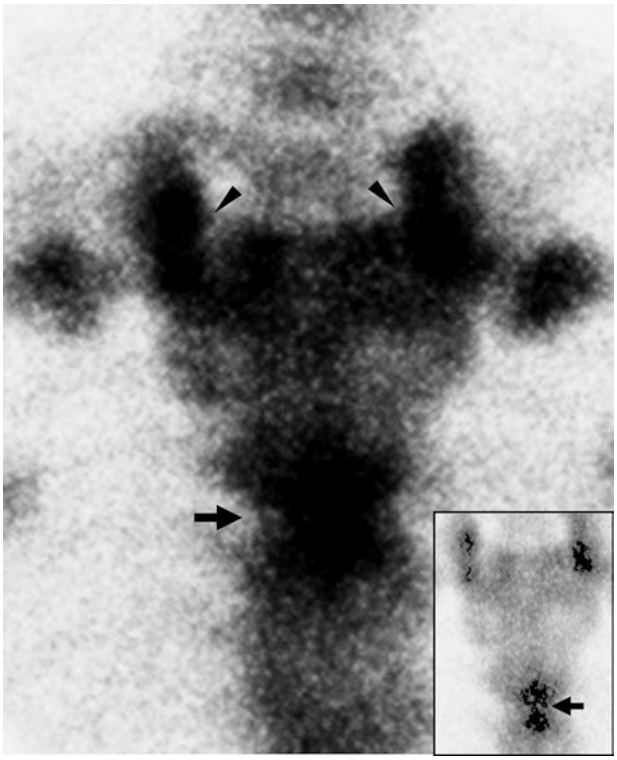

Fig. 9.31 Osteoarthritis of the manubriosternal joint. Anterior pinhole scan of the sternum in a 32-year-old woman with local pain shows hot uptake in the manubriosternal joint (*arrow*) and sternoclavicular joints (*arrowheads*). The pathological uptake is characteristically in the central region of joints. *Inset* is a gamma correction (gamma = 86) scan showing concentrated speckled hot uptake in the main degenerative bony change, including destruction and reactive bone formation (*arrow*)

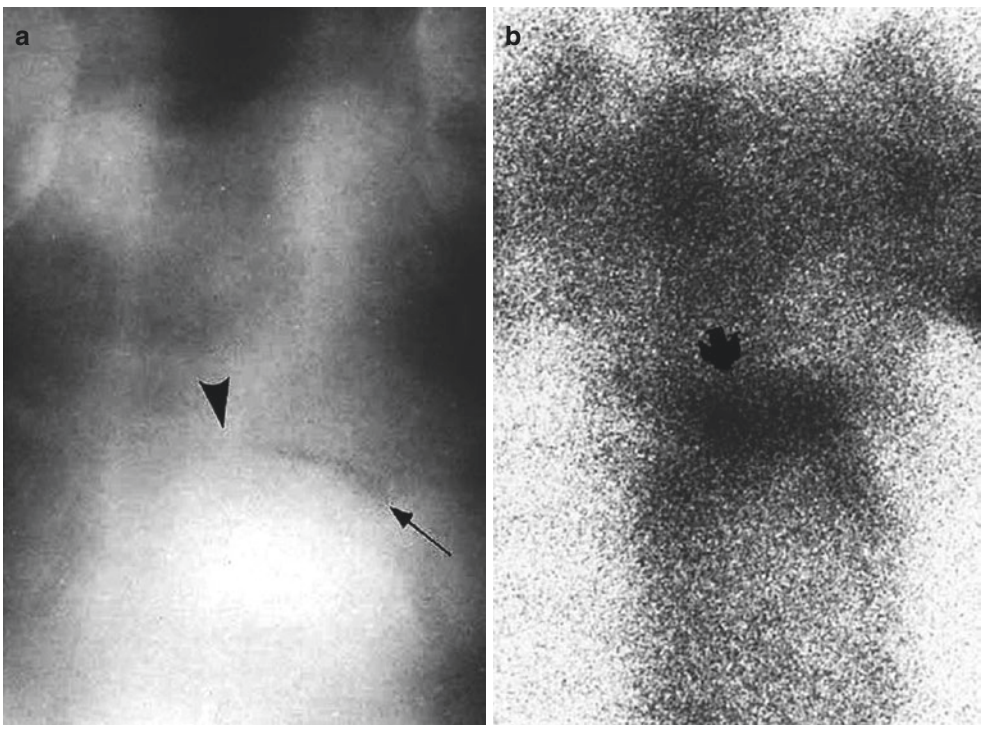

Fig. 9.30 Osteoarthritis in the manubriosternal joint. (**a**) Conventional X-ray tomography of the sternum in a 57-year-old male with chronic sternal pain shows curved linear lucency in the centro-left-lateral portion of the manubriosternal joint (*arrow*) with the obliteration of the right half (*arrowhead*). Plain radiography is not useful for the study of this thin and overshadowed joint. (**b**) Anterior pinhole scan shows a distinct band-like "hot" area in the centro-left-lateral portion of the joint denoting metabolically active arthritis (*arrow*). Planar bone scintigraphy cannot distinguish pathological uptake from physiological uptake in this joint

9.12 Elbow

The elbow joint is a compound synovial articulation that consists of two components: the humeroulnar joint and the humeroradial joint. The former is between the humeral trochlea and the ulnar trochlear notch and the latter between the humeral capitulum and the radial head. Osteoarthritis is relatively uncommon in the elbow, and it is generally secondary to trauma. The symptoms include limited motion, pain, and tender soft-tissue swelling.

Radiographic features include joint space narrowing and periarticular eburnation (Fig. 9.32a) and occasional enthesophytosis at the base of the olecranon. As elsewhere, on pinhole scintigraphy the alterations are characterized by the combination of extremely intense tracer uptake localized in the joint that is narrowed and moderately intense uptake in the surrounding periarticular bones. The trochlear notch is the site of involvement, producing the characteristic U-shaped uptake (Fig. 9.32b).

9.13 Wrist and Carpal Joints

The wrist (radiocarpal) joint is a biaxial and ellipsoid articulation formed between the distal end of the radius and the scaphoid, lunate, and triquetrum with triangular cartilage on the ulnar side. The joint is lined by synovium and surrounded by fibrous capsule and radiocarpal ligaments. In addition, there are complex intercarpal joints, interconnecting (a) the proximal carpal bones, (b) the distal carpal bones, and (c) the two carpal bone rows.

Osteoarthritis of the wrist predominantly affects the radial side with the most common sites being the trapeziometacarpal joint and the trapezioscaphoid joint (Fig. 9.33). The involvement of the radiocarpal joint, distal radioulnar joint, lunate-triquetral joint, and other intercarpal joints is not rare (Fig. 9.34). Causes are trauma in the majority of cases and calcium deposition disease in occasional cases. Symptoms include pain and tenderness, motion disturbance, and soft-tissue swelling. Osteoarthritis without an obvious or probable etiology is termed idiopathic, but its existence has been challenged.

Radiography is often not helpful in the early stage of the disease, but plays an important role in the intermediate and late stages. Radiographic changes include articular narrowing, sclerosis, osteophytosis, cystic change, bone collapse, and deformity. Characteristically, changes are limited to a single or few small joints of the wrist, and osteoporosis is not a significant feature (Fig. 9.33a). Typically, the osteoarthritis in the wrist occurs on the radial side (Fig. 9.33), but the posttraumatic type involves any joint (Fig. 9.34a). MRI and CT are extremely useful for the specific diagnosis of synovitis, cartilage destruction, and cystic change (Fig. 9.33b). Osteoarthritis of the hands in typists affects the trapeziometatarsal and trapezioscaphoid joints, causing radial subluxation and bayonet deformity in the late stage (Fig. 9.35a). The osteoarthritis secondary to rheumatoid arthritis may show localized sclerosis within diffusely porotic carpal bones (Fig. 9.36a).

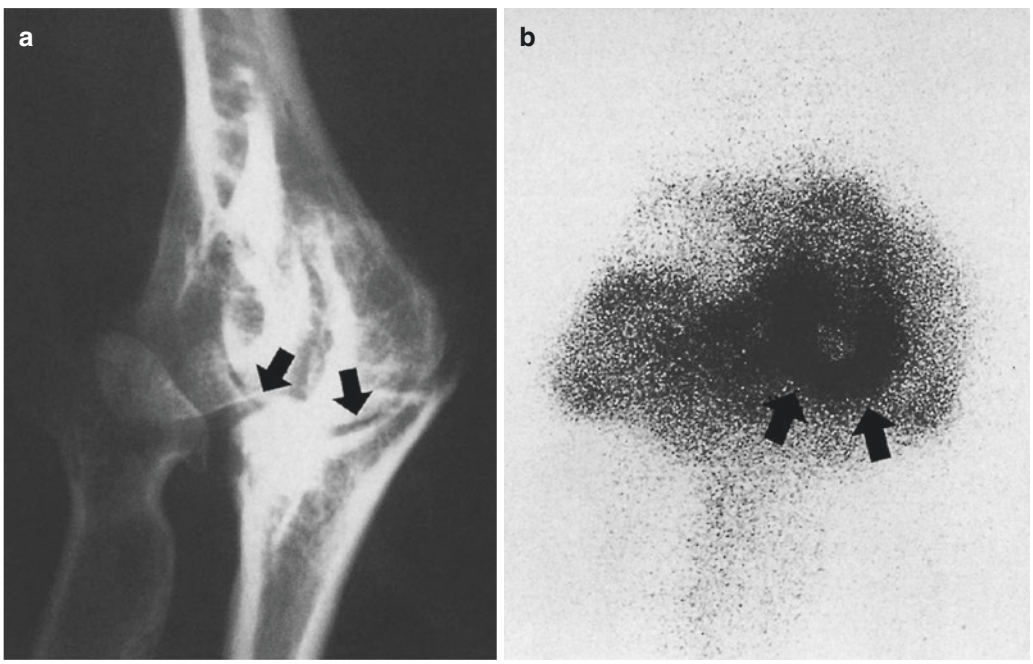

Fig. 9.32 Osteoarthritis in the elbow joint. (**a**) Oblique radiograph of the right elbow in a 47-year-old woman shows marked subarticular sclerosis with narrowing of the trochlear joint, producing a semilunar articular deformity (*arrows*). (**b**) Oblique pinhole scan reveals diffusely increased tracer uptake in the periarticular bones with the most intense uptake localized in the trochlear notch, creating the characteristic U-shaped appearance (*arrows*)

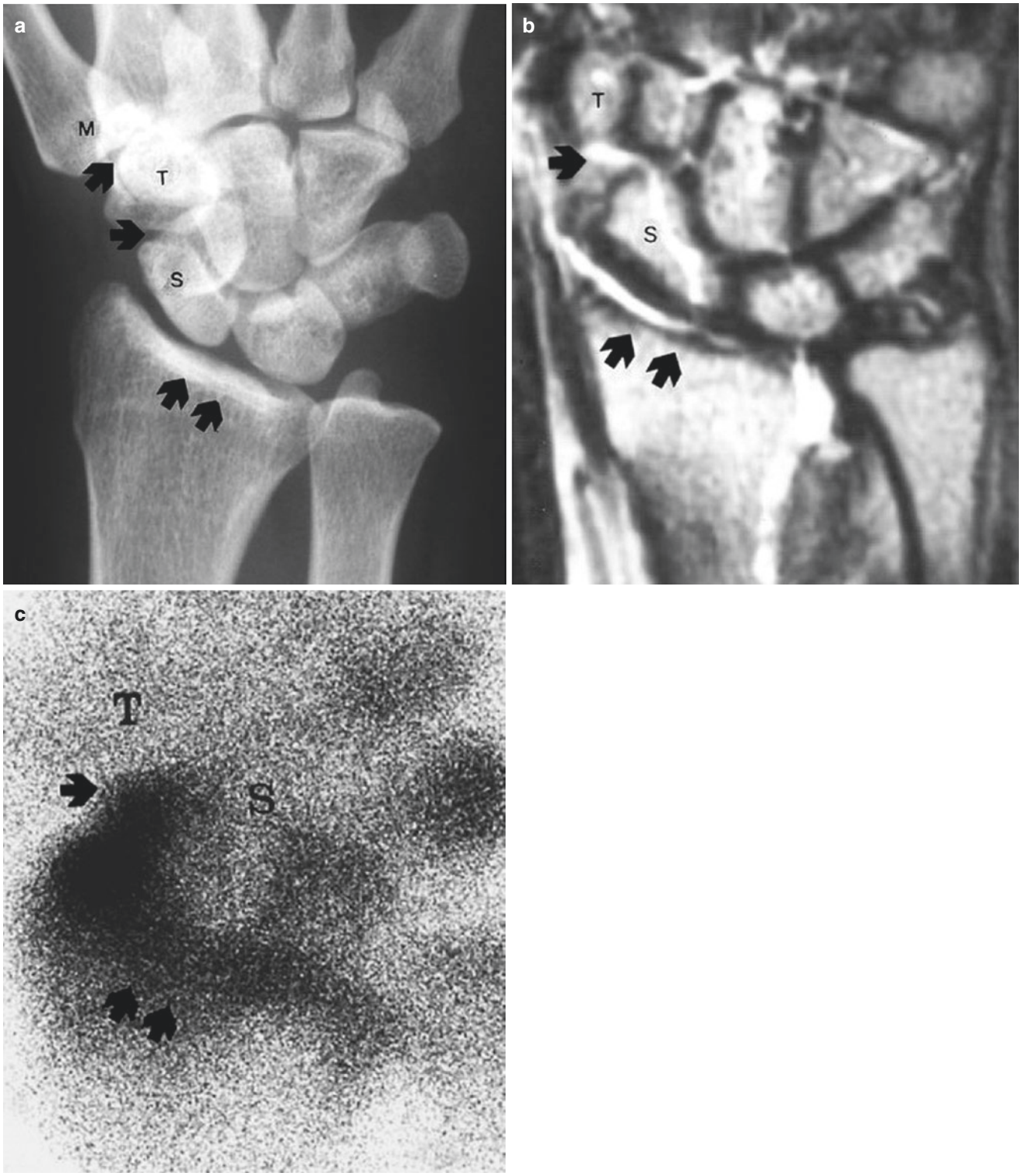

Fig. 9.33 Osteoarthritis in the radial side of the wrist. (**a**) Dorsopalmar radiograph of the right wrist in a 39-year-old female shows sclerosis in the distal radial epiphysis (*arrows*) with narrowing of the radiocarpal joint and the trapezioscaphoid and trapeziometacarpal joints (*T* triquetrum, *S* scaphoid, *M* metacarpal). (**b**) T2-weighted MRI reveals low signal in osteosclerosis (*arrows*) and bright signal of effusion in the radiocarpal and scaphotriquetral joints (*arrow* between *S* and *T*). (**c**) Dorsal pinhole scan shows intense tracer uptake in the radiocarpal joint (*twin arrows*) and the trapezioscaphoid and trapeziometacarpal joints (*single arrow*)

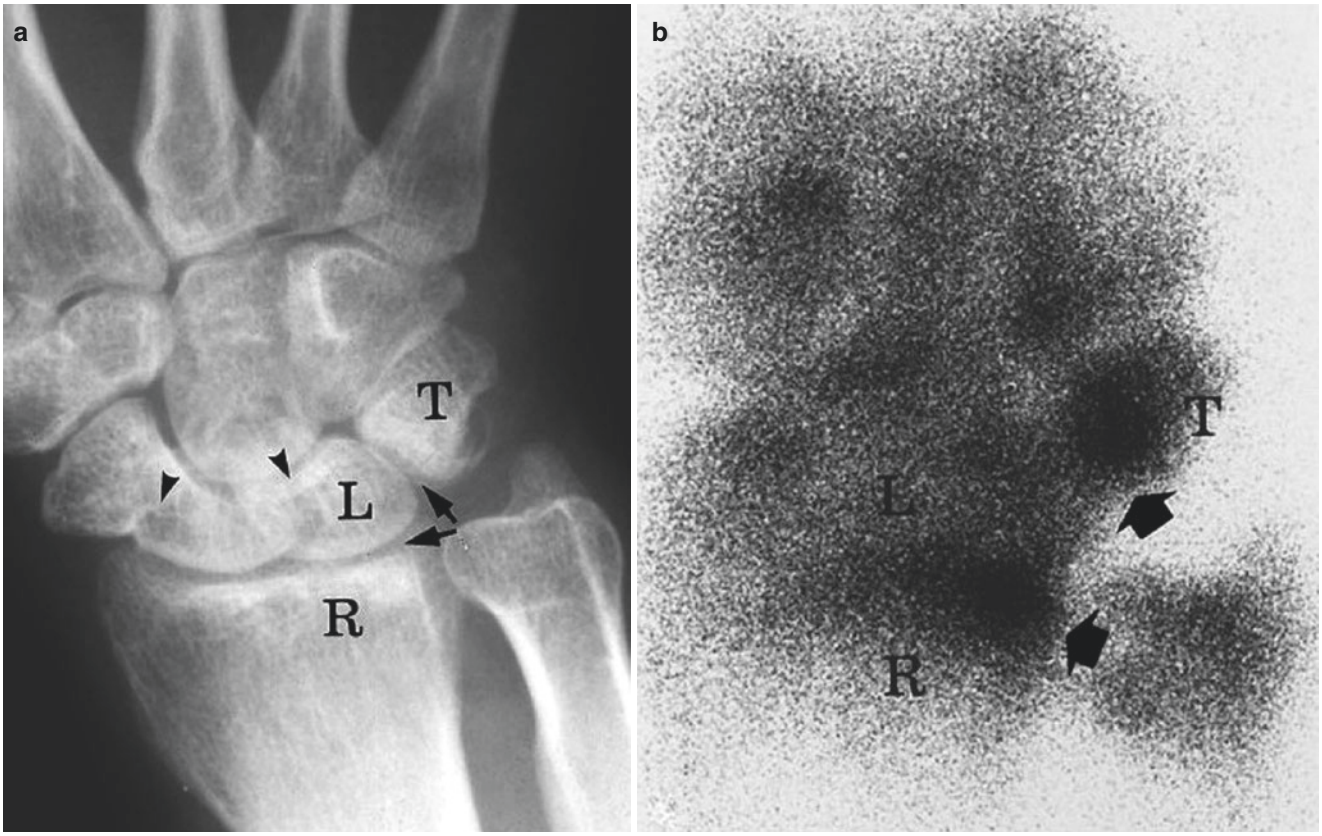

Fig. 9.34 Osteoarthritis in the ulnar side of the wrist. (**a**) Dorsopalmar radiograph of the right wrist in a 41-year-old female shows sclerosis in the distal radial epiphysis with narrowing of the radiocarpal joint and the lunate-triquetral joint (*R* radius, *L* lunate, *T* triquetrum). (**b**) Dorsal pinhole scan reveals intense tracer uptake in the radiocarpal joint (*lower arrow*) and the lunate-triquetral joint (*upper arrow*)

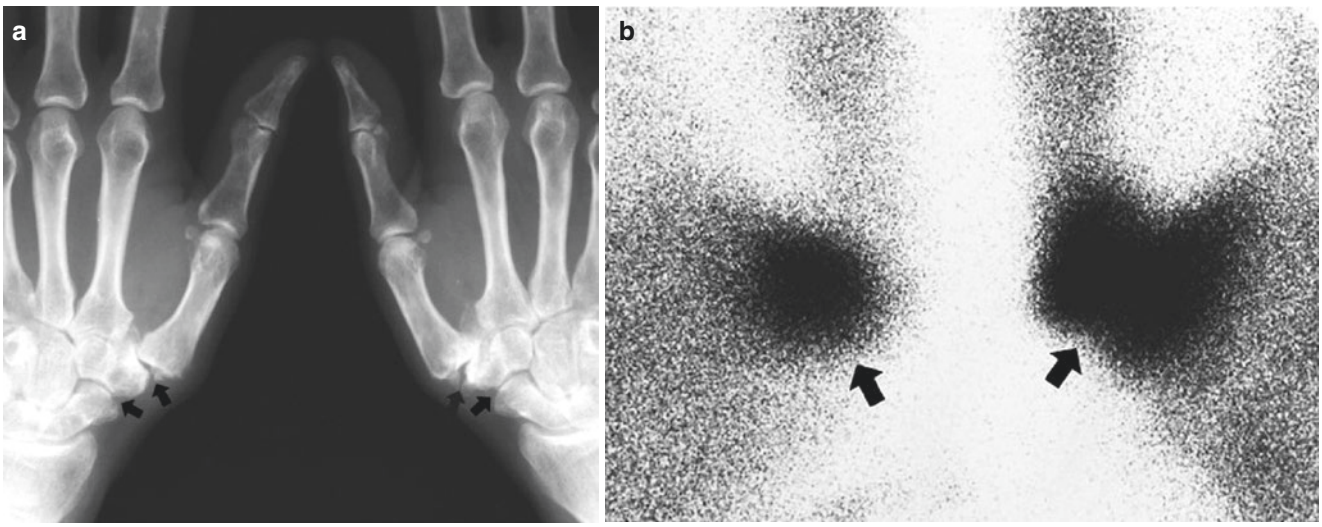

Fig. 9.35 Osteoarthritis of the hands in typists. (**a**) Dorsopalmar radiograph of both hands in a professional female typist shows osteoarthritis in the trapeziometatarsal and trapezioscaphoid joints of both hands with radial subluxation and bayonet deformity (*arrows*). (**b**) Dorsal pinhole scan reveals intense tracer uptake in classic bayonet deformity with squaring (*arrows*)

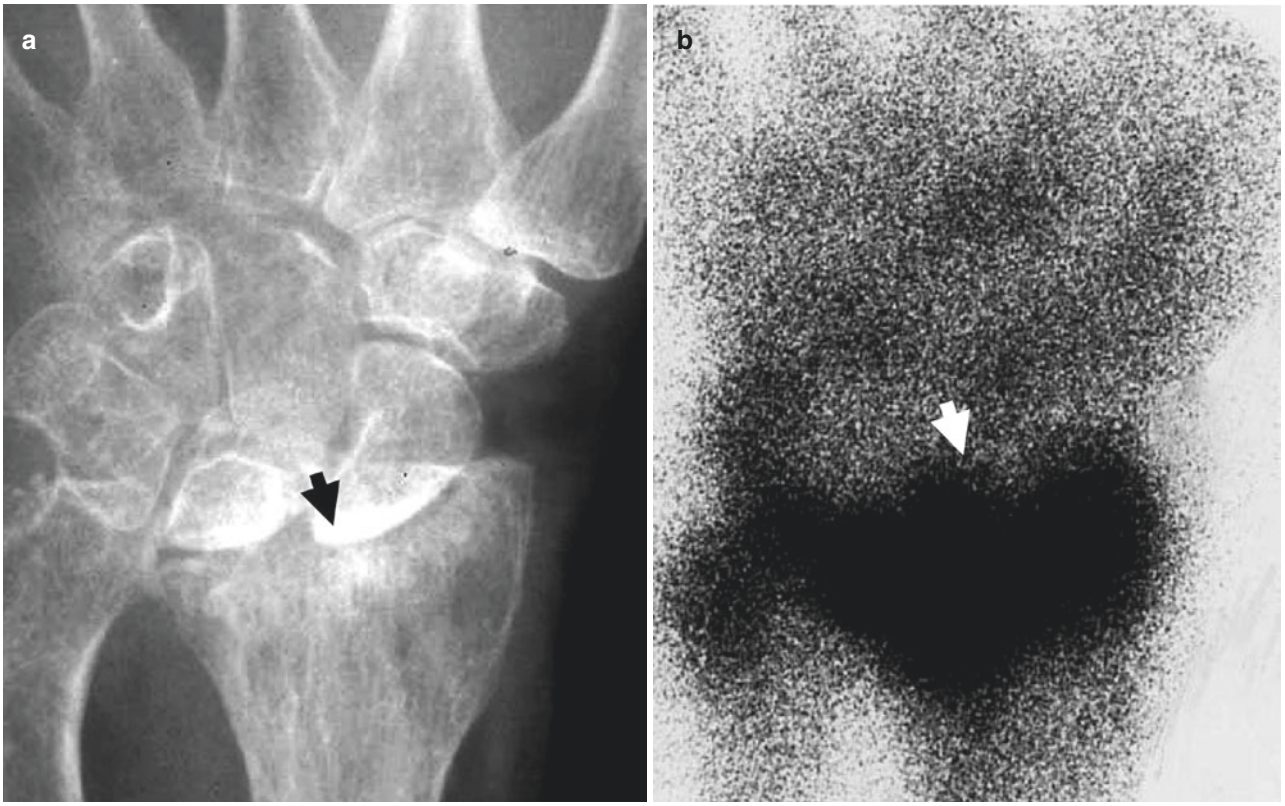

Fig. 9.36 Osteoarthritis secondary to rheumatoid arthritis. (**a**) Dorsopalmar radiograph of the left wrist in a 78-year-old female shows narrowing and obliteration of the entire carpal joints and osteoporosis, with the most prominent change occurring in the radiocarpal joint (*arrow*). (**b**) Dorsal pinhole scan reveals intense tracer uptake in the radiocarpal joint with the remaining carpal joints not accumulating tracer (*arrow*)

Pinhole scintigraphy plays an important role in the diagnosis of the early osteoarthritis with synovitis of the radiocarpal and trapeziometatarsal joints by showing tracer accumulated in the synovium and subchondral bones (Fig. 9.33c). Very subtle pathological changes localized to the proximal carpal bone can often be indicated by obvious uptake (Fig. 9.34b). Scintigraphy can also show the characteristic bayonet deformity produced by the radial subluxation of the trapeziometacarpal joint in the late stage (Fig. 9.35b). It is indeed interesting to note that the degree of tracer uptake parallels the degree of arthritic change: more intense uptake in the joints with severer pathological change and vice versa (Fig. 9.35b). The osteoarthritis secondary to long-standing rheumatoid arthritis in the wrist radiographically indicated by osteosclerosis can easily be identified and diagnosed as such by prominent tracer uptake (Fig. 9.36b).

9.14 Spine

The spine has five different articulations: the diskovertebral and apophyseal joints in throughout the spine, the costotransverse and costocorporeal joints in the thoracic spine, and the uncovertebral joints in the cervical spine. Of these, the diskovertebral joint is fibrocartilaginous in type and others are synovial except for the uncovertebral joint that is mixed in type. Based on the principal site of involvement, diskovertebral degeneration can be divided into diskovertebral osteoarthritis and spondylosis deformans. The former osteoarthritis affects the nucleus pulposus with diffuse condensation of peridiskal bones (endplate-based sclerosis) of the lower lumbar and lumbosacral vertebrae and the latter the outer or Sharpey's fibers of the annulus fibrosus with osteophytosis. On the other hand, the degenerative change of the apophyseal and costovertebral joints is considered to be a classical osteoarthritis since these joints are synovial.

Radiographically, diskovertebral osteoarthritis manifests the narrowing of the intervertebral space, endplate sclerosis, and focal osteophytes, most typically in the L4, L5, and S1 vertebrae (Fig. 9.37a). Occasionally, compression fracture may be superimposed on an endplate that is already deformed by osteoarthritis, making the diagnosis extremely difficult (Fig. 9.38b). In contrast, spondylosis deformans is characterized by multiple osteophytes, often prominent, formed in the lateral and anterior edges of the endplates (Fig. 9.39a). The diskovertebral changes such as narrowing of the intervertebral spaces and endplate scleroses are usually inconspicuous.

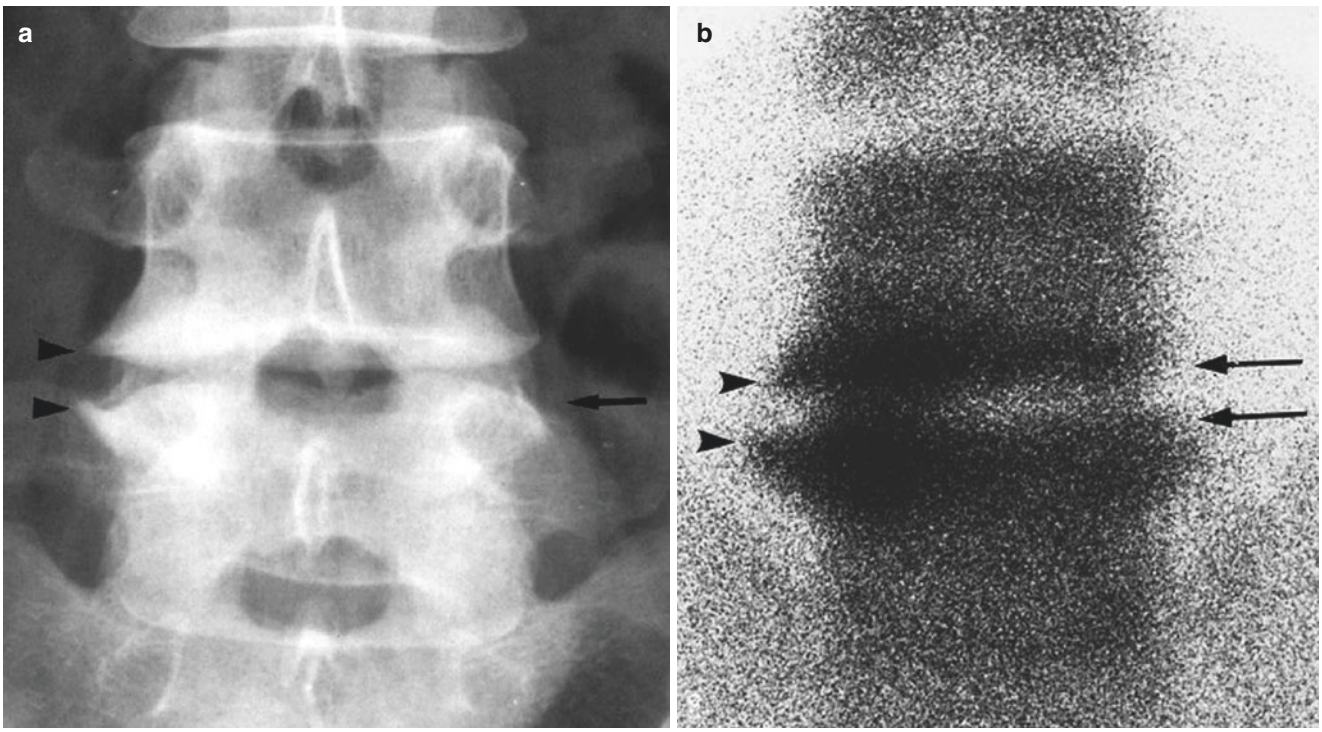

Fig. 9.37 Straightness of endplate sclerosis in intervertebral osteochondrosis in the lower lumbar spine. (**a**) Anteroposterior radiograph of the lower lumbar spine in a 37-year-old female shows typical endplate-based sclerosis in the L4 lower and L5 upper endplates with narrowing of the disk space between (*arrow*). There are small clawlike spurs at the right lateral edges (*arrowheads*). (**b**) Anterior pinhole scan shows straight tracer uptake in the sclerosed endplates with disk space narrowing (*parallel arrows*) and spur uptake (*arrowheads*)

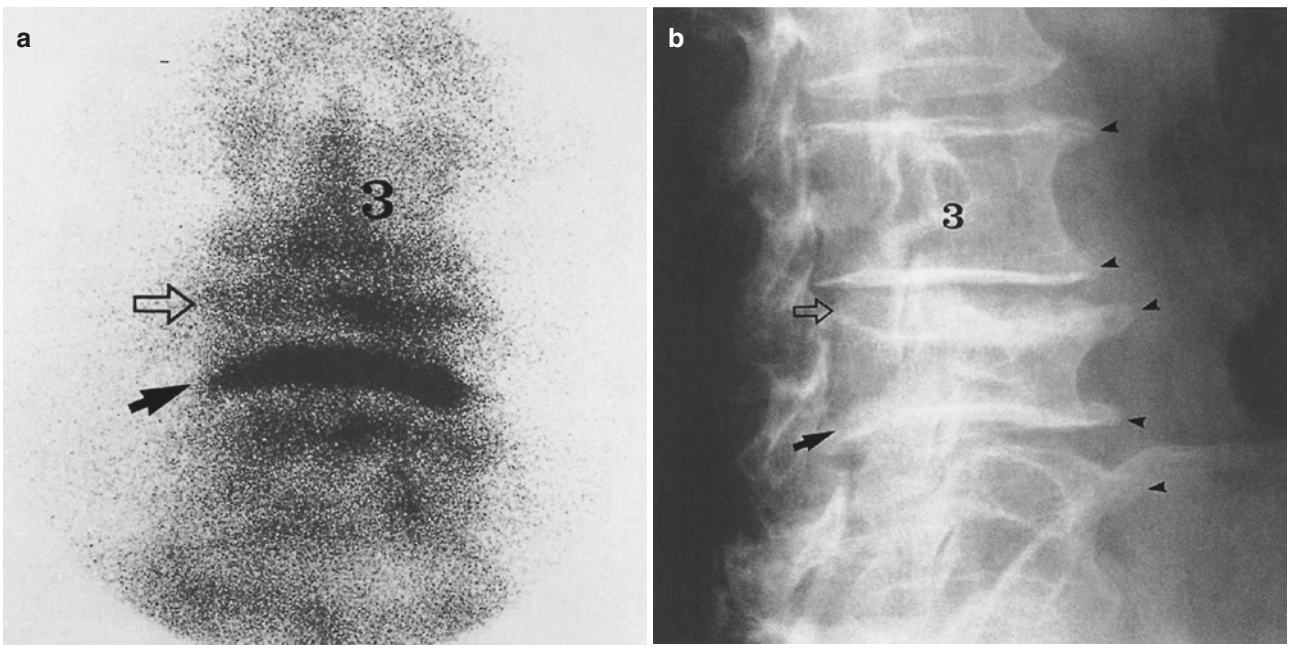

Fig. 9.38 Arcuate depression of the vertebral endplates in compression fractures of the spine. (**a**) Posterior pinhole scintigraph of the lower lumbar spine in a 67-year-old woman with old and new compression fractures of the L4 vertebra shows increased tracer uptake in the centrally depressed upper and lower endplates (*open* and *solid arrows*). Note that the tracer uptake is extremely intense in the fresh fracture of the lower endplate (*solid arrow*), whereas the uptake is minimal in the old fracture of the upper endplate (*open arrow*). (**b**) Near lateral radiograph of the same spine shows compression fractures in the upper and lower endplates of the L4 vertebra (*open* and *solid arrows*). Unlike in pinhole scintigraphy, the distinction between old and new fractures is often difficult in radiography. Note that the mature osteophytes in the nonstress areas do not concentrate tracer (*arrowheads*)

Pinhole scintigraphic manifestations of diskovertebral osteoarthrosis include tracer uptake in the vertebral endplates and marginal spurs with significant diminution of the intervertebral space (Fig. 9.37b). The endplates affected in pairs in a straight, parallel manner. Compression fractures resemble diskovertebral osteoarthritis, but fractures are rarely paired and not parallel when paired (Fig. 9.38b). Moreover, tracer uptake is markedly intensified and the disk space is preserved unless the disk is simultaneously involved in fracture. The osteophytes in spondylitis deformans are represented scintigraphically by beaklike uptake of various sizes and intensities at the lateral or anterior edges of the vertebral bodies (Fig. 9.39b). The tracer intensity in osteophytes appears to be related to age and location; the smaller and the less outgrowing the osteophyte, the more intense is the uptake and vice versa. Indeed, as in the knee (Fig. 9.5) and elsewhere, the mature osteophytes that lie in the lateral, nonstressed zones of the spine accumulate tracer only minimally, whereas the small, burgeoning spurs in the weight-bearing axis avidly concentrate tracer (Fig. 9.39b). Interestingly, old osteophytes appear imposing radiographically, while fresh ones look unimpressive. Extremely intense uptake in one or two of the many osteophytes and endplates occurs as the result of superimposed diseases such as fracture, infection, or metastasis. Thus, when fractured or abutted on another osteophyte, even a mature osteophyte conspicuously concentrates tracer (Fig. 9.40a).

The cervical spine is notorious for diskovertebral osteoarthritis, uncovertebral osteoarthritis, and apophyseal osteoarthritis. As in the lumbar and thoracic spine, diskovertebral osteoarthritis in the cervical spine is pinhole scintigraphically indicated by increased tracer uptake in the sclerosed endplates with narrowed disk space, and such findings are best appreciated on the lateral scan. It is to be noted that osteoarthritis can be confused with infective spondylitis, but radiographic findings basically differ between the two conditions: endplate sclerosis in osteoarthritis (Fig. 9.37a) and endplate lysis in infection (Fig. 6.37b).

The uncovertebral joint of Luschka is the articulation formed between the uncinate processes of the cervical vertebrae and is

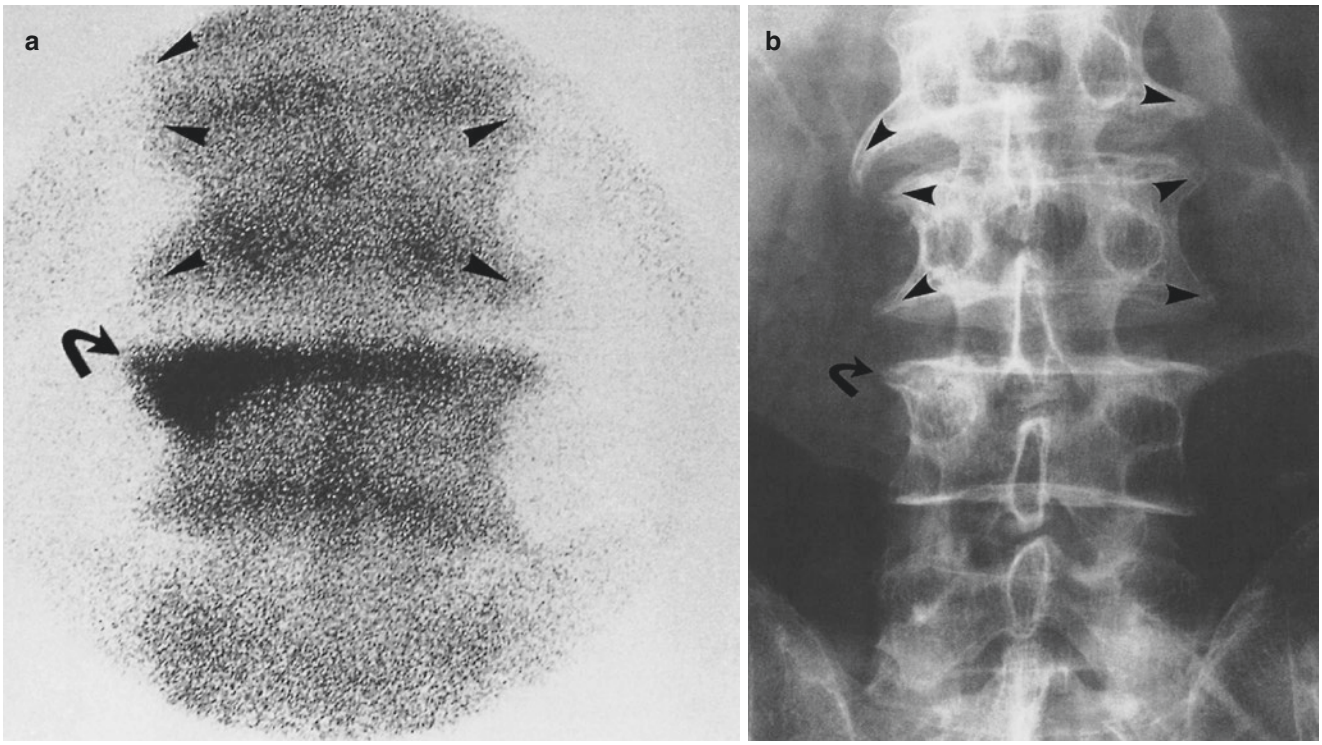

Fig. 9.39 Different intensities of tracer uptake in old and new osteophytes. (**a**) Anterior pinhole scan of the lower lumbar spine in an 80-year-old man with old and new osteophytes reveals little increase in tracer uptake in the prominent old osteophytes in the L2 and L3 vertebrae (*arrowheads*) but very intense tracer uptake in a "budding" osteophyte in the upper lateral aspect of the L4 vertebra (*curved arrow*). (**b**) Anteroposterior radiograph demonstrates prominent osteophytes in the L2 and L3 vertebrae (*arrowheads*) and an unimpressive osteophyte in the L4 vertebra (*curved arrow*)

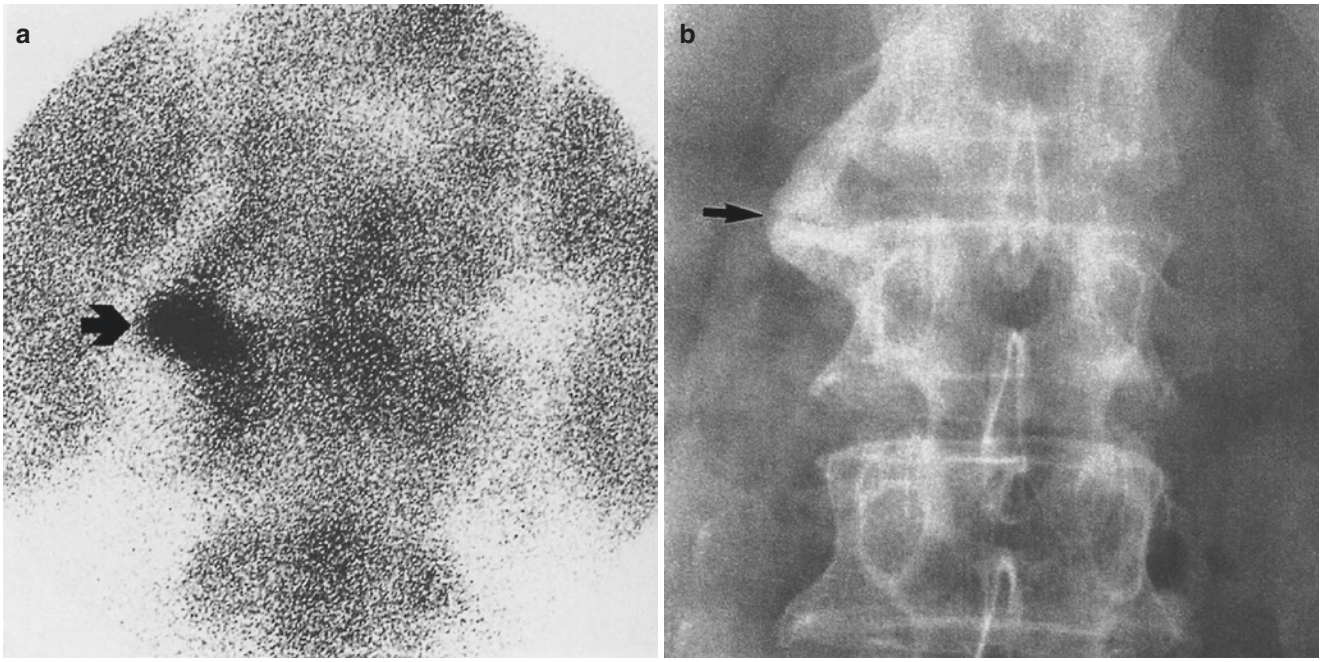

Fig. 9.40 Intense tracer uptake in abutting osteophytes. (**a**) Posterior pinhole scintigraph of the upper lumbar spine in a 72-year-old man with local pain reveals very intense trace uptake in a structure that protrudes outward from the L2–L3 vertebral junction (*arrow*). The most intense uptake occurs in the center where two osteophytes meet to fuse. (**b**) Anteroposterior radiograph shows a prominent paravertebral osteophyte formed by the two smaller, abutting osteophytes which arise separately from the lateral aspect of the lower endplate of the L1 vertebra and the upper endplate of the L2 vertebra (*arrow*). A narrow slit-like lucency at the center indicates the incompleteness of fusion (*arrow*) as confirmed by CT scan (not shown here)

found in all but the first two cervical vertebrae. Because this joint borders the medial aspect of the intervertebral foramina, their involvement is readily diagnosed by pinhole scintigraphy (Fig. 9.41b). As shown in this case, the simultaneous involvement of the uncovertebral and apophyseal joints is not uncommon.

Osteoarthritis of the apophyseal and costovertebral joints manifests as intense uptake in the respective joint. The uptake in apophyseal osteoarthritis is characterized by its lateral localization in the vertebral column on the posterior or anterior scan. It is laid more or less horizontally in the cervical and midthoracic regions (Fig. 9.41) and vertically in the lower thoracic and upper lumbar regions (Fig. 9.42). For unobstructed, viewing of individual apophyseal joints oblique pinhole scintigraphy is ideal. Apophyseal osteoarthritis may be either solitary or multiple, unilateral, or bilateral. The lumbosacral apophyses are most commonly affected, manifesting as classic spotty uptake in the lateral edge(s) of the sacral base (Fig. 9.43). In occasional cases radiographic findings are inconclusive, but scintigraphic evidence is definitive. Indeed, the diagnosis of radiographically dubious osteoarthritis in the false joint between the broad transverse process of the lowermost lumbar vertebra and the lateral part of the transitionalized sacral base can be confirmed by pinhole scintigraphy (Fig. 9.44). It is to be emphasized that planar scan or often radiography is of limited diagnostic value in this condition.

The diagnosis of osteoarthritis of the costovertebral joints, both or either of the costotransverse or costocorporeal joint, can also be established by pinhole scintigraphic portrayal of increased uptake in the respective joints. To be exact anatomically, the costotransverse joint is located in the paraspinal region and the costocorporeal joint in the immediate juxtaspinal region; the former joints lie more laterally than the latter (Fig. 9.45). As in the osteoarthritis of the apophyseal joints, the tracer uptake in costovertebral osteoarthritis is modest at most, and its occurrence is either monarticular or oligoarticular (Fig. 9.45) contrasting with multiple, intense, and usually lateralized tracer uptake in apophyseal joint fractures (Chap. 16). Apophyseal involvement in ankylosing spondylitis and other SNSA is for the most part multiple and symmetrical (Chap. 11).

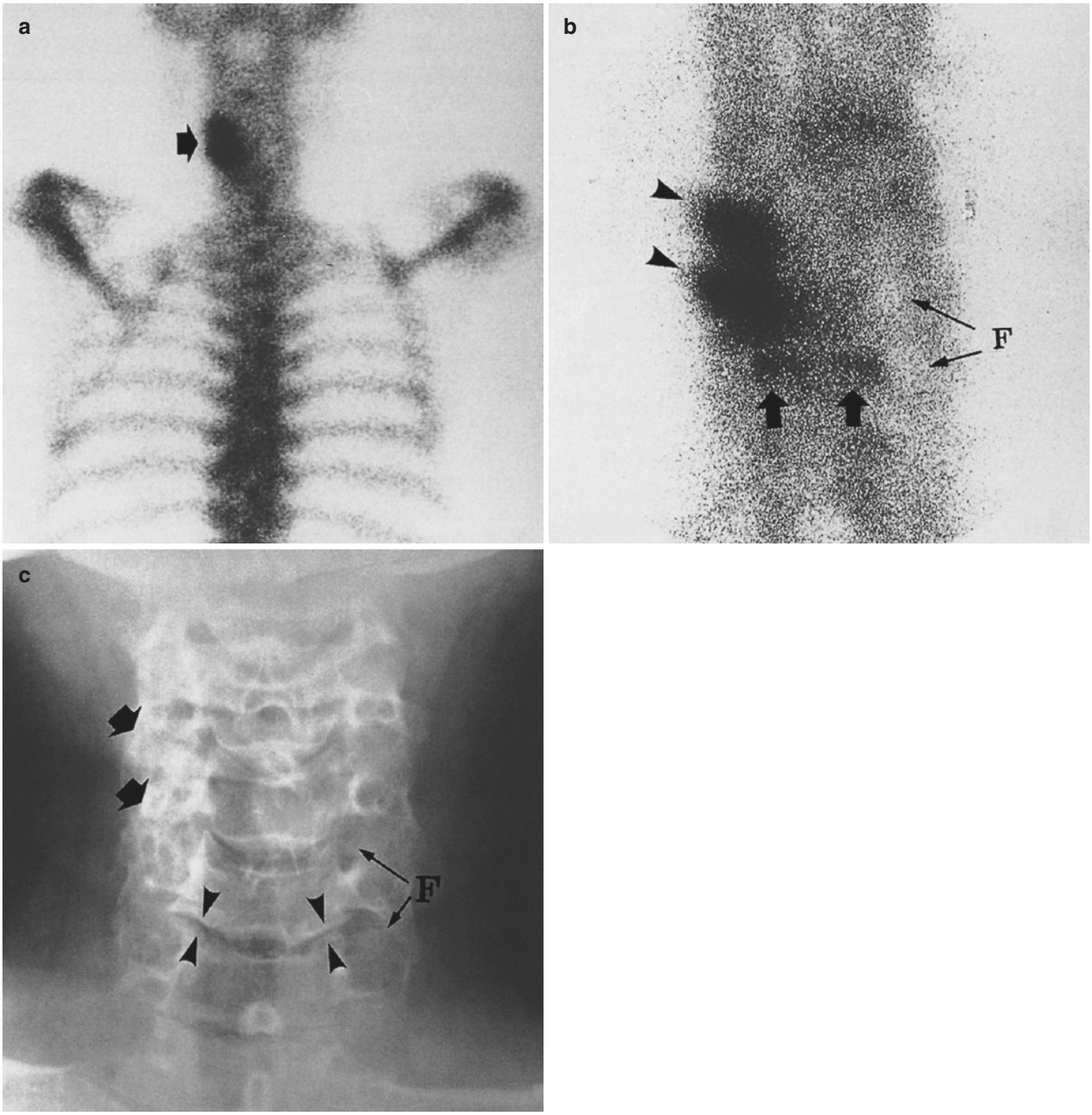

Fig. 9.41 Apophyseal and uncovertebral osteoarthritis of the cervical spine. (**a**) Posterior spot scintigraph of the cervical spine in a 62-year-old woman with posterior neck and left shoulder pain reveals intense tracer uptake in the left lateral aspect of the lower cervical spine (*arrow*). (**b**) Posterior pinhole scan shows intense tracer uptake in the apophyseal joints of C4–C6 vertebrae (*arrowheads*) and also modest tracer uptake in C6 and C7 uncovertebral joints (*arrows*). The latter joints can easily be located at the medial border of the intervertebral foramina (*F*). (**c**) Anteroposterior radiograph shows the obliteration with eburnation of the left apophyseal joints of C4–C6 vertebrae (*arrows*) and erosions in C6 and C7 uncovertebral joints (*arrowheads*). Observe the intimate positional relationship between the uncovertebral joints and the intervertebral foramina (*F*). The radiograph is printed with the right side on the left to match the scintigraph

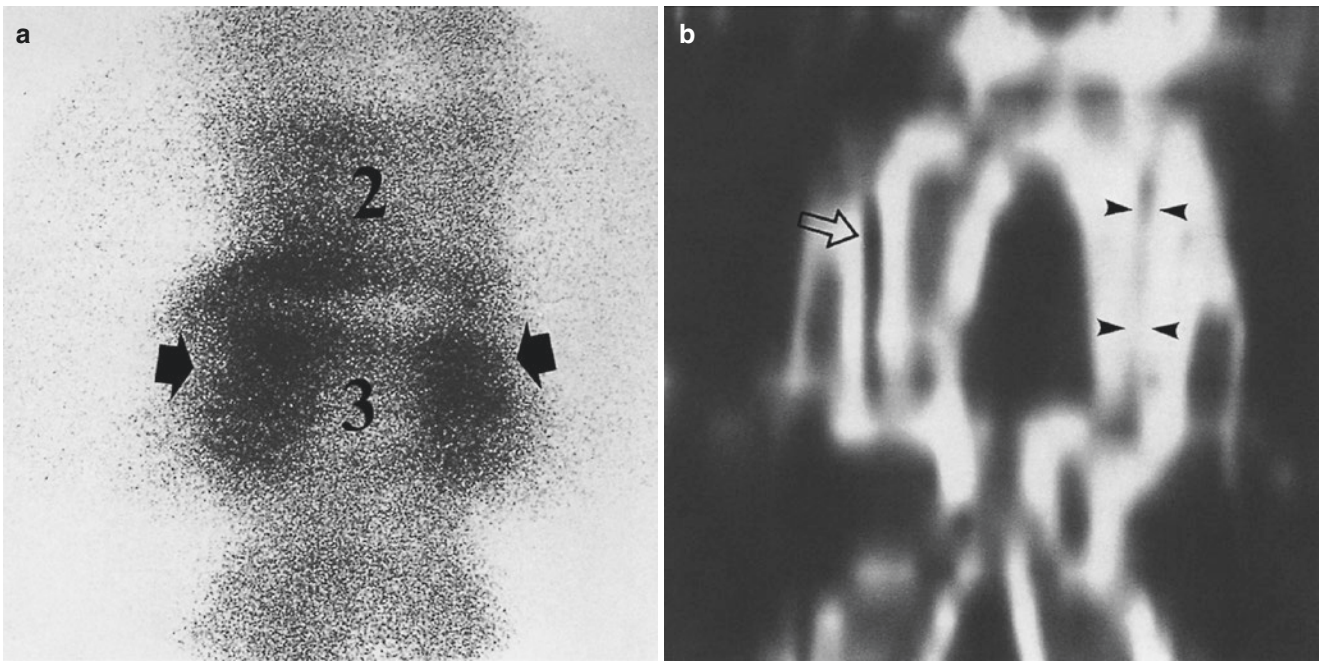

Fig. 9.42 Vertical alignment and half-astride position of the apophyseal joints in the lower lumbar spine. (**a**) Posterior pinhole scintigraph of the midlumbar spine in a 50-year-old woman with known apophyseal osteoarthritis shows intense tracer uptake in L2 and L3 apophyseal joints (*arrows*). Unlike horizontal alignment in the cervical spine (Fig. 9.41), the apophyseal joints in the lumbar spine are vertically aligned and astride in location. (**b**) Coronal CT section through the affected apophyseal joints reveals marked para-articular sclerosis with joint space narrowing on the right (*arrowheads*) and a vacuum on the left (*open arrow*). The CT image is printed with the right side on the left to match the scintigraph

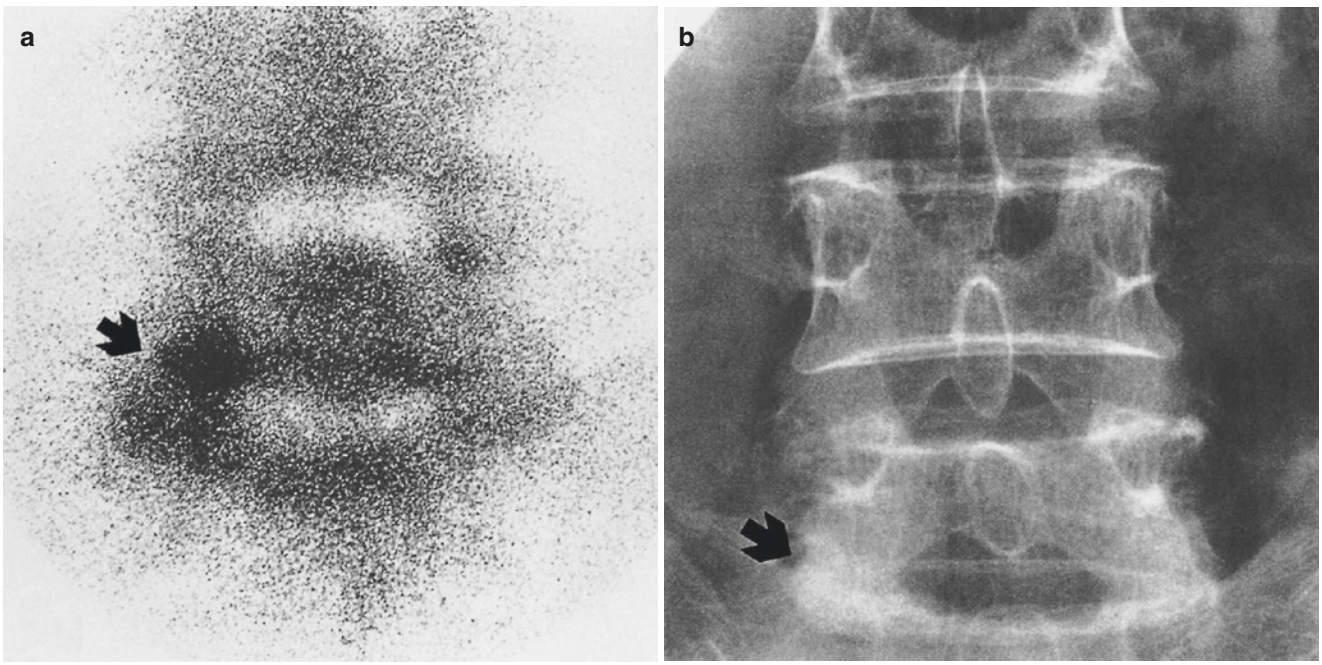

Fig. 9.43 Osteoarthritis in the lumbosacral apophyseal joint. (**a**) Posterior pinhole scintigraph of the lumbosacral region of the spine in a 59-year-old woman with local tenderness shows spotty tracer uptake in the left lumbosacral apophyseal joint (*arrow*). (**b**) Anteroposterior radiograph shows sclerosis in the left lumbosacral apophyseal joint (*arrow*). The radiograph is printed with the right side on the left to match the scintigraph

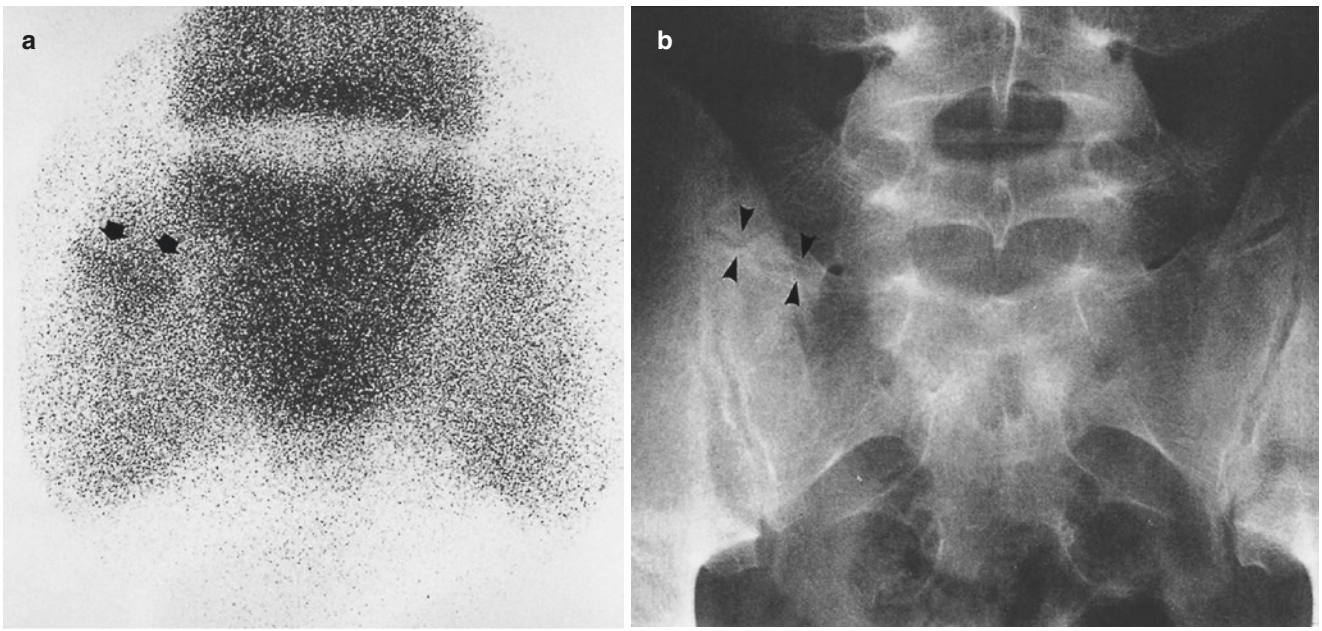

Fig. 9.44 Pinhole scintigraphic diagnosis of early osteoarthritis in transitionalized lumbosacral joint. (**a**) Anterior pinhole scan of the sacrum in a 22-year-old man with disturbing motion pain in the right lumbosacral region reveals indeed subtle tracer uptake in the anomalous lumbosacral joint (*arrows*). Ordinary scintigraph showed no abnormality (not shown here). (**b**) Anteroposterior radiograph reveals borderline para-articular sclerosis in the anomalous joint formed in the transitionalized lumbosacral spine (*arrowheads*)

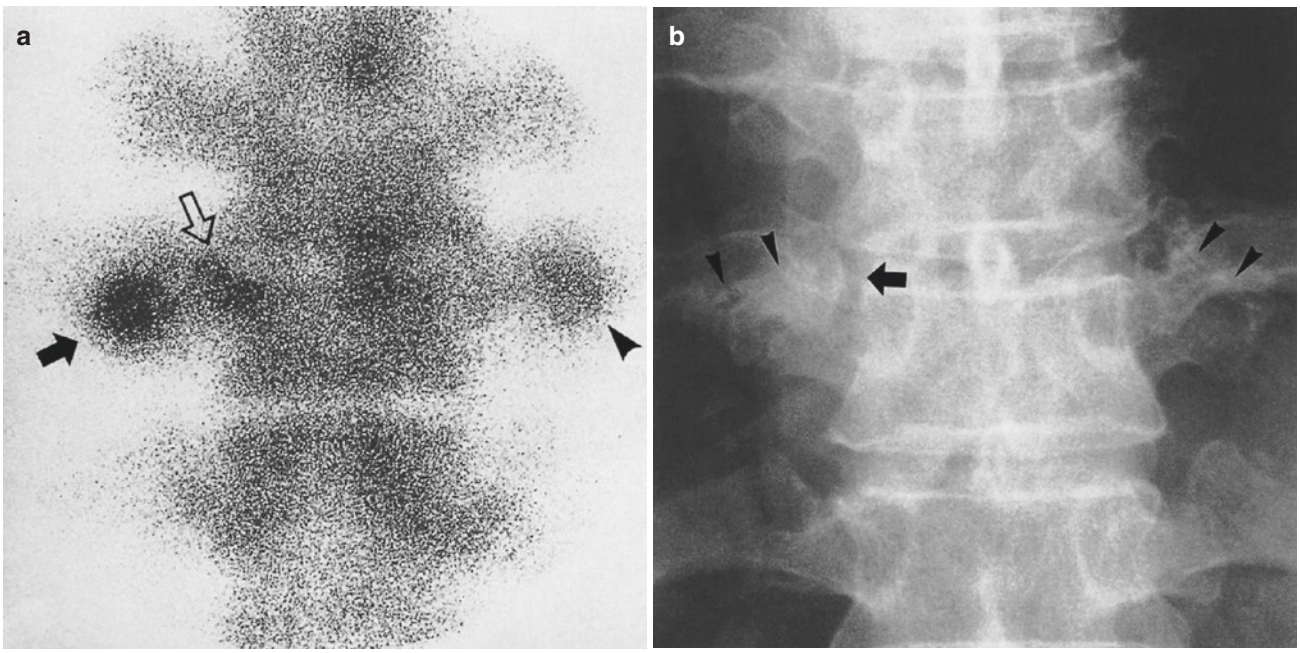

Fig. 9.45 Osteoarthritis in the costovertebral (costotransverse and costocorporeal) joints. (**a**) Posterior pinhole scintigraph of the lower thoracic spine in a 70-year-old man with local pain shows spotty tracer uptake in the left costotransverse (*solid arrow*) and costocorporeal (*open arrow*) joints of the T10 vertebra. The opposite costovertebral joint also shows minimally increased tracer uptake (*arrowhead*). (**b**) Anteroposterior radiograph shows articular narrowing and sclerosis in the costotransverse joints of the T10 vertebra on both sides (*arrowheads*). Note the more medially located costocorporeal joint with erosions (*arrow*). The radiograph is printed with the right side on the left to match the scintigraph

9.15 Other Common Sites of Osteoarthritis

Osteoarthritis commonly affects the symphysis pubis, the interphalangeal joints of the hands and feet, and the sesamoidometatarsal joint of the great toe with hallux valgus (Resnick 2002) as well as the type II accessory bone of the navicular bone (Lawson et al. 1984). As elsewhere, common radiographic features include bone erosions, eburnation, articular narrowing, and cystic formation. Scintigraphy shows increased uptake and articular narrowing. Not infrequently, the scintigraphic changes appear more prominent and impressive than the radiographic changes, especially in the early stage.

9.15.1 Symphysis Pubis

Radiography reveals mild eburnation with preserved joint space in the early stage (Fig. 9.46a) and marked eburnation with joint space narrowing in the late stage (Fig. 9.47).

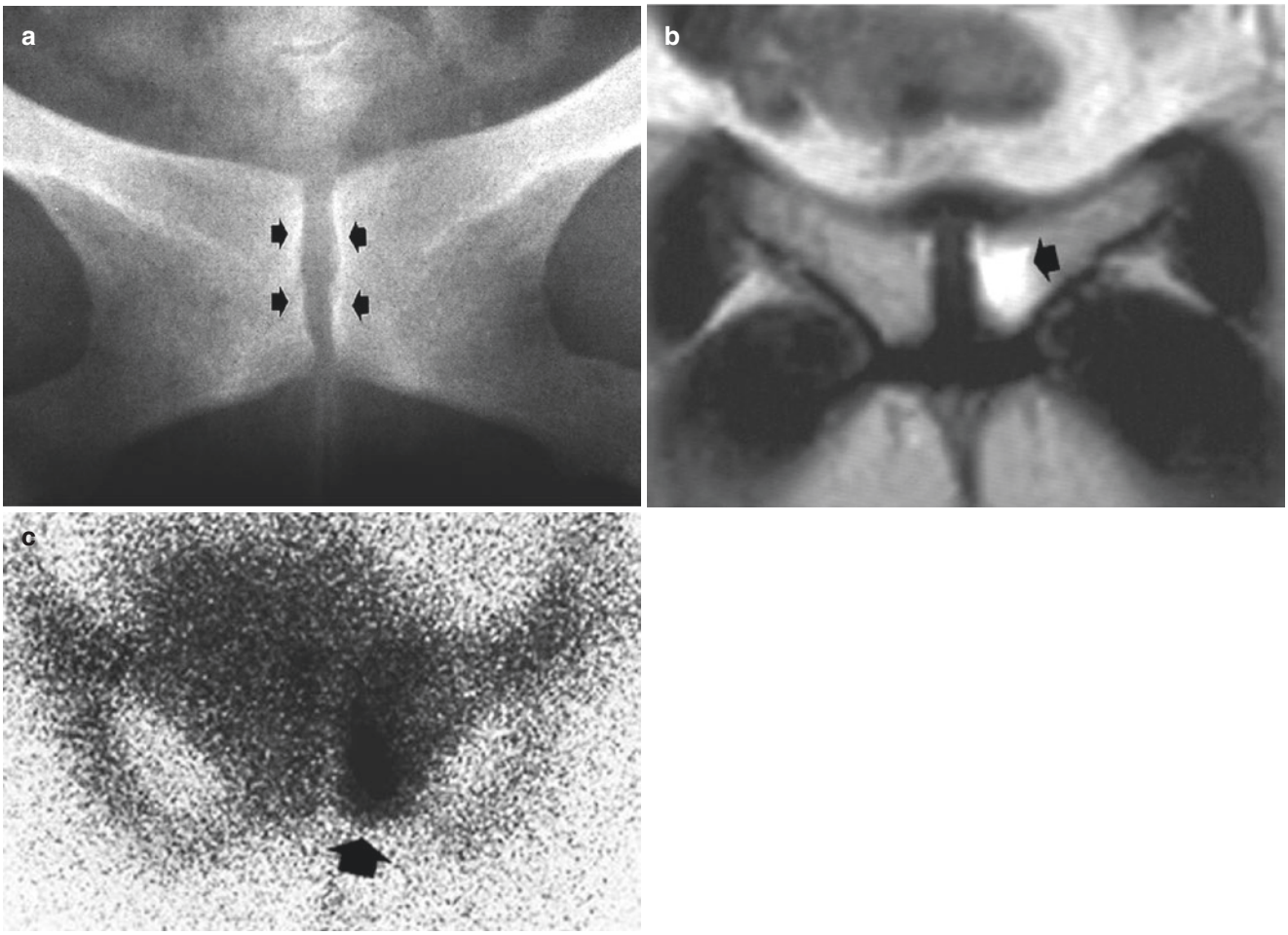

Fig. 9.46 Early osteoarthritis in the symphysis pubis. (**a**) Anteroposterior radiograph of painful pubic symphysis in a 61-year-old female shows local osteopenia and minimal eburnation with a preserved joint space (*arrows*). (**b**) Fat-suppressed T2-weighted MRI demonstrates subcortical edema in the left pubis (*arrow*). (**c**) Anterior pinhole scan shows intense tracer uptake specifically localized to the paraarticular zone of the left pubic bone (*arrow*)

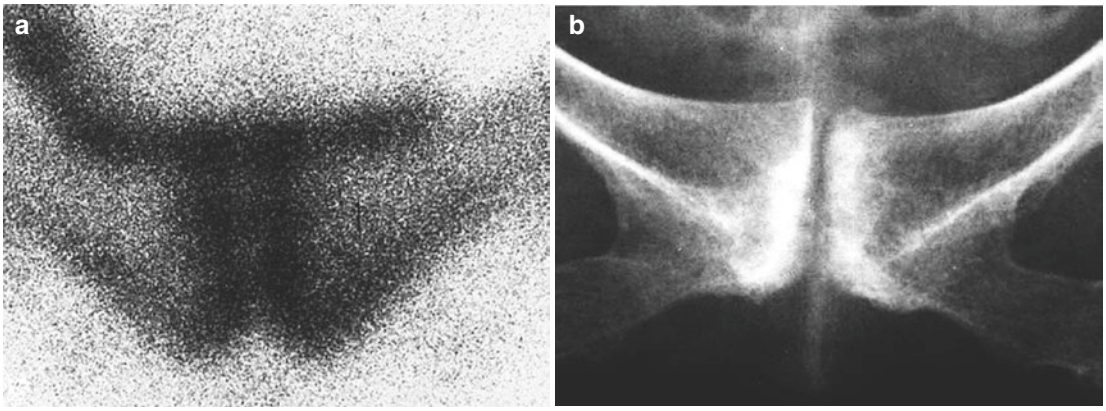

Fig. 9.47 Chronic osteoarthritis in the symphysis pubis. (**a**) Anteroposterior radiograph of painful pubic symphysis in a 72-year-old female shows local osteopenia and prominent eburnation with a narrowed joint space with vacuum shadow. (**b**) Anterior pinhole scan shows intense tracer uptake localized to the pubic bone cortices symmetrically, producing a collared neck appearance. This case suggests that the tracer uptake in pubic osteoarthritis may be linked not only to osteosclerosis but also to other causes such as osteopenia

MRI demonstrates subcortical edema (Fig. 9.46b), which coincides with the site of intense tracer uptake. The changes may be unilateral or bilateral.

9.15.2 Metatarsosesamoidal Joints

Radiography shows lateral dislocation and rotation of the sesamoids, articular narrowing, eburnation in the medial metatarsal head, and soft-tissue thickening. Pinhole scintigraphy reveals prominent tracer uptake localized to the metatarsal sesamoids (Fig. 9.48b). Nuclear angiography demonstrates increased vascularity when the arthritis is attended by active inflammation (Fig. 9.49).

9.15.3 Navicular Accessory Joint

The characteristic radiographic features of osteoarthritis of the navicular accessory bone include irregular narrowing of the navicular and navicular accessory synchondrosis or joint with the condensation of the accessory bone, mimicking avascular necrosis (Fig. 9.50a). The accessory bone avidly accumulates tracer, attesting to the fact that dense accessory bone is not due to necrosis but stimulated bone formation. Multiple "hot" areas may be seen in the neighboring or contralateral foot bones and joints in adolescents, athletes in particular, suggesting concurrent trauma. The occurrence of the navicular accessory bone is bilateral in occasional cases (Lawson et al. 1984) and if symptomatic accumulates tracer. Our recent study of 200 consecutive cases comprising 92 men and 108 women with ages ranging from 20 to 68 years showed the incidence of bilateral and unilateral "hot" navicular accessory bones to be 0.5% and 3.5%, respectively, without gender predilection (Fig. 9.51).

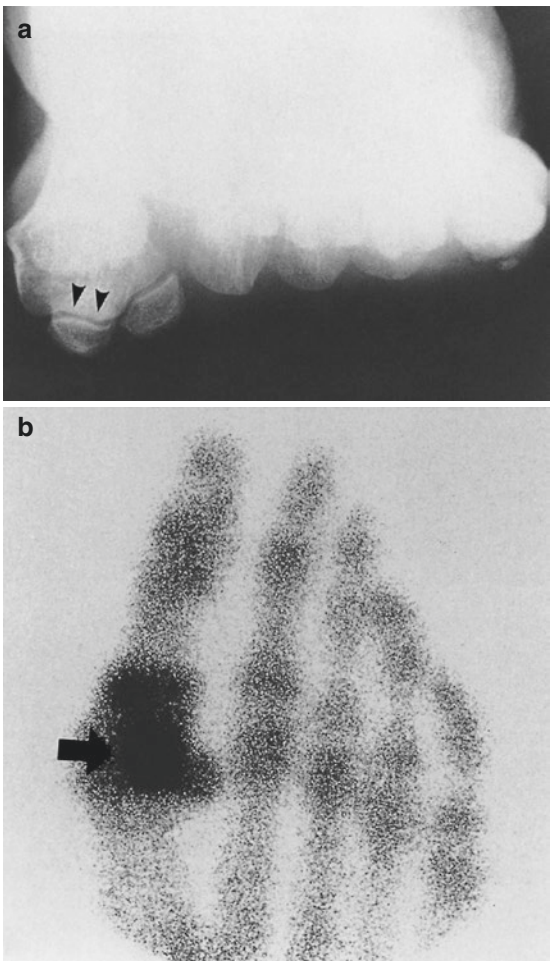

Fig. 9.48 Osteoarthritis in the "sesamoidal articulation" of the first metatarsal head. (**a**) Tangential radiograph (Lewis' view) of the plantar aspect of the painful right great toe in a 42-year-old woman shows minimal periarticular sclerosis and narrowing of the articulation formed between the medial sesamoid and the first metatarsal head (*arrowheads*). (**b**) Dorsal pinhole scan distinctly shows increased tracer uptake in the "enlarged" medial sesamoid (*arrow*) and the bones about the first metatarsophalangeal joint. Caution must be exercised not to overread physiologically increased tracer uptake in the metatarsal sesamoids (Fig. 4.39)

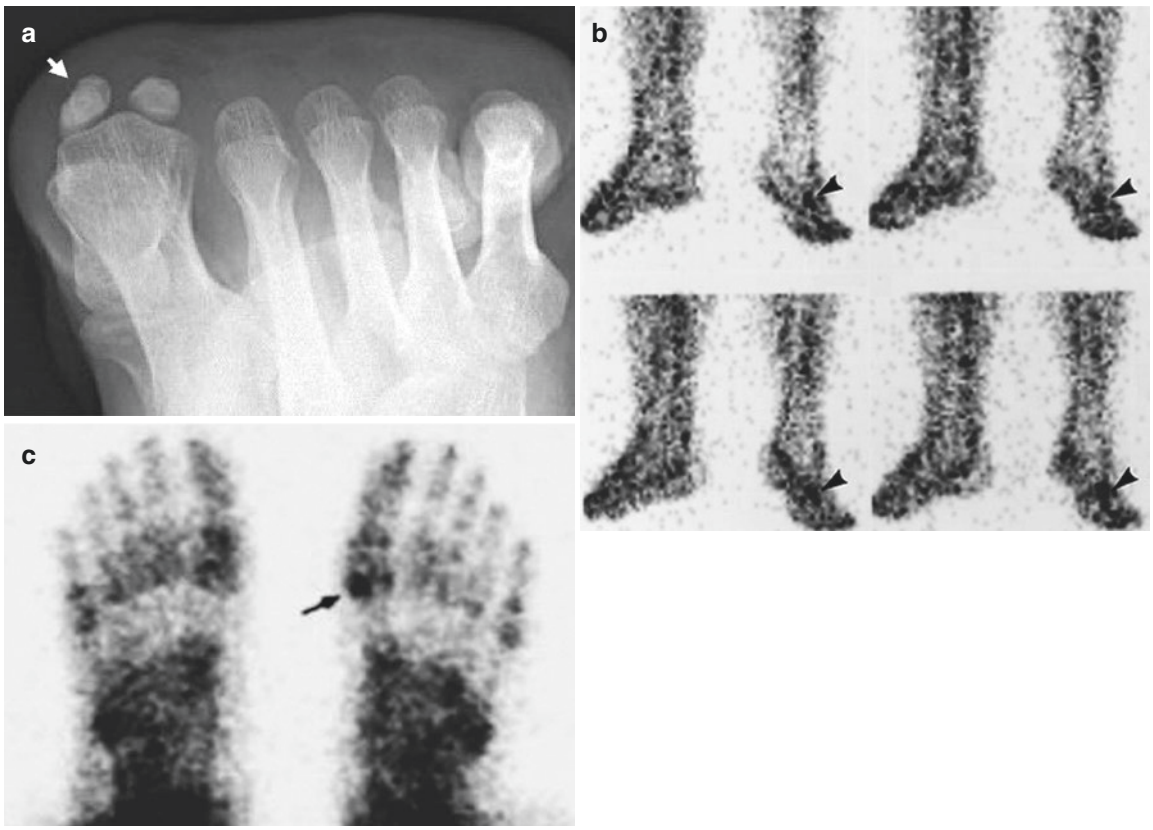

Fig. 9.49 Nuclear angiography in sesamoiditis. (**a**) Tangential view radiograph of painful left first metatarsal head sesamoids in a 35-year-old male shows mild sclerosis of the medial sesamoid bone (*arrow*). (**b**) Angiogram reveals increased blood flow and blood pool in the area in question (*arrowheads*). (**c**) Static planar bone scintigraphy shows tracer intensely accumulated in the medial sesamoid bone denoting degenerative sesamoiditis (*arrow*)

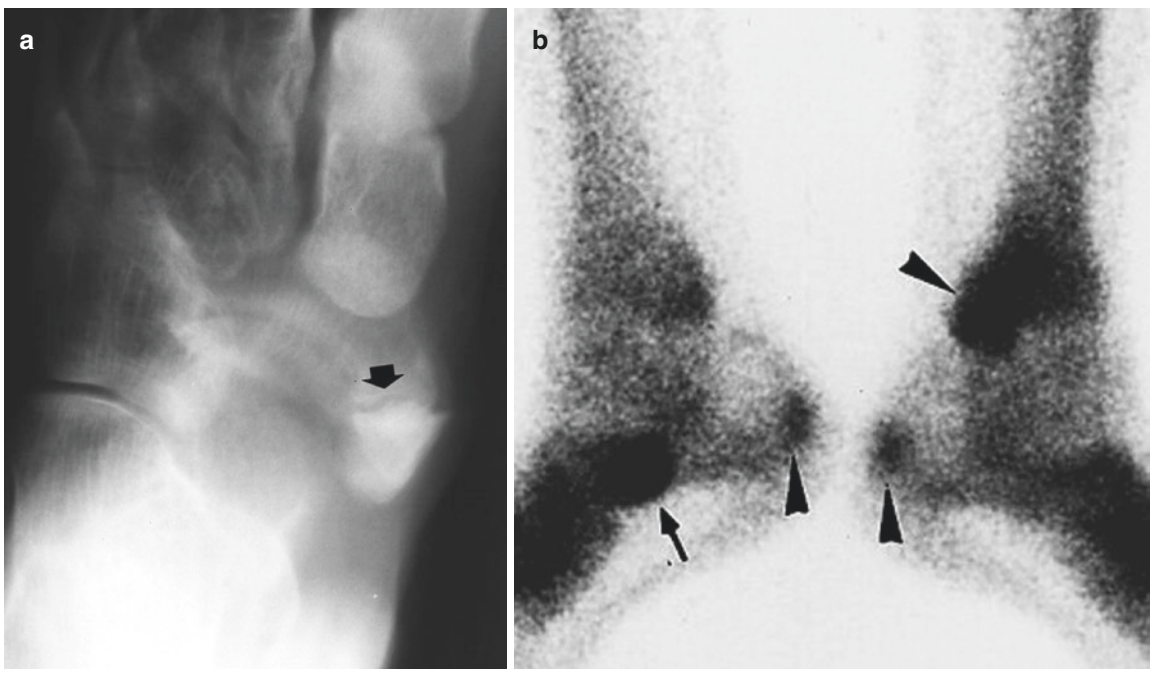

Fig. 9.50 Osteoarthritis of the navicular accessory joint. (**a**) Conventional X-ray tomogram of the right midfoot clearly demonstrates the condensed navicular accessory bone (os tibiale externum) with articular formation (*arrow*). (**b**) Lateral bone scan of both feet reveals intense tracer uptake in pathological navicular accessory bone on the right (*arrow*). The tracer uptake seen in both retrocalcaneal surfaces and left posterior tibial malleolus is likely due to trauma in this sportswoman

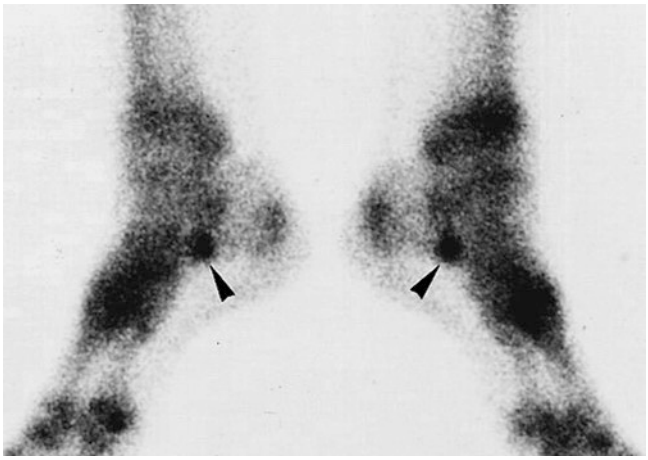

Fig. 9.51 Medial planar bone scan of both feet in a 31-year-old female incidentally shows tracer accumulated in accessory navicular bones (os tibiale externum) that were symptomless

9.16 Generalized Osteoarthritis

Generalized osteoarthritis designates a multiarticular involvement pattern of five or more joints at one time with osteoarthritis. It is divided into primary and nodal type according to the absence or presence of Heberden's nodes. Kellgren et al. (1963) have reported high rates of its occurrence in both male relatives (36%) and female relatives (49%) compared to respective expected rates of 17% and 26%. Joints commonly involved include the apophyseal joints of the spine, the knees, the proximal interphalangeal joints of the finger, the first carpometacarpal joint, and the first tarsometatarsal joint (Kellgren and Moore 1952). The hips, wrists, and lateral metatarsophalangeal joints are also involved but less commonly.

For an efficient clinical investigation of this condition, both radiography and scintigraphy are to be performed at the same time. Radiography is advantageous for the delineation of morphological changes such as bone erosion, sclerosis, and articular narrowing, and the whole-body scintigraphy is the only available imaging method for panoramic observation of multiarticular disease (Fig. 9.52). In addition, pinhole scintigraphy can uniquely provide metabolic information on the individual osteoarthritis (Fig. 9.53).

Essential radiographic features are not dissimilar to those of osteoarthritis in other joints except for multiarticular involvement and include articular narrowing, eburnation, cyst formation, and phalangeal joint osteophytosis with soft-tissue thickening. Periarticular osteophytic excrescences are termed Heberden's nodes when located on the distal interphalangeal joints and Bouchard's nodes when located on the proximal interphalangeal joints.

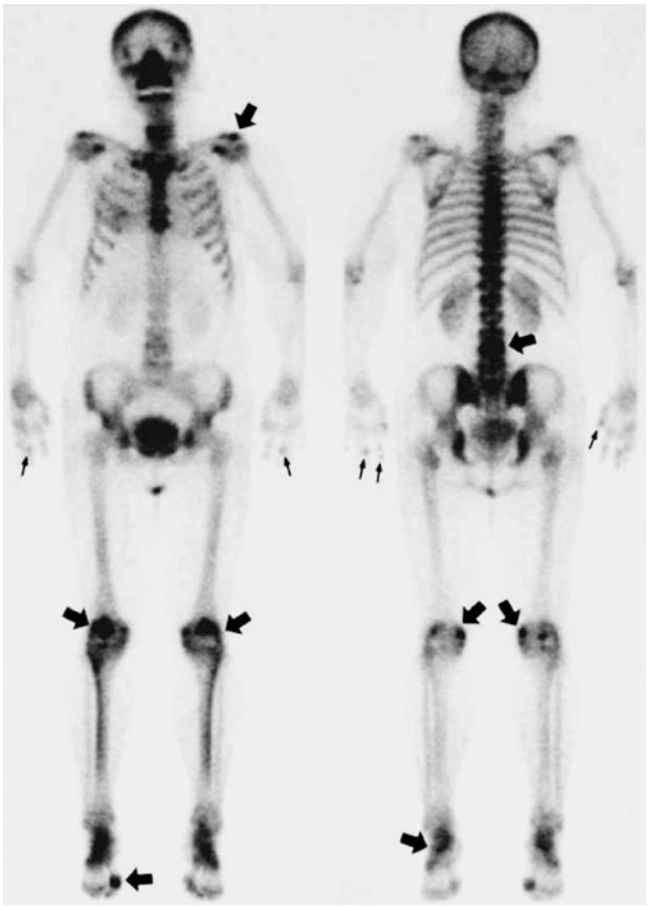

Fig. 9.52 Value of whole-body bone scintigraphy in the diagnosis of generalized osteoarthritis. Anterior (*left*) and posterior (*right*) whole-body bone scans in a 56-year-old female show asymmetrical multiarticular involvement including the lower lumbar spine

Whole-body scanning is ideally suited to the diagnosis of multiple joint involvement spread in the lumbar spine, knees, fingers, wrists, and ankles (Fig. 9.52). On the other hand, pinhole scintigraphy permits semiquantitative assessment of the extent and activity of individual arthritis by observing the intensity of tracer uptake in the individual arthritis (Fig. 9.53). Thus, arthritis in the active phase accumulates tracer intensely and in the dormant phase accumulates little tracer.

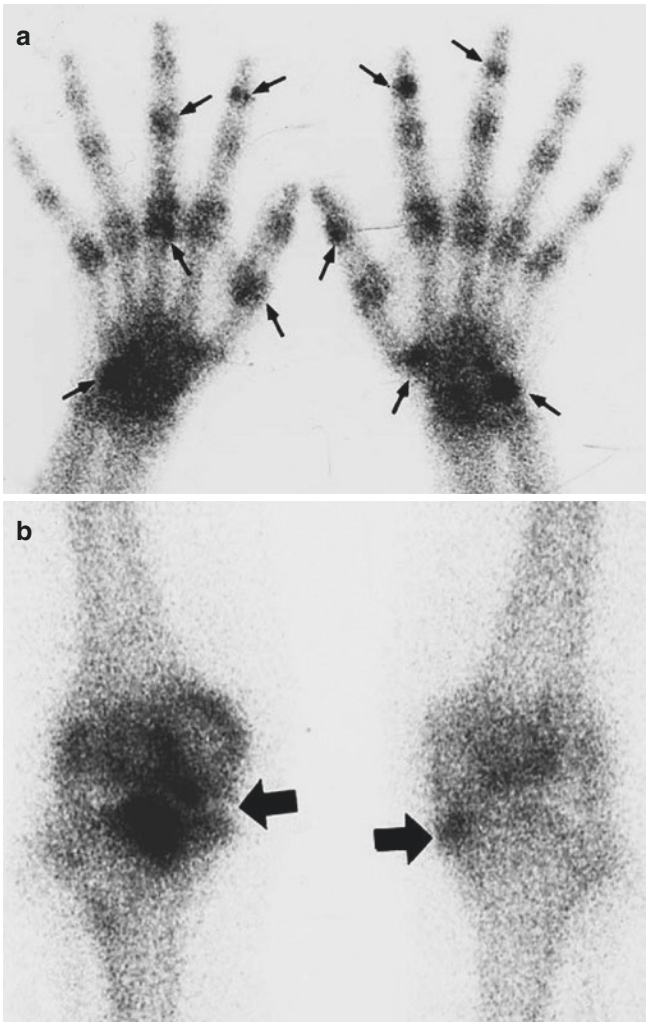

Fig. 9.53 Magnified scintigraphy can uniquely provide metabolic information on the individual osteoarthritis. (**a**) Dorsal scintigraph of both wrists and hands shows tracer uptake to be more intense in sites of active osteoarthritis (*arrows*). (**b**) Anterior pinhole scan of both knees with osteoarthritis reveals different area sizes and uptake intensities between two joints reflecting difference of disease extent and intensity (*arrows*)

9.17 Degeneration-Related Disorders of Spine

The disorders of this category include diffuse idiopathic skeletal hyperostosis (DISH), ossification of the posterior longitudinal ligament (OPPL), Schmorl's nodes, and limbus vertebra as well as spondylolysis and spondylolisthesis, and these constitute interesting objectives of bone scintigraphy that can simultaneously provide information on not only the anatomy but also the metabolic state of the individual conditions.

9.17.1 Diffuse Idiopathic Skeletal Hyperostosis

Diffuse idiopathic skeletal hyperostosis (DISH), previously known as ankylosing hyperostosis of the spine and Forestier's disease, is characterized by bony proliferation at the site of tendon and ligament attachment to bone (entheses), calcification and ossification of the anterior longitudinal ligaments, and diskovertebral osteophytosis. This is a common but not insignificant disease of the spine and extraspinal skeleton. The etiology has not been established, but some investigators consider that it may be associated with degenerative process. There are three radiographic features proposed by Resnick and Niwayama (1976) as important prerequisites for the diagnosis of DISH (Figs. 9.54a and 9.55a). They include (1) the presence of flowing-type calcification and ossification along the anterolateral aspects of four or more contiguous vertebral bodies with or without associated focal excrescences at the intervertebral level, (2) relatively preserved disk spaces without radiographic evidence of extensive disk degeneration such as the vacuum phenomenon or sclerosis, and (3) the absence of apophyseal and sacroiliac joint obliteration due to erosion, sclerosis, and bony fusion. The last feature distinguishes DISH from ankylosing spondylitis. In addition to the spine, the pelvis, trochanter, patella, calcaneus, and olecranon process are frequently involved. Osseous proliferation occurs at the entheses, producing the characteristic "whisker" sign.

Generally, scintigraphic manifestations of DISH are too subtle and complex to be recognized by ordinary scintigraphy (Paquin et al. 1983). With the aid of pinhole scintigraphy, however, DISH can be indicated more specifically by tracer uptake in the anterior and lateral aspects of vertebral bodies and disk spaces as well as the spinous processes, most commonly in the thoracic and lumbar spine. Interestingly, tracer accumulates relatively more intensely in the anterolateral aspect of the vertebral bodies than the disk spaces where radiographic hyperostosis with a bumpy contour occurs most prominently (Fig. 9.54b). Like hyperostoses elsewhere, anatomically unimpressive bony excrescences in DISH intensely accumulate tracer, obscuring the vertebral contour and disk spaces (Fig. 9.54), but larger ones accumulate little tracer rendering the spinal contour and disk spaces clearly portrayed (Fig. 9.55).

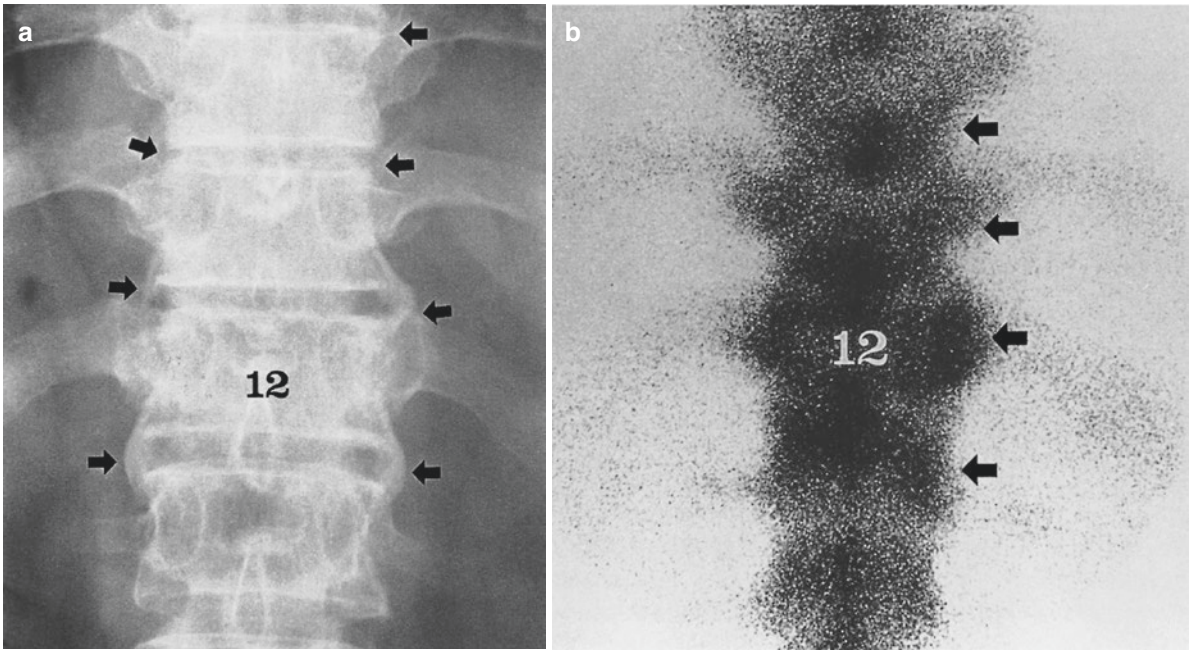

Fig. 9.54 Diffuse idiopathic skeletal hyperostosis (DISH). (**a**) Anteroposterior radiograph of the thoracolumbar spine in a 45-year-old man with DISH shows flowing ossification along the lateral aspects of T8–L1 vertebrae (*arrows*). Vertebral endplates and disk spaces appear preserved and the sacroiliac joints are not involved (not shown here). The radiograph is printed with the right side on the left to match the scintigraph. (**b**) Posterior pinhole scan shows intense tracer uptake in the costovertebral-apophyseal joints as well as the spinous processes of the thoracolumbar spine and less intense tracer uptake in the other vertebral elements (*arrows*). The individual vertebrae and disk spaces are not clearly discernible. Tracer uptake is disproportionately intense compared to relatively unimpressive radiographic changes (see Fig. 9.55)

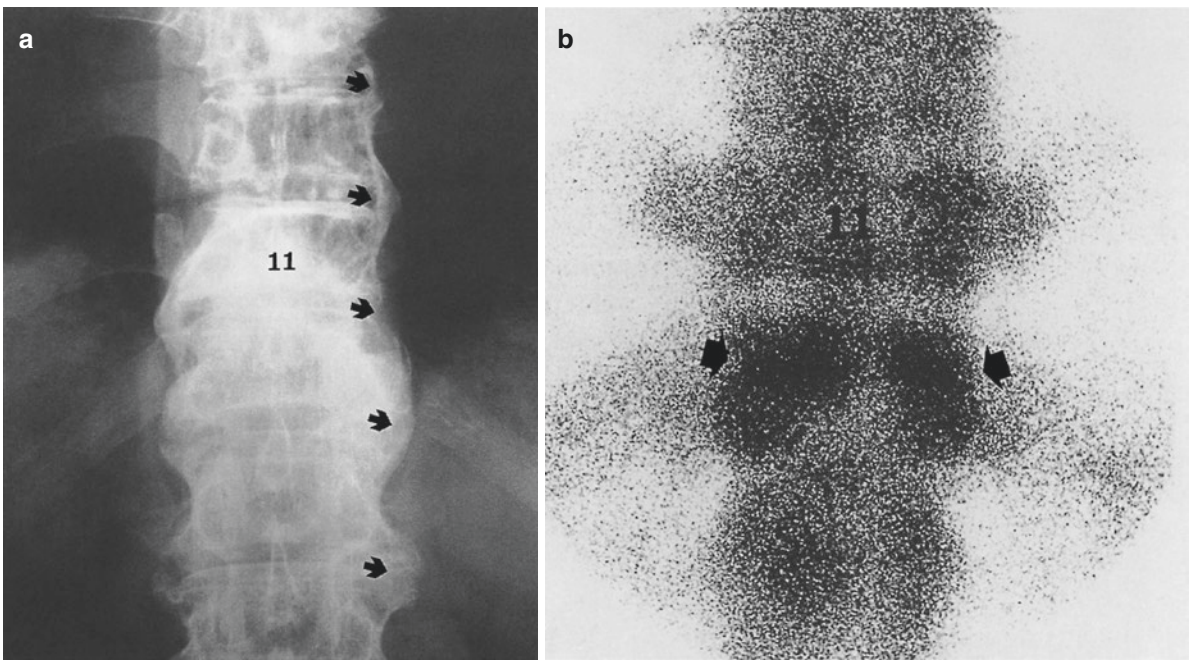

Fig. 9.55 Relatively low tracer uptake in more mature diffuse idiopathic skeletal hyperostosis (DISH). (**a**) Anteroposterior radiograph of the thoracolumbar spine in a 74-year-old man with DISH shows dense, flowing, paraspinal ossifications diffusely involving T9 through L2 vertebrae. The ossification is much more advanced than that of the case shown in Fig. 9.54. The radiograph is printed with the right side to the left to match the scintigraph. (**b**) Posterior pinhole scintigraph paradoxically shows generally reduced tracer uptake. The individual vertebrae and disk spaces are discernible. Isolated, intense tracer uptake in the costovertebral-apophyseal joints of T12 may denote the residual foci with an active pathology (*arrows*)

9.17.2 Ossification of the Posterior Longitudinal Ligament

Ossification of the posterior longitudinal ligament (OPLL) is an idiopathic disorder of the spine, in which calcification or ossification of various lengths occurs in the posterior longitudinal ligament. The middle cervical spine, T3 through T6, is most commonly affected. Pathologically, the condition is characterized by bony overgrowth of the ligament that is attached to the posterior surface of the vertebral body and intervertebral disk, compressing and flattening the spinal cord behind. The lesional bones are lamellated with well-developed Haversian canals but poorly formed marrow (Ono et al. 1977). The most typical lesion occurs in the cervical spine, although other levels are not exempted. It is a fairly common disorder with prevalence rates of 2–4% in the middle-aged and older populations in Asian countries (Ogata and Kawaguchi 2004). The disorder may pass symptomlessly or cause numbness and tingling pain in the fingers, head, and neck and severe anesthesia of the trunk and lower extremities.

The characteristic radiographic features include vertical, plaque-like ossification that is either closely or loosely attached to the posterior surfaces of cervical vertebral bodies and disk spaces (Fig. 9.56a). T2-weighted MRI presents the calcified ligament as an undulating elongated plaque of low signal intensity demarcated by bright signal intensity of the surrounding cerebrospinal fluid (Fig. 9.56b). Posterior bone scintigraphy of the neck may reveal a longitudinal strip of increased tracer uptake in the midline of the cervical spine (Fig. 9.56c).

9.17.3 Schmorl's Cartilaginous Node

Schmorl's node is the dislocation of the denatured nucleus pulposus into vertebral cancellous bone through the weakened annulus fibrosus and diskovertebral junction, creating an intravertebral defect surrounded by eburnation. Nodes are often seen in association with diskovertebral osteochondrosis, trauma, osteoporosis, or Scheuermann's disease.

Radiographically, Schmorl's node presents as an ovoid or roundish defect within the vertebral body beneath the endplate. The outline is ill defined and irregular when the lesion is relatively fresh (Fig. 9.57a) and sclerotic and well defined when old (Fig. 9.58a). The disk spaces are narrowed and endplates are eroded and sclerotic. Pinhole scintigraphy shows disk space narrowing with increased endplate uptake. Schmorl's nodes are denoted by spotty or ovoid "hot" area (Figs. 9.57b and 9.59a). The intensity of tracer uptake appears to be related to the age and size of the node: large and poorly defined nodes tend to accumulate tracer intensely (Fig. 9.57b), whereas small, well-defined, sclerotic nodes accumulate little tracer (Fig. 9.58b). CT presents the node as a hypodense area within the cancellous bone surrounded by a hyperdense rim (Fig. 9.59b).

9.17.4 Limbus Vertebra

Limbus vertebra is the marginal dislocation of nucleus pulposus, another mode of disk herniation. It occurs typically in the anterior or posterior edge of the vertebral body, radiographically manifesting as the division of a small fragment with a cleavage (Fig. 9.60a). A fragment is not present in every case (Fig. 9.61a). Pinhole scintigraphically, the limbus with sclerosis is characterized by intense uptake localized to the anterior or posterior edge of an endplate, beaking outward when fragmented (Fig. 9.60b). Apposing endplates show increased uptake and the disk space between is narrowed, reflecting diskovertebral osteochondrosis and disk degeneration.

9.17.5 Spondylolysis

Spondylolysis refers to the bone defect in the pars interarticularis. It is caused by repeated trauma or physical stress to the biomechanically vulnerable lamina between the superior and inferior articular facets. Spondylolysis divides a vertebra into the superior and inferior segment. The former segment includes the vertebral body, pedicles, transverse processes, and superior articular facet and the latter the inferior articular facet, laminae, and spinous process. Spondylolysis is an important disease that causes lasting low-back pain, especially in gymnasts (Jackson et al. 1976; Collier et al. 1985). The incidence ranges from 3% to 10%. A hereditary trait has been reported (Jackson et al. 1976).

Radiographic features vary according to disease stage: (a) osteopenic band in the early stage, (b) obvious bone defect across the lamina in the established stage, and (c) reactive sclerosis or callus formation and bony reunion in the late and cured stage (Fig. 9.62a). Spondylolysis, the bilateral form in particular, is frequently complicated by the anterior slippage or spondylolisthesis of the superior segment of the divided vertebra. CT is ideal for accurate anatomical investigation of spondylolysis and its associated lesions such as disk herniation, intervertebral foraminal narrowing, and neural canal indentation. MRI is another excellent modality for diagnosing bone defect, disk herniation, nerve compression, and soft-tissue changes.

Fig. 9.56 Ossification of the posterior longitudinal ligament (OPLL). (**a**) Lateral radiograph of the cervical spine in a 46-year-old female shows vertical, plaque-like ossification attached to the posterior surface of the middle cervical vertebral bodies (*arrows*). (**b**) T2-weighted MRI reveals undulating low signal intensity of mineralized ligament posteriorly demarcated by bright signal of cerebrospinal fluid (*arrows*). (**c**) Posterior bone scan shows longitudinal tracer uptake in OPLL in the midline of the cervical spine (*arrows*)

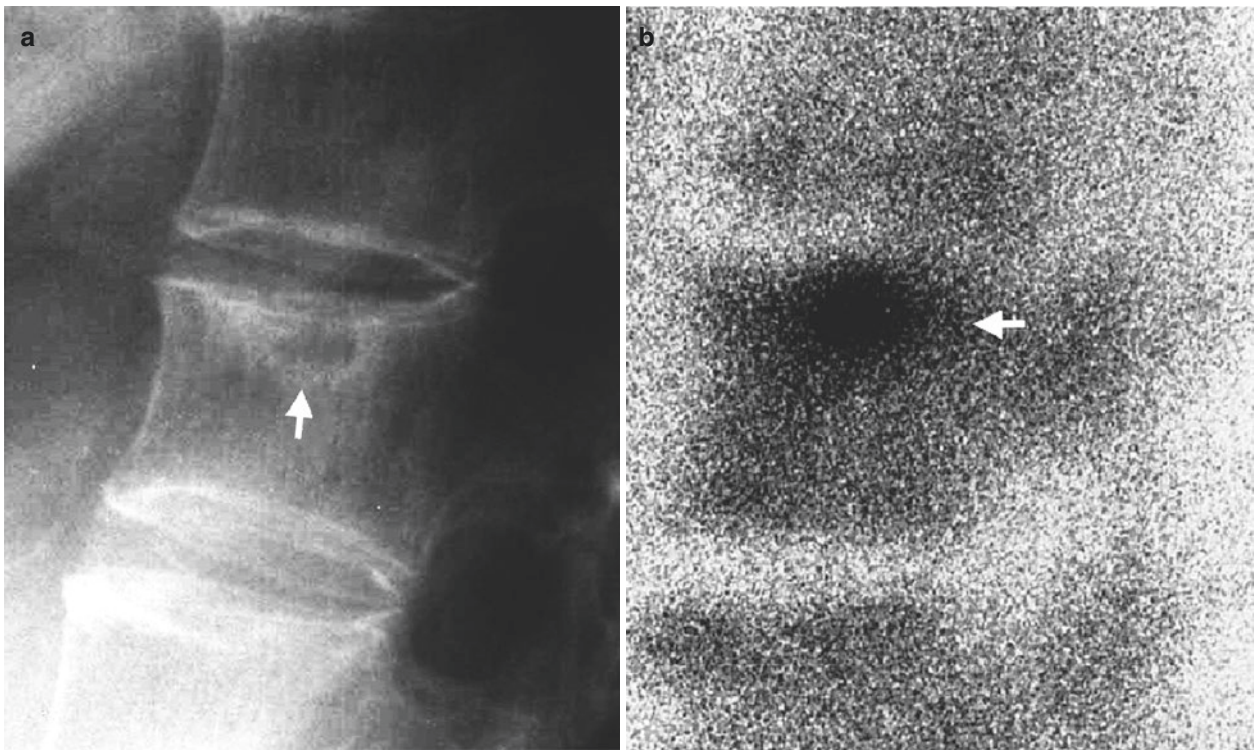

Fig. 9.57 Fresh Schmorl's node. (**a**) Lateral radiograph of L3 in a 60-year-old female with back pain shows an ill-defined ovoid bone defect within the vertebral body beneath slightly depressed endplate (*arrow*). (**b**) Lateral pinhole scan reveals an ovoid area of intense uptake, the border of which is unsharp (*arrow*)

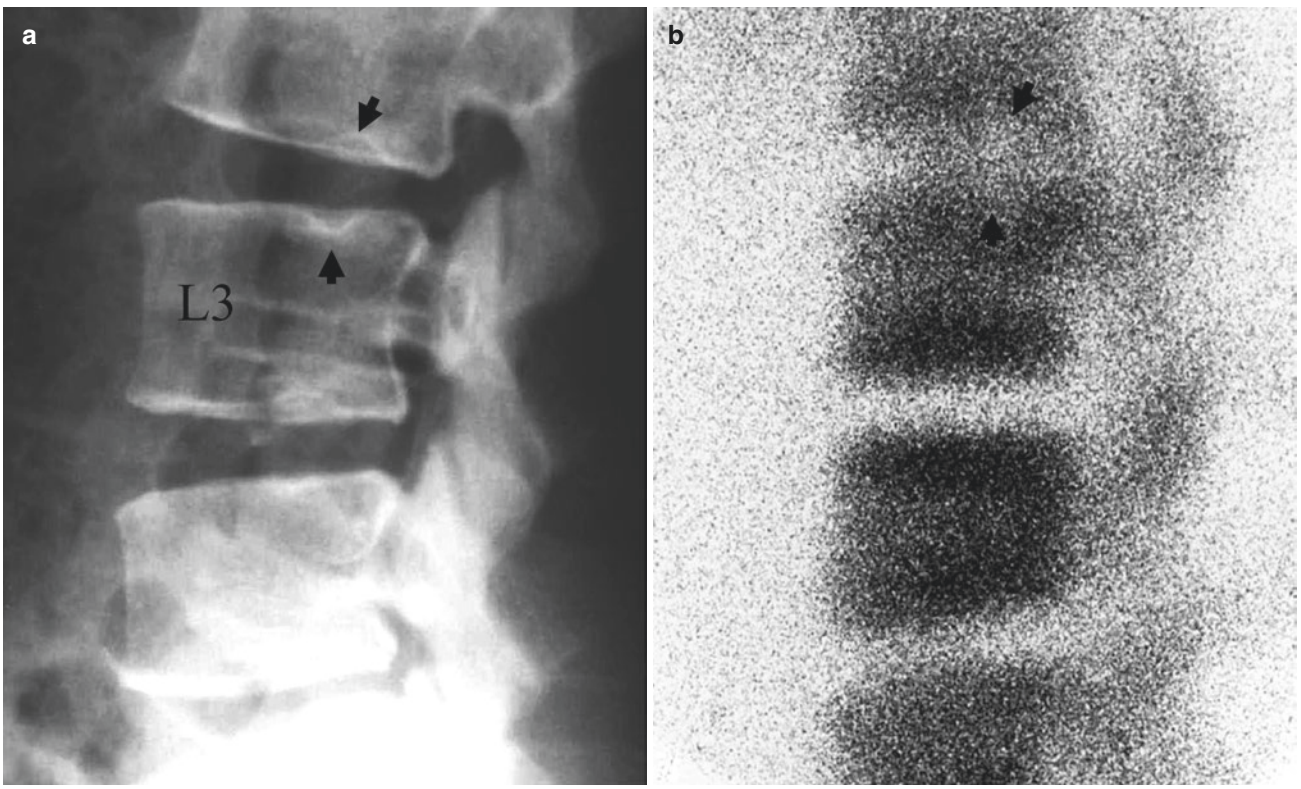

Fig. 9.58 Metabolically inert Schmorl's nodes. (**a**) Lateral radiograph of the midlumbar spine in a 33-year-old woman shows meniscoid scleroses at L2 lower and L3 upper endplates (*arrows*). (**b**) Lateral pinhole scan shows areas of decreased tracer uptake that match with the radiographic defects (*arrows*)

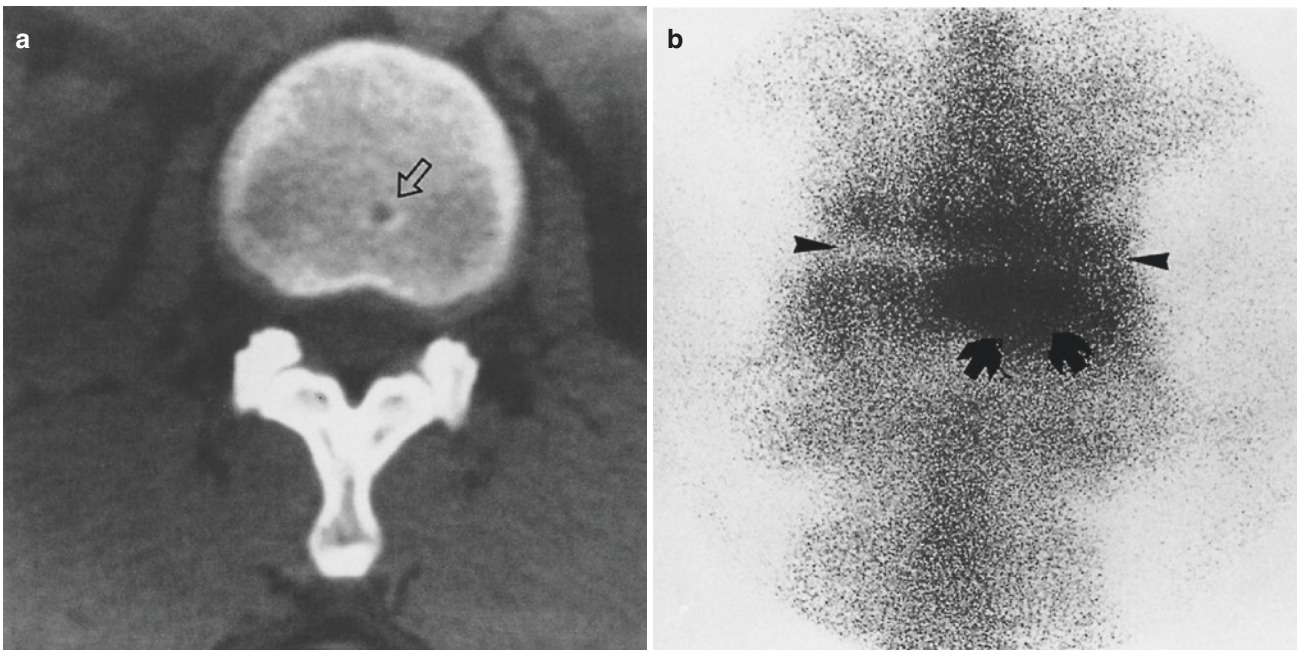

Fig. 9.59 Schmorl's node. (**a**) Axial CT scan through the upper part of the LI vertebra shows a small, round lucency surrounded by a sclerotic rim in the cancellous bone (*open arrow*). (**b**) Posterior pinhole scan shows very intense tracer uptake surrounded by less intense uptake zone in the right centrolateral aspect of the upper endplate of the LI vertebra, matching the CT scan defect (*arrows*). The disk space is moderately narrowed, and the regional endplates concentrate tracer intensely due to associated osteochondrosis (*arrowheads*)

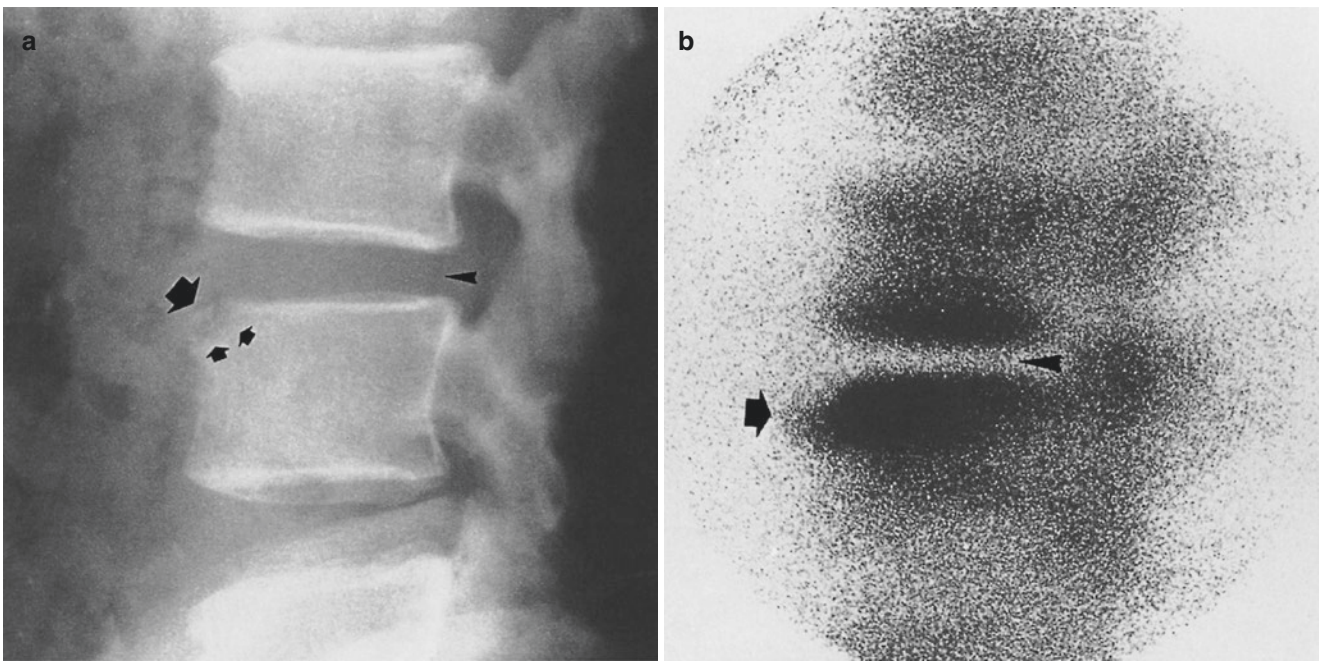

Fig. 9.60 Limbus vertebra. (**a**) Lateral radiograph of the L5 vertebra in a 53-year-old man with back pain reveals a small bone chip (*large arrow*) that is incompletely detached from the upper anterior edge with a lucent cleavage (*small arrows*). The disk space is slightly narrowed (*arrowhead*). (**b**) Lateral pinhole scintigraph shows very intense tracer uptake surrounded by less intense uptake in the area under study (*arrow*). The affected upper endplate of L5 and the apposing lower endplate of L4 concentrate tracer intensely with narrowed disk space between, indicating early osteochondrosis that may well be related to disk herniation (*arrowhead*)

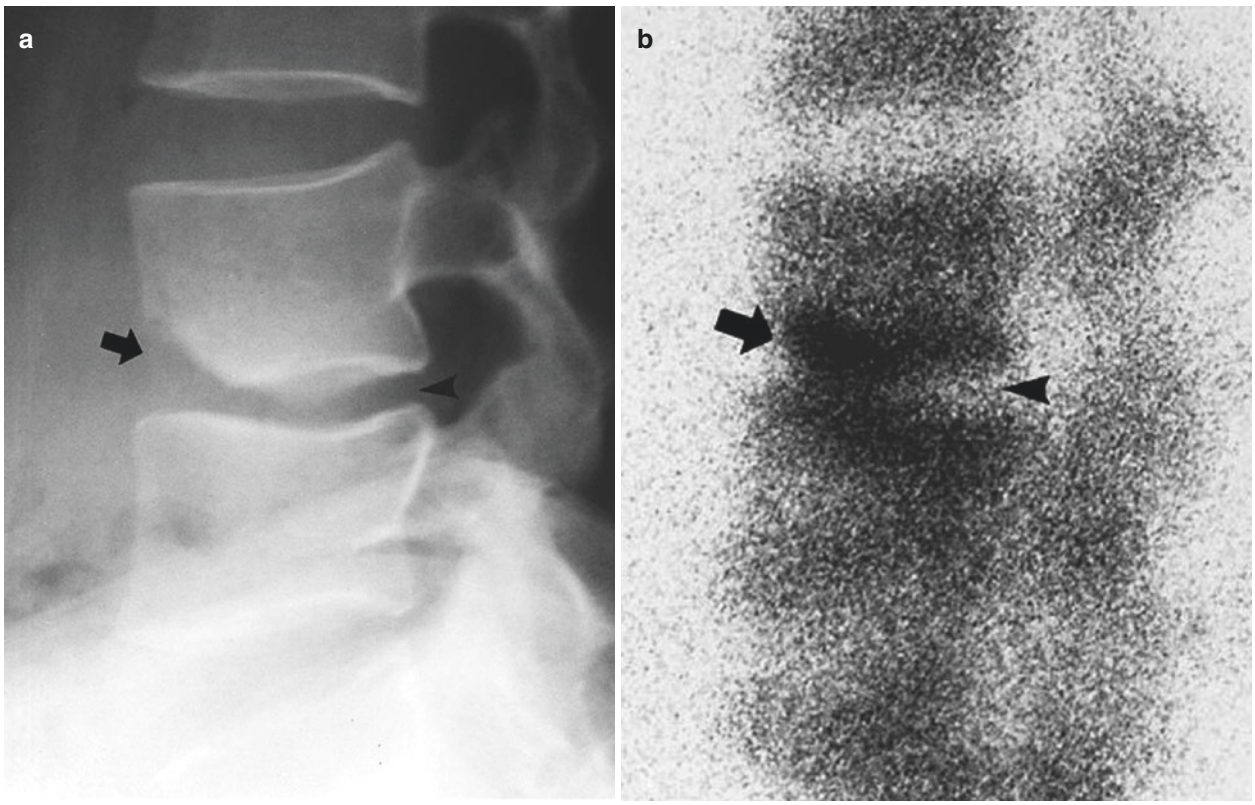

Fig. 9.61 Limbus vertebra with infraction. (**a**) Lateral radiograph of the lumbar spine in a 31-year-old female with low-back pain shows a triangular bone defect in the anterior edge of L4 lower endplate (*arrow*). The disk space is narrowed and the endplates sclerotic (*arrowhead*). (**b**) Lateral pinhole scan reveals intense tracer uptake in the triangular defect and sclerosed endplates with narrowing of the disk space (*arrowhead*)

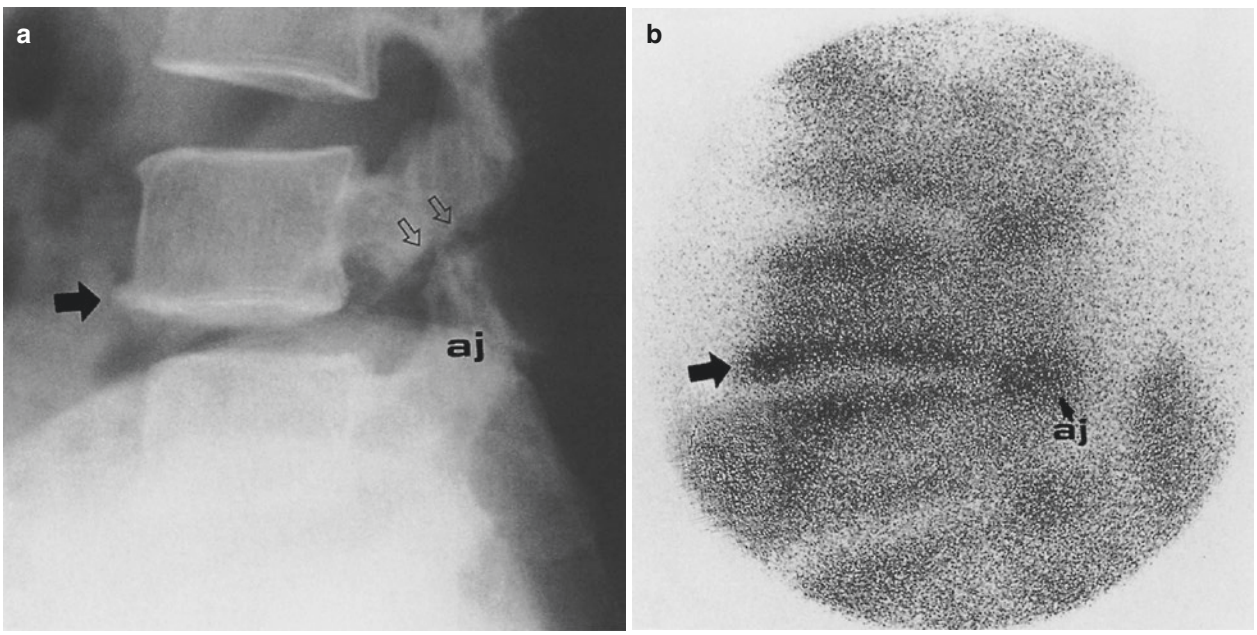

Fig. 9.62 Spondylolysis and spondylolisthesis. (**a**) Lateral radiograph of L4 and L5 vertebrae in a 45-year-old man with back pain shows a large bone defect involving the pars interarticularis of the L4 vertebra (*open arrows*) and mild anterior sliding. A small osteophyte is seen (*arrow*) (*aj* apophyseal joint). (**b**) Lateral pinhole scintigraph portrays no abnormal tracer uptake in the spondylolysis defect. However, the anterior sliding of the L4 vertebra is clearly delineated by virtue of increased tracer uptake in the osteophyte and lower endplate, the sign of the secondary osteochondrosis (*arrow*)

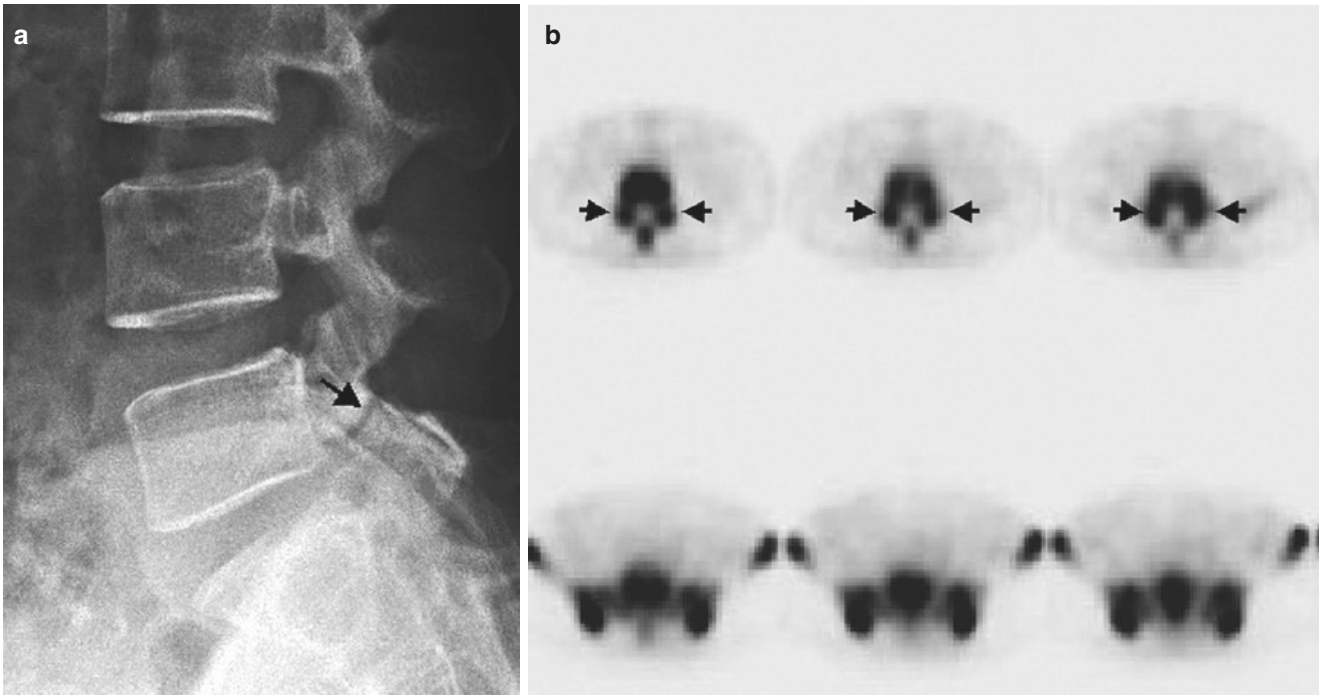

Fig. 9.63 High-resolution SPECT of acute spondylolysis. (**a**) Lateral radiograph of L5–S1 in a 41-year-old female with sudden back pain shows a band-like bone defect across the pars interarticularis (*arrow*). (**b**) High-resolution SPECT demonstrates small ovoid "hot" areas in the pars interarticularis bilaterally (*arrow*)

Planar scintigraphy is not so helpful in defining bone defects because many fail to accumulate tracer visibly (Lusins et al. 1994). Furthermore, there is no predictable pattern of correlation between the radiographic and scintigraphic findings (Gelfand et al. 1981). Indeed, we performed pinhole scintigraphy in seven patients with proven spondylolysis, but none yielded a positive result (Fig. 9.62b).

Spondylosis appears to be one of uncommon situations in which pinhole scintigraphy makes little contribution to the diagnosis. The likelier reasons are that the collimator-to-object distance is too great to image a small defect in the pars interarticularis and that old defects do not concentrate tracer visibly (Collier et al. 1985; Lusins et al. 1994). High-resolution SPECT can be recommended for acute spondylolysis as it can eliminate overlap, enhancing image contrast (Fig. 9.63). However, it is not useful for ancient or healed lesions (Collier et al. 1985; Lusins et al. 1994).

9.17.6 Spondylolisthesis

Spondylolisthesis denotes the sliding of one vertebra upon another either in the anterior or posterior direction (retrolisthesis). The sliding may be associated with spondylolysis or degenerative diseases such as apophyseal osteoarthritis and diskovertebral osteoarthritis. The latter type is aptly termed degenerative spondylolisthesis or spondylolisthesis with intact neural arch.

Radiographic features include vertebral slippage and endplate eburnation, most commonly in the two lowermost lumbar vertebrae and the lumbosacral joint (Figs. 9.62a and 9.64a). The anterior downward tilt of the displaced vertebral body seen on the lateral view is another diagnostic sign. On the anterior view, the downward tilt is indicated by the change of quadrilateral shape of the vertebral body into ovoid shape, arbitrarily termed the "ovoid vertebra" sign. Interestingly, pinhole scintigraphy shows prominent uptake in the ovoid vertebra, which is densely sclerosed (Fig. 9.64b).

9.17.7 Baastrup's Disease

Baastrup's disease is a painful condition of the spine in which the spinous processes of neighboring vertebrae come into contact with each other due to excessive lordosis of the lumbar spine created by various causes. The condition can be diagnosed by simple conventional radiography and MRI or PET/CT (Lin 2007). Recently, we encountered a patient in whom this disease was successfully diagnosed using pinhole scan (Fig. 9.65a). The pinhole scan showed a discoid hot area interposed between the lower endplate of a cranially

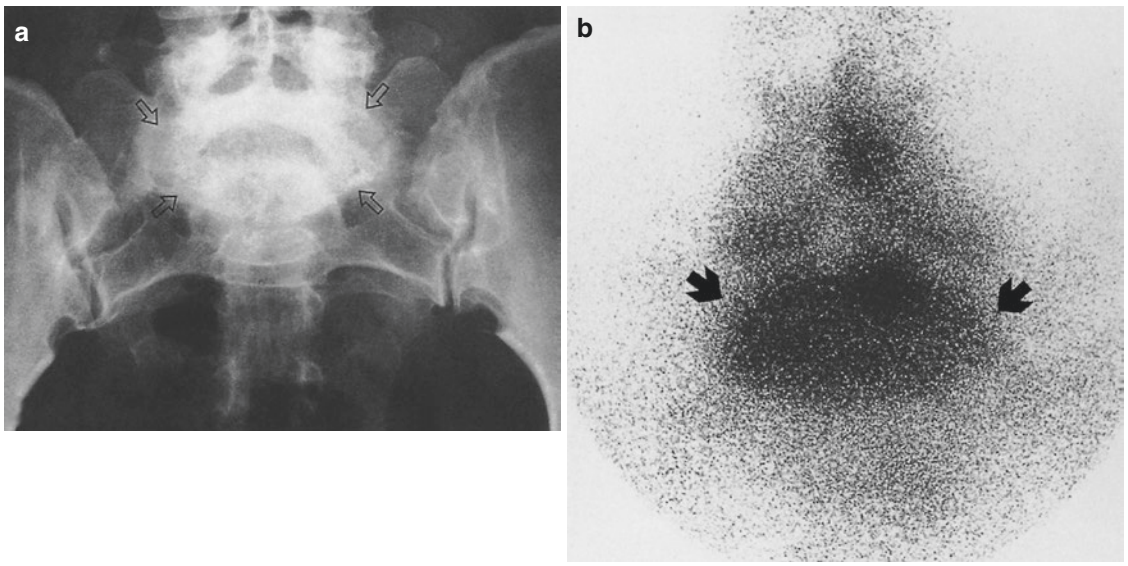

Fig. 9.64 Spondylolisthesis. (**a**) Anteroposterior radiograph of the lumbosacral spine in a 47-year-old man with disabling back pain demonstrates an ovoid "double bone density" overlapping the base of the sacrum (*open arrows*). (**b**) Anterior pinhole scintigraph shows the characteristic "ovoid vertebra" sign, indicating anterior and downward sliding of the L5 vertebra (*arrows*)

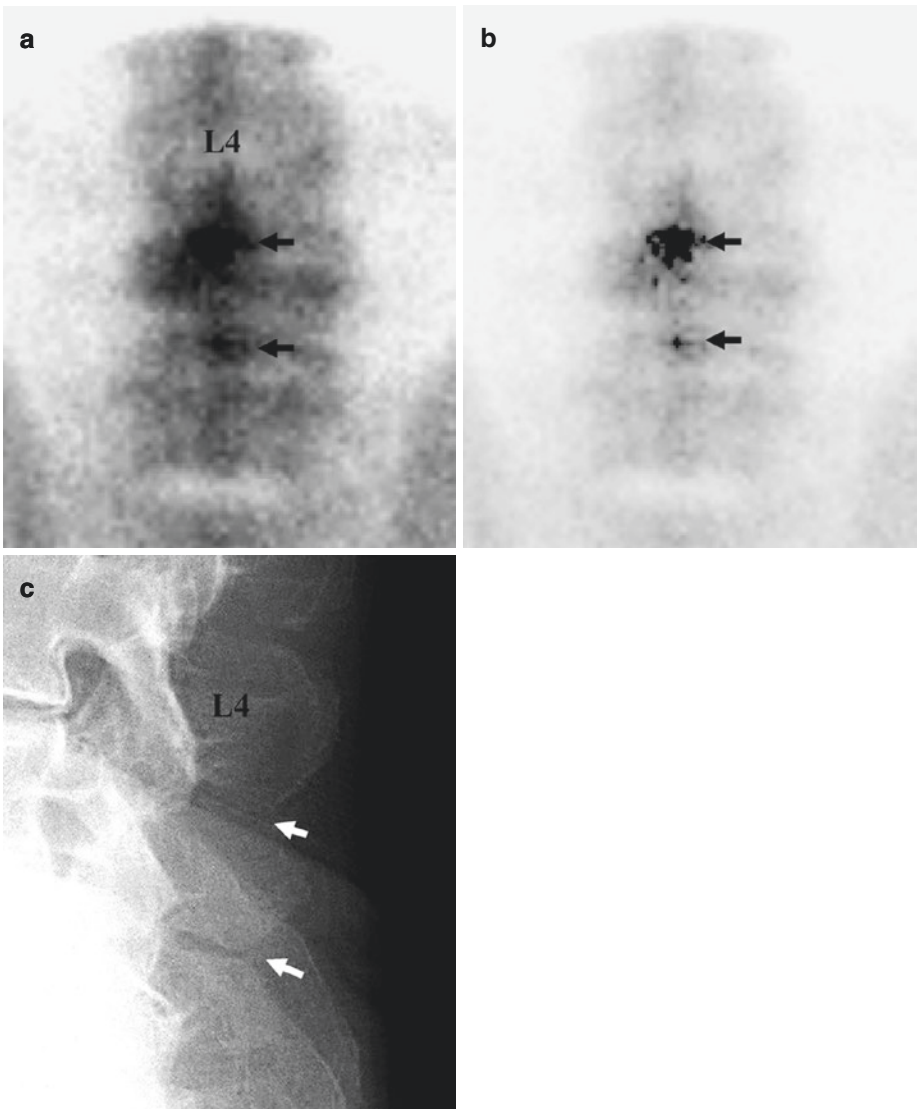

Fig. 9.65 Baastrup's disease of L3–5 spinous processes. (**a**) Posterior pinhole scan in a 77-year-old man with low-back pain shows prominent tracer uptake at the spinous processes of L4 and 5, which are in close contact (*top arrow*), and less intense uptake in the L5 and S1 spinous processes (*bottom arrow*). (**b**) Gamma correction (gamma =81) scan shows washout of lower tracer uptake in edema and hyperemia with preserved speckled uptake in injured spinous processes (*arrows*). (**c**) Lateral radiograph shows contact of L4 and 5 spinous processes (*top arrow*) and approximation of L5 and S1 processes (*bottom arrow*)

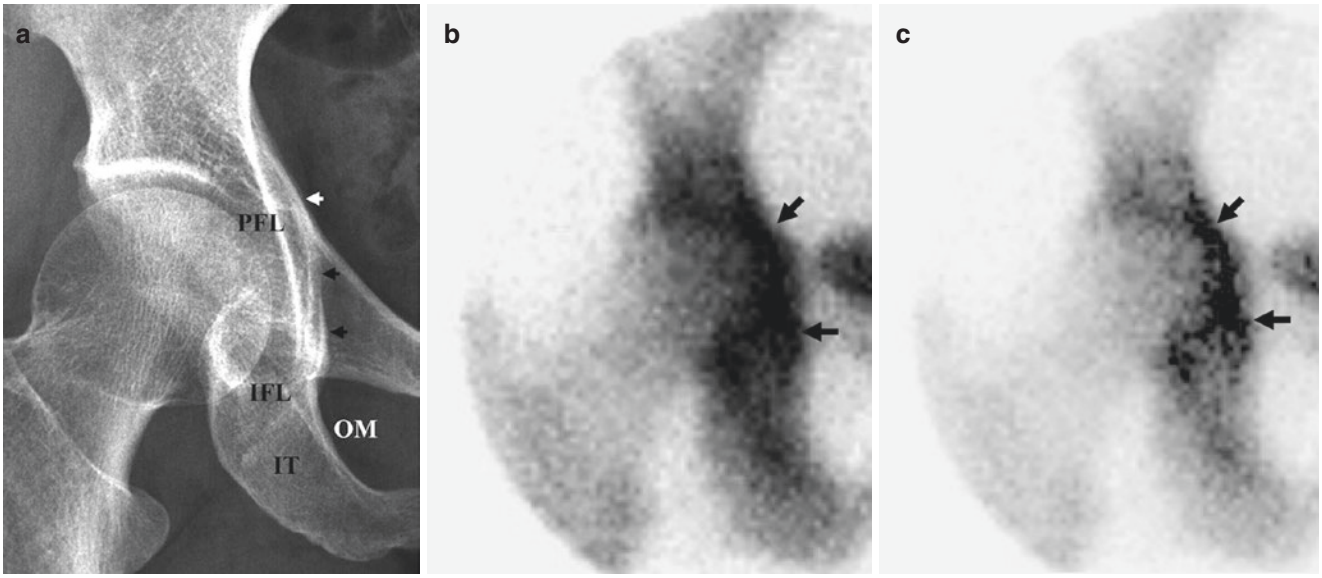

Fig. 9.66 Degenerative enthesopathy in the right iliopubic eminence and upper ischial tuberosity. (**a**) Anteroposterior radiograph of the right hip in a 56-year-old woman with chronic hip pain on sitting shows a blurred profile of the iliopubic eminence (*arrows*) and upper ischial tuberosity (*IT*). This finding is of no practical significance. The eminence is where the pubofemoral ligament (*PFL*), iliofemoral ligament (*IFL*), and obturator membrane (*OM*) are attached. (**b**) Anterior pinhole scan shows increased tracer uptake in the iliopubic eminence and upper ischial tuberosity (*arrows*). (**c**) Gamma correction (gamma = 69) scan shows washout of tracer uptake due to edema and congestion, distinctly leaving reactive osteogenesis behind, as in occult fracture (*arrows*)

situated vertebra and the upper endplate of the subjacent vertebra. Impressively, the gamma correction scan depicted the exact location of the "kissing uptake" with washout of tracer uptake in edema and congestion (Fig. 9.65b). The scintigraphic information on bone metabolic activity in this disease is considered to be useful for semiquantitative analysis of reactive bone changes.

9.18 Degenerative Enthesopathy

Degenerative enthesopathy is an inflammatory disorder that affects the attachments of tendons, ligaments, and interosseous membranes at bones. The disease occurs in any joints, the most commonly affected being the hip joint in adults (Imhof et al. 2009). Radiographically, enthesopathy itself is not diagnosable simply because pathologic changes in entheses are invisible unless indirectly indicated by the formation of calcific spur or hyperostosis (Fig. 9.66a). In contrast, MR imaging can reveal early changes such as edema and hyperemia in the cartilage, synovium, and subchondral bone and tears and defects in the cartilage. We found that pinhole scan can sensitively depict specific findings that reflect both enthesopathy with edema and osteopathy with speckled reactive bone formation. Characteristically, tracer uptake occurs at and around attachments of tendons, ligaments, and interosseous syndesmoses. In the hip joint, for example, tracer accumulates at the iliopubic eminence and the upper ischial tuberosity to which the pubofemoral and ischiofemoral ligaments and obturator membrane are attached (Fig. 9.66b). Gamma correction scan can more specifically demonstrate osteopathy (Fig. 9.66c).

References

Bahk YW, Park YH, Chung SK, Kim SH, Shinn KS (1994) Pinhole scintigraphic sign of chondromalacia patellae in older subjects: a prospective assessment with differential diagnosis. J Nucl Med 35:855–862

Brower AC (1988) The sacroiliac joint. In: Arthritis in black and white. WB Saunders, Philadelphia, pp 103–120

Cicuttini FM, Spector TD (1997) What is the evidence that osteoarthritis is genetically determined? Bailieres Clin Rheumatol 11:657–669

Collier BD, Johnson RP, Carrera BF et al. (1985) Painful spondylolysis and spondylolisthesis studied by radiography and single photon emission tomography. Radiology 54:207–211

de Palma AF (1957) Degenerative change in sternoclavicular and acromioclavicular joints in various decades. Charles C Thomas, Springfield

Dye SF, Boll DA (1986) Radionuclide imaging of the patellofemoral joint in young adults with anterior knee pain. Orthop Clin North Am 17:249–262

Gelfand MJ, Strife JL, Kereiakes JG (1981) Radionuclide bone imaging in spondylolysis of the lumbar spine in children. Radiology 140:191–195

Goodfellow J, Hungerford DS, Woods C (1976) Patellofemoral joint mechanics and pathology. 2. Chondromalacia patellae. J Bone Joint Surg Br 58:291–299

Howell DS, Sapolsky AL, Pita JC, Woessner JF (1976) The pathogenesis of osteoarthritis. Semin Arthritis Rheum 4:365–383

Imhof H, Nöbauer-Huhmann I, Trattnig S (2009) Coxarthrosis—an update. Radiologe 49:400–409

Jackson DW, Wilste LL, Cirincoine RJ (1976) Spondylolysis in the female gymnast. Clin Orthop 117:68–73

Kellgren JH, Moore R (1952) Generalized osteoarthrosis and Heberden's nodes. Br Med J 1:181–187

Kellgren JH, Lawrence JS, Bier F (1963) Genetic factors in generalized osteoarthrosis. Ann Rheum Dis 22:237–255

Lawson JP, Ogden JA, Sella E, Barwick KW (1984) The painful accessory navicular. Skeletal Radiol 12:250–266

Lin E (2007) Baastrup's disease (kissing spine) demonstrated by FDG PET/CT. Skeletal Radiol 37:173–175

Lund F, Nilsson BE (1980) Radiologic evaluation of chondromalacia patellae. Acta Radiol Diagn 21:413–416

Lusins JO, Elting JJ, Cicoria AD, Goldsmith SJ (1994) SPECT evaluation of lumbar spondylolysis and spondylolisthesis. Spine 19:608–612

Mitchel NS, Cruess RL (1977) Classification of degenerative arthritis. Can Med Assoc J 117:763–765

Ogata N, Kawaguchi H (2004) Ossification of the posterior longitudinal ligament of spine (OPLL). Clin Calcium 14:42–48

Ono K, Ota H, Tada K et al. (1977) Ossification of the posterior longitudinal ligament. Spine 2:126–138

Paquin J, Rosenthall L, Esdaile J et al. (1983) Elevated uptake of ^{99m}technetium methylene diphosphonate in the axial skeleton in ankylosing spondylitis and Reiter's disease: implications for quantitative sacroiliac scintigraphy. Arthritis Rheum 26:217–220

Radin EL, Paul IL, Rose RM (1977) Current concepts of the etiology of idiopathic osteoarthrosis. Bull Hosp Joint Dis 31:117–120

Resnick D (2002) Degenerative disease of extraspinal locations. In: Resnick D (ed) Diagnosis of bone and joint disorders, 4th edn. WB Saunders, Philadelphia, PA, pp 1271–1381

Resnick D, Niwayama G (1976) Radiographic and pathologic features of spinal involvement in diffuse idiopathic skeletal hyperostosis (DISH). Radiology 119:559–568

Spencer JM, Loughlin J, Clipsham K, Carr AJ (2005) Genetic background increases the risk of hip osteoarthritis. Clin Orthop Relat Res 431:134–137

Wiles P, Andrews PS, Devas MB (1956) Chondromalacia of the patella. J Bone Joint Surg Br 38:95–113